IOPscience iopscience.iop.org

Home Search Collections Journals About Contact us My IOPscience

Metastable charged sparticles and the cosmological ^{7}Li problem

This content has been downloaded from IOPscience. Please scroll down to see the full text.

JCAP12(2012)037

(http://iopscience.iop.org/1475-7516/2012/12/037)

View the table of contents for this issue, or go to the journal homepage for more

Download details:

IP Address: 137.138.125.164
This content was downloaded on 25/11/2013 at 10:09

Please note that terms and conditions apply.

Journal of Cosmology and Astroparticle Physics
An IOP and SISSA journal

Metastable charged sparticles and the cosmological ^{7}Li problem

Richard H. Cyburt,[a] **John Ellis,**[b,c] **Brian D. Fields,**[d] **Feng Luo,**[b,e] **Keith A. Olive**[e,f] **and Vassilis C. Spanos**[g]

[a]Joint Institute for Nuclear Astrophysics (JINA),
National Superconducting Cyclotron Laboratory (NSCL),
Michigan State University, East Lansing, MI 48824, U.S.A.
[b]Theoretical Physics and Cosmology Group, Department of Physics, King's College London, London WC2R 2LS, U.K.
[c]TH Division, Physics Department, CERN, CH-1211 Geneva 23, Switzerland
[d]Departments of Astronomy and of Physics, University of Illinois, Urbana, IL 61801, U.S.A.
[e]School of Physics and Astronomy, University of Minnesota, Minneapolis, MN 55455, U.S.A.
[f]William I. Fine Theoretical Physics Institute, School of Physics and Astronomy, University of Minnesota, Minneapolis, MN 55455, U.S.A.
[g]Institute of Nuclear Physics, NCSR "Demokritos", GR-15310 Athens, Greece
E-mail: cyburt@nscl.msu.edu, John.Ellis@cern.ch, bdfields@illinois.edu, feng.luo@kcl.ac.uk, olive@physics.umn.edu, spanos@inp.demokritos.gr

Received September 13, 2012
Accepted November 26, 2012
Published December 21, 2012

Abstract. We consider the effects of metastable charged sparticles on Big-Bang Nucleosynthesis (BBN), including bound-state reaction rates and chemical effects. We make a new analysis of the bound states of negatively-charged massive particles with the light nuclei most prominent in BBN, and present a new code to track their abundances, paying particular attention to that of ^{7}Li. Assuming, as an example, that the gravitino is the lightest supersymmetric particle (LSP), and that the lighter stau slepton, $\tilde{\tau}_1$, is the metastable next-to-lightest sparticle within the constrained minimal supersymmetric extension of the Standard Model (CMSSM), we analyze the possible effects on the standard BBN abundances of $\tilde{\tau}_1$ bound states and decays for representative values of the gravitino mass. Taking into account the constraint on the CMSSM parameter space imposed by the discovery of the Higgs boson at the LHC, we delineate regions in which the fit to the measured light-element abundances is as good as in standard BBN. We also identify regions of the CMSSM parameter space in which the bound state properties, chemistry and decays of metastable charged sparticles can solve the cosmological ^{7}Li problem.

Keywords: big bang nucleosynthesis, dark matter theory, particle physics - cosmology connection, supersymmetry and cosmology

ArXiv ePrint: 1209.1347

© 2012 IOP Publishing Ltd and Sissa Medialab srl
doi:10.1088/1475-7516/2012/12/037

JCAP12(2012)037

Contents

1 Introduction **1**

2 Bound-state properties **3**

3 Bound-state reactions and abundances **6**
3.1 Formalism 6
3.2 Reaction rates 8

4 Bound-state chemical effects **10**

5 Decays of the NLSP in gravitino dark matter scenarios **13**

6 NLSP lifetimes in the CMSSM with gravitino LSP **14**

7 Light-element constraints in the CMSSM with a metastable Stau NLSP **16**
7.1 Summary of light-element abundance constraints 16
7.2 Application to the CMSSM with a metastable Stau NLSP 20
7.3 Bound-state effects and uncertainties 28

8 Summary **31**

A Recombination of X bound states **32**

B Specification of the supersymmetric model framework **34**

C Three-body Stau decays **35**

1 Introduction

The agreement of standard Big-Bang Nucleosynthesis (BBN) calculations with the measured abundances of the light elements imposes important constraints on scenarios for new physics that involve massive metastable particles [1] -[48]. If these particles are neutral, only the effects of particles produced in the showers following their decays need to be taken into account, but in the case of negatively-charged metastable particles X^-, the formation of (AX^-) bound states should also be considered, and are very important [24, 27–30, 32, 35–37, 42, 45].

The emergence of the primordial 'lithium problem' adds cosmological motivation to the studying the effects of metastable particles on BBN. As reviewed in refs. [40, 45, 49, 50], WMAP and other observations [51] have determined precisely the cosmic baryon density and thus pinned down the one free parameter of standard BBN [52]. Using this as an input, BBN makes precise predictions for light-element abundances, and those of deuterium and ^{4}He are in good agreement with obervations. But the BBN expectations for ^{7}Li/H based on the WMAP baryon density are *higher* than the observed abundances by factors of $2-4$, amounting formally to a $4-5\sigma$ discrepancy; this is the cosmological lithium problem [53, 54]. Nuclear uncertainties [54–57] and/or resonances are all but excluded as solutions to the

JCAP12(2012)037

problem [57–62]. There is the possibility that depletion plays a role in altering the ^{7}Li abundance [63]. However, these solutions typically have difficulty in explaining the thinness of the ^{7}Li plateau [64] for [Fe/H] $\gtrsim -3$ (see ref. [65]) as well as the observation of ^{6}Li in some halo stars [66]. The temperature scale used in the ^{7}Li abundance determination has also been considered [67, 68] and it seems unlikely that a significant change in the ^{7}Li abundance is possible within reasonable uncertainties in the effective temperature.

We note that two recent developments alter the observational lithium picture. Halo-star measurements at very low metallicities [Fe/H] < -3 show a large dispersion and apparently a decrease in Li/H towards low metallicity [65]. The origin of this trend is not clear, nor is its relation to the still-thin Spite plateau at higher metallicity. On the other hand, recent observations of lithium in the interstellar medium of the metal-poor Small Magellanic Cloud test these systematics and are consistent with the halo-star results [69]. Thus, the cosmological lithium problem seems increasingly likely to be real, and to point to new physics during or after BBN.

In a previous paper [44], we extended analyses of the effects of particle showers in the decays of metastable particles to include the most relevant uncertainties in nuclear reaction rates. We applied our analysis to scenarios within the constrained minimal supersymmetric extension of the Standard Model (CMSSM, see appendix B for its specification) in which the lightest neutralino χ is the lightest supersymmetric particle (LSP), and the heavier, neutral gravitino is metastable. Not only did we find regions of this CMSSM parameter space where the cosmological light-element abundances agreed with the measured values at least as well as in standard BBN, but we also identified regions of this CMSSM parameter space where the cosmological ^{7}Li problem is alleviated and even potentially solved. In this paper, we extend the analysis of [44] to include the (AX^-) bound-state effects expected in the case of a negatively-charged metastable particle X^-.

Bound-state effects were also discussed in [27], and here we update and supersede that analysis incorporating qualitatively and quantitatively new rates and processes that were not available at the time. To this end, we first review our calculations of bound-state properties, and then turn to their effects on BBN. These include calculations of (1) bound-state recombination, which fixes the abundances of various exotic 'ions' such as (pX^-), $(^4\mathrm{He}X^-)$, $(^7\mathrm{Be}X^-)$, etc., and (2) bound-state catalysis, which causes additional changes in light-element production and destruction rates beyond the non-thermal reactions considered in [44]. Our new calculations of bound-state properties such as binding energies and charge radii are in reasonable agreement with other work, and we use them to discuss the effects of uncertainties in the nuclear inputs. For this purpose, we have compiled a complete and up-to-date list of the relevant reactions, tabulated below. We have verified, using a simple driver code, that our recombination rates give (pX^-) and $(^4\mathrm{He}X^-)$ abundances in good agreement with previous results [24]. We have then updated the BBN code used in [27, 41, 44] to include the recombination and catalysis rates, in a more complete, accurate and systematic way than previously.

As an example of the application of our code, we consider the case of a supersymmetric model in which the gravitino is the LSP, and the lighter stau slepton, $\tilde{\tau}_1$ is the metastable NLSP. We work within the framework of the CMSSM, and seek regions of its parameter space where the consistency with the measured light-element abundances of standard BBN calculations is at least maintained, and also look for regions where the cosmological ^{7}Li problem may be alleviated or even solved. We find that this is possible for generic values of the CMSSM parameters where the lifetime of the NLSP $\sim 10^3$ s (as in [16, 17]), and that

JCAP12(2012)037

there are more extended regions of parameter space where the cosmological ^{7}Li is at least no worse than in standard BBN calculations.

The paper is organized as follows. In section 2 we discuss the relevant properties of X^- bound states, including the Coulomb radii of several nuclides and our three-body model for the $(\alpha + \alpha + X)$ system, and various choices for binding energies. In section 3, we discuss relevant nuclear interaction rates involving bound states, and our implementation of them in the BBN network. In section 4, we briefly describe the chemical reactions involving bound states. In section 5, we introduce the supersymmetric framework we use to produce our numerical results. In particular, we consider models where the lighter stau slepton is our candidate for the metastable charged particle X^-, and results for stau lifetimes are summarized in section 6. Our main results are given in section 7, which includes a discussion of the light element abundance observations and the abundances we find from BBN with stau bound states. Our results are summarized in section 8.

2 Bound-state properties

Before considering the impact of a new electromagnetically-charged particle on BBN predictions, we first study the properties of its bound states with light nuclei. To this end, we solve the time-independent Schrödinger equation with an interaction potential given by the Coulomb potential between a finite-sized nuclide and a point-like X^- particle. The Coulomb potential is determined by the charge and the rms charge radius of the nuclide of interest. Here we adopt the latest rms charge radii measurements of He, Li and Be isotopes, and assume the charge distribution of the nuclide to be Gaussian.[1]

When solving the Schrödinger equation, we first define dimensionless variables for the energy and a typical length scale. This makes the equations a function of a single parameter, the ratio of the rms charge radius $R_{\rm c}$ to the Bohr radius $R_{\rm B}$. We have verified that our solutions interpolate smoothly between Coulombic bound-state energies at small $R_{\rm c}/R_{\rm B}$ and harmonic oscillator energy levels at large $R_{\rm c}/R_{\rm B}$, and that our numerical solutions match analytic solutions.

Numerical results for bound states for the nuclides of interest for BBN are shown in table 1. We note that the rms charge radii of many of the nuclides considered have been determined experimentally. However, in other cases we must rely on phenomenological estimates, and table 1 gives some ranges in these cases. In particular, the charge radii for the two nuclei relevant for crossing the $A = 8$ divide, namely ^{8}Be and the first excited state of ^{9}Be, are not known experimentally. Given that ^{8}Be is a barely bound state of two α particles (^{4}He nuclei) that are hardly touching, it is expected that the rms charge radius of ^{8}Be should be close to twice the rms charge radius of ^{4}He, i.e., $R_{\rm c,8} = 3.362\,$fm. This estimate is in good agreement with the value given in [77], namely $R_{\rm c,8} = 3.39\,$fm, after correcting for the poor binding energy determination in [79]. For comparison, we also consider the value $R_{\rm c,8} = 2.50\,$fm [78]; an estimate chosen close to the ^{9}Be charge radius, though likely an underestimate.

The $(^8{\rm Be}X^-)$ state can play an important role in primordial ^{9}Be synthesis, if the state exists and has appreciable abundance. As we will see in the next section, the significance of $(^8{\rm Be}X^-)$ depends not only to the qualitative issue of whether this system is bound, but also on the value of the binding energy. For this species, therefore, we have gone beyond the 2-body model that has been used to calculate the other binding energies appearing in table 2.

[1] As long as one reproduces the rms charge radius, the detailed form of the charge distribution is not important for our purposes.

JCAP12(2012)037

Nuclide	Mass (amu)	R_c (fm)	B_A (MeV)
^{1}H	1.00782503	0.8750 ± 0.0068 [70]	0.02493
^{2}H	2.01410178	2.1303 ± 0.0010 [71]	0.04879
^{3}H	3.01604927	1.63 ± 0.03 [72]	0.07264
^{3}He	3.01602931	1.9506 ± 0.0014 [73]	0.2677
^{4}He	4.00260325	1.681 ± 0.004 [74]	0.3474
^{6}Li	6.01512228	2.517 ± 0.030 [75]	0.8000
^{7}Li	7.01600405	2.39 ± 0.030 [75]	0.8893
^{7}Be	7.01692925	2.647 ± 0.015 [76]	1.2879
^{8}Be	8.00530509	3.390 [77]	1.1679
		2.50 [78]	1.408 [78]
		N/A*	0.492
^{9}Be	9.01218213	2.519 ± 0.012 [76]	1.4699
^{9}Be*	9.01398998	2.519	1.4700
		2.880 [79]	1.3527
		3.390	1.2173
^{8}B	8.037675026	2.65	1.8547

*Our result for B_A in this case is based on our three-body calculation.

Table 1. Properties of X^- bound states with relevant nuclides. The table lists relevant nuclides together with their (unbound) masses and rms charge radii R_c in Coulombic parameterizations of the potentials. Bound-state binding energies B_A come from our 2-body calculations based on the given charge radii (except where otherwise noted). Experimental values and ranges of R_c are listed, where available for some nuclides, and ranges of theoretical estimates of R_c for other nuclides.

To analyze the bound state properties of the 3-body system ($\alpha + \alpha + X$), we have utilized the Variational Monte Carlo (VMC) method [80]. This method assumes a suitable form of wavefunction with parameters to be determined by Monte Carlo variation. Parameters are randomly chosen after some initial guess; the expectation value of the Hamiltonian is then computed and, if it is lower than the initial expectation value, the current parameters are set as the adopted values. This variation is repeated until some convergence criteria are met, such as small (or no) changes in the expectation value of the Hamiltonian with decreasing step size. The complexity of the adopted wave function can be increased, with added parameters, allowing for another test of convergence. Note that, as with the 2-body case, the 3-body binding energy is expressed with respect to free ^{8}Be+X; this is larger than the binding relative to free $\alpha + \alpha + X$ by $m(^{8,\text{free}}\text{Be}) - 2m_\alpha = -Q_{8,\text{free}} = 92$ keV.

We have adopted wavefunctions with the forms of exponentials with Gaussian cutoffs and extra Gaussian terms with decreasing dispersion with respect to the cutoff scale. The method was validated with the three-body systems of the neutral He-atom and the negatively charged H-atom, using finite-sized Coulomb potentials with the p and α rms charge radii. The VMC method reproduced the binding energies for these Coulomb-only systems quite quickly, agreeing with the observed values. For the $\alpha + \alpha + X$ system, we similarly adopt finite-sized Coulomb interactions, plus an added nuclear $\alpha + \alpha$ interaction from [81, 82]. The adopted nuclear $\alpha + \alpha$ potential reproduces elastic scattering data and the ^{8}Be ground state resonance energy. We find that $^8\text{Be} + X$ is bound, but with $B_8 = 492 \pm 50$ keV. This is more fragile than found when assuming a two-body ($^8\text{Be}X^-$) structure with an appropriate rms charge radius. The Coulomb repulsion of the two α particles loosens the binding of the three-body system.

JCAP12(2012)037

For $(^8\mathrm{Be}X^-)$ to allow substantial ^{9}Be production, two conditions must be satisfied:

1. Production of $(^8\mathrm{Be}X^-)$ must be possible and effective, and
2. Production of ^{9}Be must proceed resonantly through the first excited state in $(^9\mathrm{Be}^*X^-)$, that is, $(^8\mathrm{Be}X^-) + n \to (^9\mathrm{Be}^*X^-) \to {}^9\mathrm{Be} + X^-$ [78].

The requirement that $(^8\mathrm{Be}X^-)$ production is possible merely demands that this state is stable, as we and others have found. But, as we will see, in the early Universe $(^4\mathrm{He}X^-)$ is the dominant bound state. Consequently, $(^8\mathrm{Be}X^-)$ production occurs via $(^4\mathrm{He}X^-) + {}^4\mathrm{He} \to (^8\mathrm{Be}X^-) + \gamma$. This channel is only effective if it has $Q > 0$, which demands that

$$B_8 > B_8^{\mathrm{min}} = B_4 - Q_{8,\mathrm{free}} = 0.439 \text{ MeV}\,. \tag{2.1}$$

We find that all estimates of B_8 satisfy this constraint, though our 3-body result does so by a much smaller margin than the others.

The second requirement for ^{9}Be production depends on the position of the first excited state of $(^9\mathrm{Be}^*X^-)$, to which we now turn. In ordinary ^{9}Be, this is a cluster state that is poorly described by shell-model calculations. Its structure is that of two α particles and a neutron and, to first order, this state is the $^8\mathrm{Be} + n$ ground state. Therefore, a first guess for the rms charge radius would be $R_{\mathrm{c},9^*} = R_{\mathrm{c},8}$. However, the presence of the neutron impacts the structure, and the excited state of ^{9}Be should have a radius larger than the ground state. This constrains our estimate of the impact of the neutron on the rms ^{9}Be charge radius to the range $R_{\mathrm{c},9^*} \in (2.519, 3.39)$ fm, where the low value is just the ground-state value $R_{\mathrm{c},9}$, and the upper value is the estimate of $R_{\mathrm{c},8}$ given in [77]. This range includes the result for the rms charge radius given in [79], namely $R_{\mathrm{c},9^*} = 2.88$ fm. If one assumes the same relative shift in the rms charge radius as for ^{8}Be, one finds $R_{\mathrm{c},9^*} = 3.11$ fm. However, it may be larger, given that the level energy calculated is less accurate in the ^{9}Be case than in the ^{8}Be case.

Figure 1 shows the level structure for the ^{9}Be system when either in the ordinary unbound state (left, [83]) or bound to an X^- particle (right, our calculations). The zero-point of energy is taken to be that of unbound, free particles. Thus, for example, unbound $^8\mathrm{Be} + n$ lies at $-Q_{8,\mathrm{free}} = +0.092$ MeV. The level positions for each of the bound states are shifted relative to the corresponding unbound case due to the binding energy: level i lies at energy $E_{(iX)} = E_{i,\mathrm{free}} - B_i$. Thus, level *spacings* are shifted by *differences* in binding: $E_{(jX)} - E_{(iX)} = E_{j,\mathrm{free}} - E_{i,\mathrm{free}} - B_j + B_i$. For example, the $(^9\mathrm{Be}^*X)$ excited state lies above the ground state by an amount that is the sum of the unbound ^{9}Be level spacing 1.684 MeV, minus the difference $B_{9^*} - B_9$. If the bindings are the same, then the first excited state spacing is also the same as in the ordinary case. But if the excited state is more weakly bound, then the level spacing is larger than in ordinary ^{9}Be.

The three strips for the $(^8\mathrm{Be}X^-)$ bound state represent the three values as determined by this work (highest strip), as well that of [77, 78] (the lower two strips, as labelled). The thick box for the excited $(^9\mathrm{Be}^*X^-)$ state corresponds to the range of possible charge radii $R_{\mathrm{c},9^*} \in (2.519, 3.39)$ fm. Even with the broad range of possible rms charge radii for the first excited state in ^{9}Be, one can see that the excited state probably lies substantially below the $(^8\mathrm{Be}X^-)$ entrance level. If this is so, this drives the reaction away from resonance, substantially reducing or even eliminating the mechanism discussed in [78], and thus suppressing ^{9}Be production via bound states. Ultimately, however, a true determination of the first exited state position would require a four-body calculation of $(\alpha\alpha nX^-)$. This challenging work has

JCAP12(2012)037

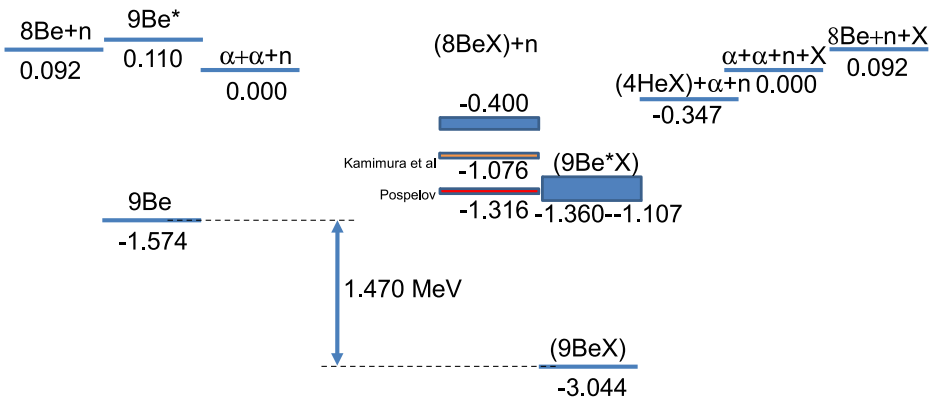

Figure 1. Level schemes calculated for unbound and bound X^- states in the ^{9}Be system. State labels appear above the corresponding level. Level values shown are based on table 1, and all levels are shifted such that zero energy corresponds to the free-particle state. In the case of (^{8}BeX^-), we show the result of our 3-body calculation (a blue band whose the width corresponds to the uncertainty), as well as the 2-body calculations of Kamimura et al. [77] and of Pospelov [78] (labelled). In the case of (^{9}Be$^*X^-$), we consider a range of level values including our and Pospelov's estimates.

not been done, and lies beyond the scope of our paper. Note also that our 2-body and 3-body calculations of (^{8}BeX^-) gave significantly different binding energies, underscoring the importance of detailed calculations for these states with relatively high Z. Consequently, we cannot exclude the possibility that the (^{8}BeX^-) entrance channel will be near resonance.

Clearly, the situation regarding ^{9}Be is uncertain, reflecting the poor state of knowledge regarding the (^{8}BeX^-) and (^{9}BeX^-) nuclear properties. In this paper, our approach is to illustrate the ability of ^{9}Be to constrain supersymmetric models, within the most optimistic scenario in which the resonant production discussed in [78] occurs. Thus, for most of our calculations we adopt this (constant) resonant rate for (^{8}BeX^-)$+n \to {}^9$Be$+X^-$ [78]. However, the reader should bear in mind that the resulting ^{9}Be abundances and resulting constraint therefore represent a 'most optimistic' scenario. Consequently, we also make comparisons with calculations in which this production channel is suppressed, considering the cases:

1. Bound state structure and resonant rate from [78].

2. (^{8}BeX^-) is more tightly and more weakly bound.

3. The resonant rate set to zero for (^{8}BeX^-) $+ n \to {}^9$Be $+ X^-$.

It goes without saying that there is a pressing need for precise and accurate calculations of (^{8}BeX^-) and (^{9}BeX^-) properties.

3 Bound-state reactions and abundances

3.1 Formalism

In looking at the effects of bound states of X^-, we must track the abundances of its bound states with various nuclei, e.g., (pX^-), (^{4}HeX^-) and (^{7}BeX^-). For this purpose, we need to

JCAP12(2012)037

incorporate reactions that affect these bound-state abundances, namely: (1) recombination and photodissociation processes on each nuclear species i, such as

$$i + X^- \leftrightarrow (iX^-) + \gamma \ , \tag{3.1}$$

and (2) charge-exchange processes between (iX^-) bound states and other nuclides j, such as

$$(iX^-) + j \leftrightarrow i + (jX^-) \ . \tag{3.2}$$

We refer to these processes collectively as 'bound-state chemistry', and solve the rate equations for the processes (3.1) and (3.2) to determine the corresponding chemical abundances.

Denoting the total X^- number density by $n_{X^-} = Y_{X^-} n_{\rm B}$, we decompose it into the free and bound abundances, respectively $n_{X^-,\rm free}$ and $n_{(jX^-)}$, with $j \in p, d, \ldots$. To remove the effect of cosmic expansion, as usual we follow the evolution of the 'mole fractions'

$$Y_i \equiv \frac{n_i}{n_{\rm B}}, \tag{3.3}$$

where the states i include: (a) ordinary *unbound*, free nuclei, (b) X^- bound states, and (c) free X^-. Thus, we treat these in a manner completely parallel to the usual BBN accounting for ordinary (unbound) nuclides. Note that the total abundance of a nuclear species i sums its unbound and bound states $Y_{i,\rm tot} = Y_{i,\rm free} + Y_{(iX^-)}$, while the total abundance of X^- is $Y_{X^-,\rm tot} = Y_{X^-,\rm free} + \sum_i Y_{(iX^-)}$.

For two-to-two reactions of the form $ab \to cd$, the reaction rate per unit volume is $n_a n_b \langle \sigma_{ab\to cd} v \rangle$, with $\langle \sigma_{ab\to cd} v \rangle$ the appropriate thermally-averaged rate coefficient. The reaction rate per particle a is thus

$$\Gamma_{ab\to cd} = \langle \sigma_{ab\to cd} v \rangle \, n_b = N_{\rm Avo} \langle \sigma_{ab\to cd} v \rangle \ \rho_{\rm B} Y_b \equiv \lambda_{ab\to cd} \, \rho_{\rm B} Y_b, \tag{3.4}$$

where $N_{\rm Avo} = 1/m_u$ is Avogadro's number, and $\lambda_{ab\to cd} = N_{\rm Avo} \langle \sigma_{ab\to cd} v \rangle$ is the form in which thermonuclear rates are normally tabulated. Thus the *total* rate per target b nucleus is

$$\Gamma^{\rm tot}_{ab\to cd} = \Gamma_{ab\to cd} + \Gamma_{(aX)b\to cdX} = \langle \sigma_{ab\to cd} v \rangle \, n_{\rm B} Y_{a,\rm free} + \left\langle \sigma_{(aX)b\to cdX} v \right\rangle n_{\rm B} Y_{(aX)} \, , \tag{3.5}$$

which can be substantially larger than in the ordinary case if the catalyzed rate coefficient has a large enhancement and if there is a substantial (aX) abundance.

With these definitions, the evolution of bound state (iX), with $i \in p, d, \ldots$ can be expressed as a sum over several kinds of processes:

$$\frac{\partial}{\partial t} Y_{(iX)} = \frac{\partial}{\partial t} Y_{(iX)} \bigg|_{\rm chem} + \frac{\partial}{\partial t} Y_{(iX)} \bigg|_{\rm nuc} + \frac{\partial}{\partial t} Y_{(iX)} \bigg|_{\rm decay} \ . \tag{3.6}$$

The bound-state chemistry reactions do not change the type of nuclides in the initial state, and are

$$\frac{\partial}{\partial t} Y_{(iX)} \bigg|_{\rm chem} = \\ - \left(\Gamma_{\gamma(iX)\to iX} + \sum_j \Gamma_{j(iX)\to i(jX)} \right) Y_{(iX)} + \Gamma_{iX\to\gamma(iX)} Y_{X,\rm free} + \sum_j \Gamma_{i(jX)\to j(iX)} Y_{(jX)} \ . \tag{3.7}$$

JCAP12(2012)037

Bound-state nuclear reactions have final-state nuclides different than those in the initial state, and take the form

$$\frac{\partial}{\partial t} Y_{(iX)}\bigg|_{\rm nuc} = -\left(\sum_{k\ell} \Gamma_{j(iX)\to k\ell X}\right) Y_{(iX)} + \sum_{k\ell} \Gamma_{\ell(kX)\to j(iX)} Y_{(kX)}\,, \tag{3.8}$$

where the last term includes only those reactions that produce bound (iX^-) rather than free i. Finally, the decays of X^- with lifetime τ_X destroy bound states:

$$\frac{\partial}{\partial t} Y_{(iX)}\bigg|_{\rm decay} = -\Gamma_X Y_{(iX)}\,, \tag{3.9}$$

where the decay rate $\Gamma_X = 1/\tau_X$.

Turning to free X^-, we have

$$\frac{\partial}{\partial t} Y_{X,\rm free} = -\sum_i \frac{\partial}{\partial t} Y_{(iX)}\bigg|_{\rm chem} - \sum_i \frac{\partial}{\partial t} Y_{(iX)}\bigg|_{\rm nuc} - \Gamma_X Y_{X,\rm free}\ . \tag{3.10}$$

The bound-state contribution to the evolution of a species of unbound, free nuclei i is given by

$$\begin{aligned}\frac{\partial}{\partial t} Y_{i,\rm free}\bigg|_{\rm BS} = &-\frac{\partial}{\partial t} Y_{(iX)}\bigg|_{\rm chem} - \frac{\partial}{\partial t} Y_{(iX)}\bigg|_{\rm decay} \\ &- \left(\sum_j \Gamma_{i(jX)\to k\ell X}\right) Y_{i,\rm free} + \sum_{k\ell} \Gamma_{\ell(kX)\to ijX} Y_{(kX)}\,,\end{aligned} \tag{3.11}$$

where the last term includes only bound-state reactions that produce free i in the final state.

3.2 Reaction rates

Tables 2 and 3 summarize the treatments of bound-state chemistry and nuclear rates in our work and in the recent literature. Entries for recent literature are given to the best of our knowledge; in some cases full details were not given in the published papers. Blank entries mean that to the best of our knowledge no rate was assigned, effectively setting the rate to zero.

Wherever possible, we adopted the most up-to-date chemistry and nuclear rates from the literature. In many cases, rates were not available for channels we wished to examine. Thus we adopted simple rules to estimate the needed rates from published ones; these cases are identified in the tables. In the case of bound-state chemistry, we adopted recombination rates for nuclide i using the scaling $\sigma_{\rm rec} \propto Z_i^2 B_{(iX)}$.

As we see below, bound state chemistry strongly favors $({}^4{\rm He}X^-)$ production, which essentially locks up all of the X^-, for the cases of physically interesting abundances where $Y_{X^-} < Y_\alpha$. Consequently, nuclear reactions involving $({}^4{\rm He}X^-)$ are the most important. On the other hand, (pX^-) reactions are relatively unimportant due to the small abundance of this state, and (dX^-) and (tX^-) have negligible effects.

In general, bound states enhance nuclear rates. This is in part because they reduce the Coulomb barrier, to which the rates are exponentially sensitive. For nuclides and channels for which bound-state nuclear rates were not available in the literature, we estimated the rates assuming this is the only source of perturbation. In these cases, we adopted the ordinary thermonuclear rates, but with a Gamow penetration factor appropriate for a nucleus of effective charge $Z^{\rm eff}_{(iX)} = Z_i - 1$.

JCAP12(2012)037

Reaction	CEFOS 2006 [27]	Bailly et al 2009 [38]	Pospelov et al 2008 [37]	Kamimura et al 2009 [77]	This Work
$p + X^- \to (pX^-) + \gamma$	simple scaling	Kamimura 09 [77]	estimated		Pospelov [37]
$d + X^- \to (dX^-) + \gamma$	simple scaling				scaled Pospelov [37]
$t + X^- \to (tX^-) + \gamma$	simple scaling				scaled Pospelov [37]
${}^3\mathrm{He} + X^- \to ({}^3\mathrm{He}X^-) + \gamma$	simple scaling				scaled Pospelov [37]
$\alpha + X^- \to (\alpha X^-) + \gamma$	simple scaling	"	Pospelov 07 [24]		Pospelov [37]
${}^6\mathrm{Li} + X^- \to ({}^6\mathrm{Li}X^-) + \gamma$	simple scaling	"			$\sigma_{\mathrm{rec}} \propto Z^2 B$ scaling
${}^7\mathrm{Li} + X^- \to ({}^7\mathrm{Li}X^-) + \gamma$	simple scaling	"			$\sigma_{\mathrm{rec}} \propto Z^2 B$ scaling
${}^7\mathrm{Be} + X^- \to ({}^7\mathrm{Be}X^-) + \gamma$	simple scaling	"	Bird 08 [29]		Bird 08 [29]
$({}^8\mathrm{Be}X^-) + \gamma \to {}^8\mathrm{Be} + X^-$	simple scaling				$\sigma_{\mathrm{rec}} \propto Z^2 B$ scaling
${}^9\mathrm{Be} + X^- \to ({}^9\mathrm{Be}X^-) + \gamma$					$\sigma_{\mathrm{rec}} \propto Z^2 B$ scaling
${}^8\mathrm{B} + X^- \to ({}^8\mathrm{B}X^-) + \gamma$					$\sigma_{\mathrm{rec}} \propto Z^2 B$ scaling
$(pX^-) + \alpha \to (\alpha X^-) + p$		"	estimated	QM 3-body	Kamimura 09 [77]
$(dX^-) + \alpha \to (\alpha X^-) + d$		"		QM 3-body	Kamimura 09 [77]
$(tX^-) + \alpha \to (\alpha X^-) + t$		"		QM 3-body	Kamimura 09 [77]

Table 2. Summaries of the treatments of bound-state chemistry rates assumed in our work and in the recent literature (I).

Bound State Nuclear					
Reaction	CEFOS 2006 [27]	Bailly et al 2009 [38]	Pospelov et al 2008 [37]	Kamimura et al 2009 [77]	This Work
$(dX^-)+\alpha \to {}^6\mathrm{Li}+X^-$		Kamimura 09		QM 3-body	Kamimura 09 [77]
$(\alpha X^-)+d \to {}^6\mathrm{Li}+X^-$	simple scaling	"		QM 3-body	Kamimura 09 [77]
$(tX^-)+\alpha \to {}^7\mathrm{Li}+X^-$		"		QM 3-body	Kamimura 09 [77]
$(\alpha X^-)+t \to {}^7\mathrm{Li}+X^-$	simple scaling	"		QM 3-body	Kamimura 09 [77]
$(\alpha X^-)+{}^3\mathrm{He} \to {}^7\mathrm{Be}+X^-$	simple scaling	"		QM 3-body	Kamimura 09 [77]
$(\alpha X^-)+{}^4\mathrm{He} \to ({}^8\mathrm{Be}X^-)+\gamma$					Pospelov 07 [78]
$(\alpha X^-)+{}^6\mathrm{Li} \to ({}^{10}\mathrm{B}X^-)+\gamma$					scaling from Caughlan 88 [84]
$(\alpha X^-)+{}^7\mathrm{Li} \to ({}^{11}\mathrm{B}X^-)+\gamma$					scaling from Angulo 99 [85]
$(\alpha X^-) + {}^7\mathrm{Be} \to ({}^{11}\mathrm{C}X^-) + \gamma$					scaling from Angulo 99 [85]
$({}^6\mathrm{Li}X^-)+p \to \alpha+{}^3\mathrm{He} + X^-$	simple scaling	"		QM 3-body	Kamimura 09 [77]
$({}^6\mathrm{Li}X^-)+n \to t+\alpha+X^-$					Caughlan 88 [84]
$({}^6\mathrm{Li}X^-)+d \to {}^7\mathrm{Li}+p+X^-$					scaling Malaney 89 [86]
$({}^6\mathrm{Li}X^-)+d \to {}^7\mathrm{Be}+n+X^-$					scaling Malaney 89 [86]
$(pX^-)+{}^6\mathrm{Li} \to {}^4\mathrm{He}+{}^3\mathrm{He}+X^-$		"	estimated		Pospelov [37]
$({}^7\mathrm{Li}X^-)+p \to \alpha+\alpha+X^-$	simple scaling			QM 3-body	Kamimura 09 [77]
$(pX^-)+{}^7\mathrm{Li} \to {}^8\mathrm{Be}+X^-$		"		QM 3-body	Kamimura 09 [77]
$({}^7\mathrm{Be}X^-)+n \to {}^7\mathrm{Li}+p+X^-$					scaling from Cyburt 04 [87]
$({}^7\mathrm{Be}X^-)+p \to {}^8\mathrm{B}+X^-$		"		QM 3-body†	Kamimura 09 [77]
$(pX^-)+{}^7\mathrm{Be} \to {}^8\mathrm{B}+X^-$		"		QM 3-body	Kamimura 09 [77]
$({}^7\mathrm{Be}X^-)+d \to p+2\alpha+X^-$					Caughlan 88 [84]
$({}^8\mathrm{Be}X^-)+n \to {}^9\mathrm{Be}+X^-$			estimated	$\star$	Pospelov [37]
$({}^8\mathrm{Be}X^-)+d \to {}^{10}\mathrm{B}+X^-$					scaled from Coc 12 [88]
$({}^8\mathrm{Be}X^-)+d \to {}^6\mathrm{Li}+\alpha+X^-$					scaled from Coc 12 [88]
$({}^8\mathrm{B}X^-) \to {}^8\mathrm{Be}+X^-$					β lifetime Matt 64 [89]

† This rate is m_X-dependent.

$\star$ The reaction $({}^8\mathrm{Be}X^-) + n$ is argued in [77] to be non-resonant, which would reduce the ^{9}Be production from the levels given by this rate.

Table 3. Summaries of the treatments of bound-state nuclear rates assumed in our work and in the recent literature (II).

JCAP12(2012)037

In many cases, bound states also enhance nuclear channels through catalysis effects, which may be described as follows [24]. Consider the important example of catalyzed ^{6}Li formation,

$$(^4\mathrm{He}X^-) + d \to {}^6\mathrm{Li} + X^- \quad . \tag{3.12}$$

The corresponding ordinary process is the $^4\mathrm{He} + d \to {}^6\mathrm{Li} + \gamma$ radiative capture reaction, which is suppressed because it must proceed through the E2 mode. The bound-state rate does not require the emission of a photon and is substantially larger than the ordinary rate in the typical situation in which the $(^4\mathrm{He}X^-)$ abundance is large.

We have included rates for the formation and processing of $(^8\mathrm{Be}X^-)$ which, as we will see, can lead to substantial ^{9}Be production under optimistic nuclear physics assumptions. We also have included rates for ^{10}B and ^{11}B production via rates involving (αX^-). We find that boron production is indeed increased over the (very small) standard BBN level. However, the B/H abundance always remains many orders of magnitude below the levels seen in halo stars. Thus we find that boron is not a promising signature of decaying particle effects.

We have also studied whether reionization by the emitted XLyα photons could inhibit the net rates for the NLSP recombination reactions $A + X^- \to (AX^-) + \gamma$, as is the case in ordinary hydrogen recombination. As discussed in appendix A, we find that, whereas the optical depth for reionization by XLyα photons emitted by NLSP recombination is much smaller than that for ordinary hydrogen and helium recombination, it is still very large, so that the net rate of recombination might be very suppressed. However, as we also show in appendix A, XLyα photons Compton scatter rapidly off free electrons. This rapidly degrades the energies off resonance, so that they are ineffective for reionization. We conclude that NLSP recombination to the ground state proceeds unimpeded, unlike the case of ordinary hydrogen and helium recombination.

4 Bound-state chemical effects

We present later results from a code that treats self-consistently the bound states as separate nuclei, which then can have their own set of bound-state chemical and nuclear reactions with other species. As a warm-up exercise, we first present some results with catalysis effects turned off, and so only incorporate bound-state chemistry, i.e., recombination onto bound states. We include decays as part of the chemistry, i.e., decays remove free and bound X^-, but we turn off nonthermal decay effects. This exercise tests our code and illustrates the interplay between recombination and charge transfer.

For this purpose, we choose an initial X^- abundance $Y^{\mathrm{init}}_{X^-,\mathrm{tot}} = 10^{-2}$, which is typical for interesting supersymmetric models, and we vary the lifetime τ_X, to show the sensitivity to this parameter.

In figures 2–4, we show the abundances $Y_i \equiv n_i/n_\mathrm{B}$ for both bound and free species, as functions of the temperature T. The solid black line corresponds to the abundance of free X^-'s, whereas the other solid lines are the abundances of the bound states, as labeled by colour, and dashed lines of the same color are the corresponding free states, e.g., the solid red line represents the $(^4\mathrm{He}X^-)$ abundance, while the dashed red represents that of free ^{4}He. Figure 2 illustrates the case of a very long-lived X^-. Focusing first on the bound states (solid colored lines) we see that ^{7}Be recombines first, followed by ^{7}Li, then ^{4}He, and finally protons. These results were to be expected, given that recombination occurs at $T_{Rec} \sim B/|\ln \eta| \sim B/25$, where $B \sim Z^2$, with $\eta \equiv n_\mathrm{B}/n_\gamma$ the baryon-to-photon ratio.

Comparing the solid lines, we see that free X^- particles dominate until ^{4}He recombines, leading to the first kink in the black curve, after which most X^- are in $(^4\mathrm{He}X^-)$

JCAP12(2012)037

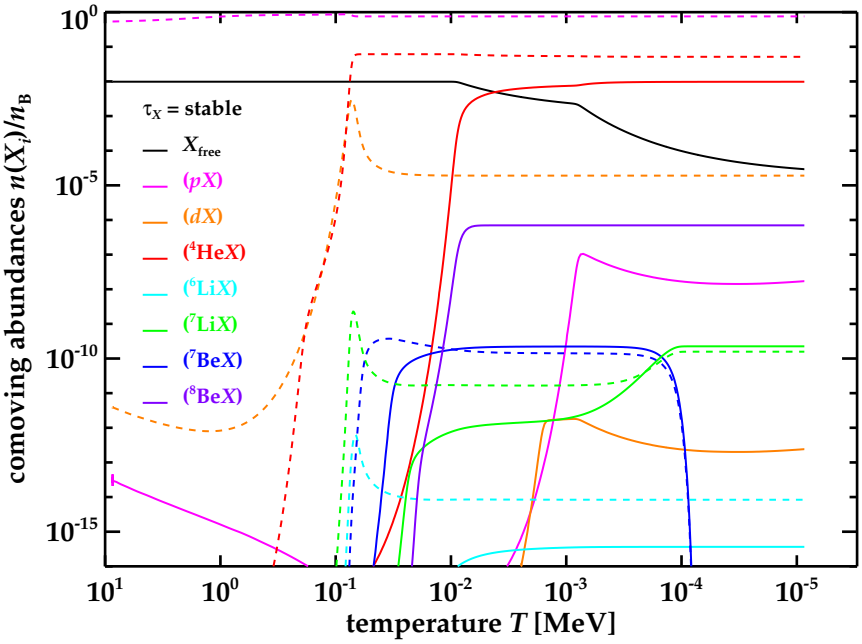

Figure 2. The abundances of free nuclei (dashed lines) and nuclear bound states (solid lines) as functions of temperature. The black line corresponding to the abundance of free X^- particles, which is assumed to be 10^{-2} initially. In this case the X lifetime τ_X is assumed to be infinite.

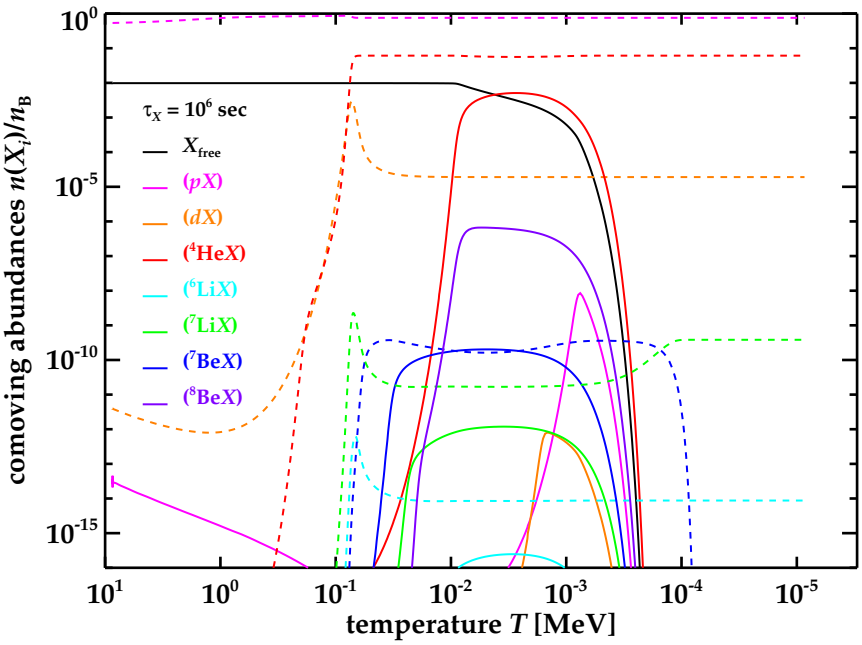

Figure 3. As in figure 2, but with an assumed lifetime $\tau_X = 10^6$ s.

JCAP12(2012)037

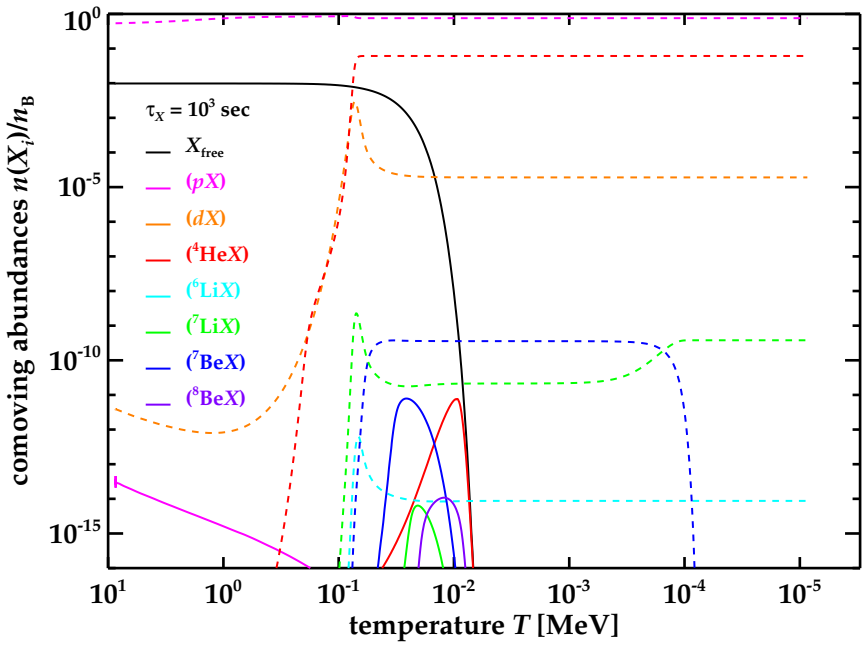

Figure 4. As in figure 2, but with an assumed lifetime $\tau_X = 10^3$ s.

bound states[2]. Subsequently the protons recombine, and this leads to the second kink in the black free X^- curve, as well as a small rise in the ^{4}He curve. This is because, immediately after the (pX^-) states recombine, the important (pX^-) + ^{4}He $\rightarrow$ p + $(^4\mathrm{He}X^-)$ charge-exchange process converts (pX^-) states into more $(^4\mathrm{He}X^-)$ bound states. The (dX^-) state actually form earlier than (pX^-) states, because the deuteron states are more tightly bound. However, deuterons are much rarer, and thus the (dX^-) abundance is always quite small, and ultimately the $(dX^-)/(pX^-)$ ratio is comparable to the ordinary D/H ratio.

Turning attention now to the $A = 7$ states (blue and green curves), we see that recombination into these nuclei occurs mostly after they are formed. The $(^7\mathrm{Be}X^-)$ state has almost the same abundance as the free ^{7}Be state, whereas the abundance of $(^7\mathrm{Li}X^-)$ is smaller than that of free ^{7}Li. At late times $T \sim 10^{-5}$ MeV, the $(^7\mathrm{Be}X^-)$ captures an electron and converts to $(^7\mathrm{Li}X^-)$, which remains bound because here Q is smaller than the difference in binding energies. Looking at the ^{6}Li abundances, we see that the bound state has a much smaller abundance than the free nucleus.

Finally, we turn to the special case of $(^8\mathrm{Be}X^-)$. Because this state has no analogue nuclide in standard BBN, there is no $^8\mathrm{Be} + X^-$ recombination, and thus $(^8\mathrm{Be}X^-)$ does not emerge when the temperature drops below its binding. Rather, production occurs via $(^4\mathrm{He}X^-) + {}^4\mathrm{He} \rightarrow (^8\mathrm{Be}X^-) + \gamma$, and thus we see that the abundances rises after that of $(^4\mathrm{He}X^-)$.

Our results are similar to those shown in [37], apart from ^{6}Li, where we have purposely removed catalysis effects for this exercise only. One difference is that we use the charge-

[2]Note that it is important for this analysis that $Y_{X^-} < Y_{^4\mathrm{He}}$, so that all X^- particles can find ^{4}He partners.

JCAP12(2012)037

exchange rates of [77], which are larger than those used in [37], and thus give a *smaller* (pX^-) abundance due to the more efficient (pX^-) conversion.

Figures 3 and 4 are for $\tau_X = 10^6$ and 10^3 s, respectively, and reveal few surprises. They are similar to the case of long-lived X until the time $t \sim \tau_X$, where $t \sim 1/T^2_{\rm MeV}$, at which stage the X particles decay away. A corollary of this exercise is that if $\tau_X < 10^3$ s, recombination cannot form bound states before the X particles decay, and hence bound-state chemical effects are negligible.

5 Decays of the NLSP in gravitino dark matter scenarios

As in [27], we base our discussion here on the CMSSM, as described in appendix B. The mass of the gravitino is a free parameter in the CMSSM, and is the LSP and constitutes the dark matter if its mass, $m_{3/2}$ is chosen to be less than $\min(m_\chi, m_{\tilde\tau})$. The abundances of the light elements provide some of the most important constraints on such a gravitino dark matter (GDM) scenario [18, 20, 21, 23, 27, 34, 36, 38, 90–93]. Their abundances also impose important constraints on neutralino LSP scenarios, since a gravitino NLSP could decay sufficiently slowly to affect them. Here, however, we restrict our attention to GDM scenarios with either a stau or neutralino NLSP, later focusing more closely on the stau NLSP case.

In the process of calculating the lifetime of the NLSP, we calculate the partial widths of the dominant relevant decay channels of the NLSP and hence the various NLSP decay branching ratios. We also calculate the resulting electromagnetic (EM) and hadronic spectra, which impact the light-element abundances. The decay products that yield EM energy obviously include directly-produced photons, and also indirectly-produced photons (e.g., via the decays of neutral pions, π^0), and charged leptons (electrons and muons) that may be produced via the secondary decays of gauge and Higgs bosons. Hadrons (nucleons and mesons such as the K^0_L, $K^\pm$ and $\pi^\pm$) are produced through quark-antiquark pairs and via the secondary decays of gauge and Higgs bosons, as well as (in the case of mesons) via the decays of τ leptons. We note that mesons other than pions decay before interacting with the hadronic background, and that the pion decays are only important for lifetimes $\lesssim 100$ sec [14, 90, 91]. We include pion decays, but these generally do not play an important role in our analysis. Thus the hadronic injections on which we focus our attention are those that produce nucleons, namely the decays via gauge and Higgs bosons and quark-antiquark pairs.

In the case of the neutralino NLSP, we include the two-body decay channels $\chi \to \widetilde{G}\, H_i$ and $\chi \to \widetilde{G}\, V$, where $H_i = h, H, A$ and $V = \gamma, Z$, and also the dominant three-body decays $\chi \to \widetilde{G}\,\gamma^* \to \widetilde{G}\, q\bar{q}$ and $\chi \to \widetilde{G}\, W^+W^-$. In the case of $\chi \to \widetilde{G}\, W^+W^-$ we have included all the contributing tree-level amplitudes, as was done in [41], thus treating correctly the longitudinal components of the W bosons. In general, the two-body channel $\chi \to \widetilde{G}\,\gamma$ dominates the χ NLSP decays and yields the bulk of the injected EM energy. When the χ is heavy enough to produce a real Z boson, the next most important channel is $\chi \to \widetilde{G}\, Z$, which is also the dominant channel for producing hadronic injections in this case. The Higgs boson channels are smaller by a few orders of magnitude, and those to heavy Higgs bosons (H, A), in particular, become kinematically accessible only for heavy χ in the large-$m_{1/2}$ region.

Turning to the three-body channels, the decay through the virtual photon to a $q\bar{q}$ pair can become comparable to the subdominant channel $\chi \to \widetilde{G}\, Z$, injecting nucleons even in the kinematical region $m_\chi < m_{3/2} + M_Z$, where direct on-shell Z-boson production is not possible. In principle, one should also include $q\bar{q}$ pair production through the virtual Z-boson channel

JCAP12(2012)037

$\chi \to \widetilde{G}\, Z^* \to \widetilde{G}\, q\overline{q}$ [19] and the corresponding interference term. However, this process is suppressed by a factor of $M_Z^4/m(\bar{q}q)^4$ with respect to $\chi \to \widetilde{G}\,\gamma^* \to \widetilde{G}\, q\overline{q}$, and the interference term is suppressed by $M_Z^2/m(\bar{q}q)^2$. Numerically, these contributions are unimportant, and we drop them in our calculation. Finally, we note that the three-body decays to W^+W^- pairs and a gravitino are usually at least five orders of magnitude smaller. Analytical results for the amplitudes for these gravitational decays of a neutralino NLSP have been presented in [41]. There, they were calculated for the inverse processes $\widetilde{G} \to \chi + X$, but the decay amplitudes are the same, and the only adjustment needed is to interchange the neutralino and gravitino mass in the phase space.

We presented in [41] our method of estimating the EM and the hadronic decays of the direct products of the χ decays using the `PYTHIA` event generator [94]. We first generate a sufficient number of spectra for the secondary decays of the gauge and Higgs bosons and the quark pairs. Then, we perform fits to obtain the relation between the energy of the decaying particle and the quantity that characterizes the hadronic spectrum, namely dN_h/dE_h, the number of produced nucleons as a function of the nucleon energy. These spectra and the fraction of the energy of the decaying particle that is injected as EM energy are then used to calculate the light-element abundances. We use the same approach here.

An analogous procedure is followed for the $\tilde{\tau}$ NLSP case. In [27], we assumed that the lighter stau was right-handed, so we ignored the stau mixing effects and the stau interactions with the $W^\pm$. However, in this analysis here we include the full effects of stau mixing. The decay rate for the dominant two-body decay channel, namely $\tilde{\tau} \to \widetilde{G}\,\tau$, was given in [92]. However, this decay channel does not yield any nucleons. Therefore, one must calculate some three-body decays of the $\tilde{\tau}$ to obtain any protons or neutrons. The most relevant channels are $\tilde{\tau} \to \widetilde{G}\,\tau^* \to \widetilde{G}\, Z\,\tau$, $\tilde{\tau} \to Z\,\tilde{\tau}^* \to \widetilde{G}\, Z\,\tau$, $\tilde{\tau} \to \tau\widetilde{\chi}_i^{0*} \to \widetilde{G}\, Z\,\tau$ and $\tilde{\tau} \to \widetilde{G}\, Z\,\tau$. In addition, so as to include the full effects of stau mixing, we included the processes $\tilde{\tau} \to \widetilde{G}\,\tau^* \to \widetilde{G}\, W^-\,\nu_\tau$, $\tilde{\tau} \to W^-\,\widetilde{\nu}_\tau^* \to \widetilde{G}\, W^-\,\nu_\tau$, $\tilde{\tau} \to \nu_\tau\widetilde{\chi}_i^{-*} \to \widetilde{G}\, W^-\,\nu_\tau$ and $\tilde{\tau} \to \widetilde{G}\, W^-\,\nu_\tau$.

Analytical results for three-body stau decays can be found in appendix C. We then use `PYTHIA` to obtain the hadronic spectra and the EM energy injected by the secondary W, Z-boson and τ-lepton decays. As in the case of the χ NLSP, this information is then used for the BBN calculation.

6 NLSP lifetimes in the CMSSM with gravitino LSP

As discussed above, we study the constraints from the cosmological light element abundances in the context of the CMSSM. The recent discovery of a new boson with mass $\sim$ 125 to 126 GeV with properties that resemble those of the Standard Model Higgs boson [95] motivates us to concentrate on regions of the CMSSM parameter space where the lightest neutral Higgs boson has a mass close to this range, taking into account the theoretical uncertainty in the calculation of its mass for any fixed values of the CMSSM parameters [96]. As discussed in [97], this mass range favours large values of A_0 and $\tan\beta$: see also [98, 99]. On the other hand, the constraint from $B_s \to \mu^+\mu^-$ [100] disfavours very large $\tan\beta$ [101, 102]. Accordingly, in this paper we discuss one example of a $(m_{1/2}, m_0)$ plane with $\tan\beta = 10$ and two examples with $\tan\beta = 40$ [97]. In many models of supersymmetry breaking, the soft trilinear supersymmetry-breaking parameter $A_0 \propto m_0$. For $\tan\beta = 10$ we consider the single value $A_0 = 2.5\, m_0$, and in the $\tan\beta = 40$ case we consider the two options $A_0 = 2\, m_0, 2.5\, m_0$. In the absence of clear indications on the gravitino mass $m_{3/2}$, in each case we consider two options: fixed $m_{3/2} = 100\,\text{GeV}$ and $m_{3/2} = 0.1 m_0$. We also consider in less detail two

JCAP12(2012)037

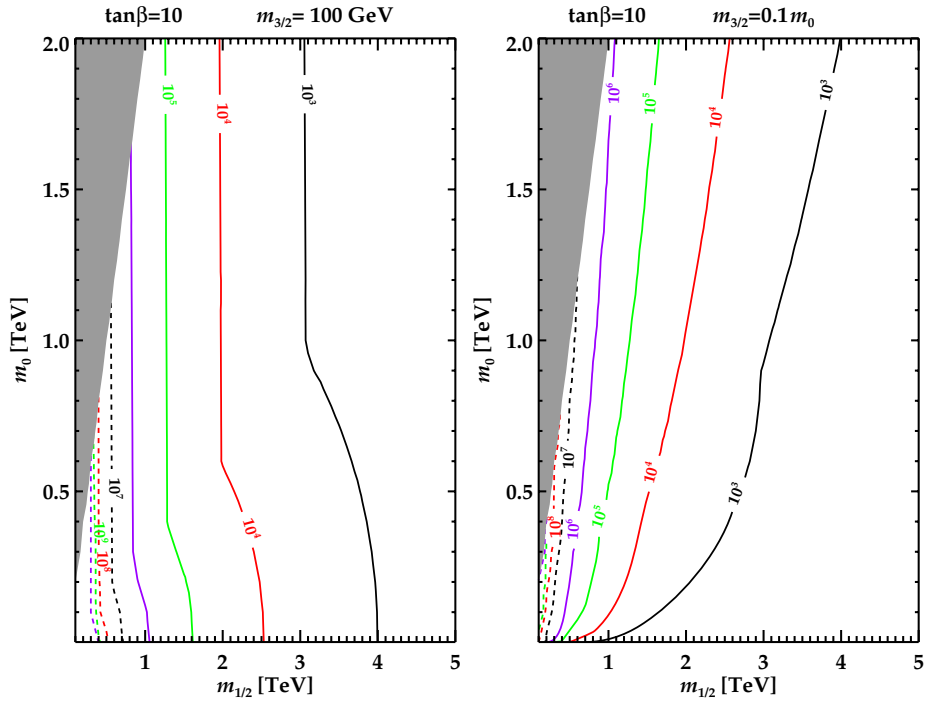

Figure 5. The NLSP lifetime $\tau_{\rm NLSP}$ in the $(m_{1/2}, m_0)$ plane for $A_0 = 2.5\, m_0$, $\tan\beta = 10$ and $m_{3/2} = 100\,$GeV (left) and $m_{3/2} = 0.1\, m_0$ (right).

examples of $(m_{1/2}, A_0)$ planes with fixed $\tan\beta = 40$ and $m_{3/2} = 100\,$GeV, namely with $m_0 = 1000, 3000\,$GeV.

An important ingredient in understanding the morphology of our results in the $(m_{1/2}, m_0)$ planes is provided by the NLSP lifetime $\tau_{\rm NLSP}$. Figure 5 displays contours of $\tau_{\rm NLSP}$ in the first cases studied above, namely the $(m_{1/2}, m_0)$ planes for $\tan\beta = 10$, $A_0 = 2.5\, m_0$ and $m_{3/2} = 100\,$GeV (left) and $m_{3/2} = 0.1\, m_0$ (right). In the upper part of the left panel, where the lightest neutralino is the NLSP, we see that the lifetime contours are essentially vertical, since they depend mainly on the relationship of m_χ (and hence $m_{1/2}$) to $m_{3/2}$. These contours appear only when the gravitino is the LSP, i.e., for $m_\chi > m_{3/2}$, and there is a vertical band at small $m_{1/2}$ where this condition is not satisfied. Also, we note that the lighter stop squark is either the NLSP or tachyonic in the grey shaded triangular regions in the small-$m_{1/2}$, large-m_0 corners of these panels. In the lower part of the left panel of figure 5 where the lighter stau is the NLSP, the contours of constant NLSP lifetime curve, track the relationship between $m_{1/2}$ and $m_{\tilde\tau_1}$. The lifetime contours in the right panel of figure 5, for $m_{3/2} = 0.1\, m_0$, are everywhere sloping up from left to right.

Figure 6 displays the corresponding contours of $\tau_{\rm NLSP}$ for the cases $\tan\beta = 40$, $A_0 = 2\, m_0$ and $m_{3/2} = 100\,$GeV (left) and $m_{3/2} = 0.1\, m_0$ (right). These exhibit similar features to the previous case, except that the stau NLSP region is now larger, as a result of the larger value of $\tan\beta$, and now we see a difference in the behaviours of the lifetime contours in the stau and neutralino NLSP regions. The vertical band at small $m_{1/2}$ where the gravitino is not the LSP is now fully visible. In this case, there is a triangular region at small $m_{1/2}$ and large m_0 where the gravitino is no longer the LSP.

JCAP12(2012)037

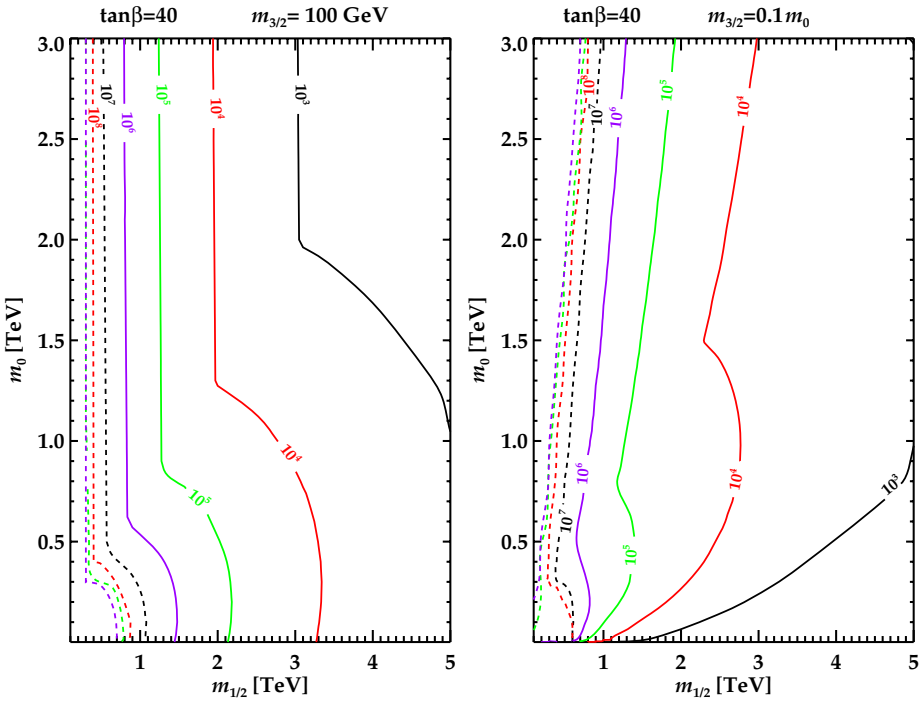

Figure 6. The NLSP lifetime in the $(m_{1/2}, m_0)$ plane for $A_0 = 2\,m_0$, $\tan\beta = 40$ and $m_{3/2} = 100\,\mathrm{GeV}$ (left) and $m_{3/2} = 0.1\,m_0$ (right).

Finally, figure 7 displays the corresponding contours of τ_{NLSP} for the cases $\tan\beta = 40$, $A_0 = 2.5\,m_0$ and $m_{3/2} = 100\,\mathrm{GeV}$ (left) and $m_{3/2} = 0.1\,m_0$ (right). This is qualitatively similar to figure 6, though we note that the stau NLSP region has expanded again, this time as a result of the larger value of A_0. Note also that the triangular region where the stop is light (or tachyonic) has reappeared at the larger value of A_0.

7 Light-element constraints in the CMSSM with a metastable Stau NLSP

We display in figure 8 the light-element abundances we calculate in the $(m_{1/2}, m_0)$ plane for the first example introduced above, namely $A_0 = 2.5\,m_0$, $\tan\beta = 10$ and $m_{3/2} = 100\,\mathrm{GeV}$. In this and subsequent figures, the stau is the NLSP in a wedge of each plane at low m_0 and large $m_{1/2}$. (The outline of this wedge can be seen in each of the preceding lifetime plots by connecting the points where the lifetime vs. $m_{1/2}$ changes from a curve to a straight line.) In most of the planes at larger m_0 the lightest neutralino is the NLSP. However, when $A_0 = 2.5m_0$, there are also wedges at large m_0 and small $m_{1/2}$, shaded grey, in which the NLSP is the lighter stop squark. Indeed for very low $m_{1/2}$, the stop mass squared is negative and hence for parameter choices inside this grey wedge the sparticle spectrum is not physical. There is only a very narrow strip along the wedge where the stop is actually the NLSP. We do not consider this case in the present work (see however [103]), discussing only the neutralino and stau NLSP cases.

7.1 Summary of light-element abundance constraints

As in subsequent similar figures, the upper left panel of figure 8 displays the D/H ratio, the upper middle panel displays the ^{3}He/D ratio, the upper right panel displays the ^{4}He

JCAP12(2012)037

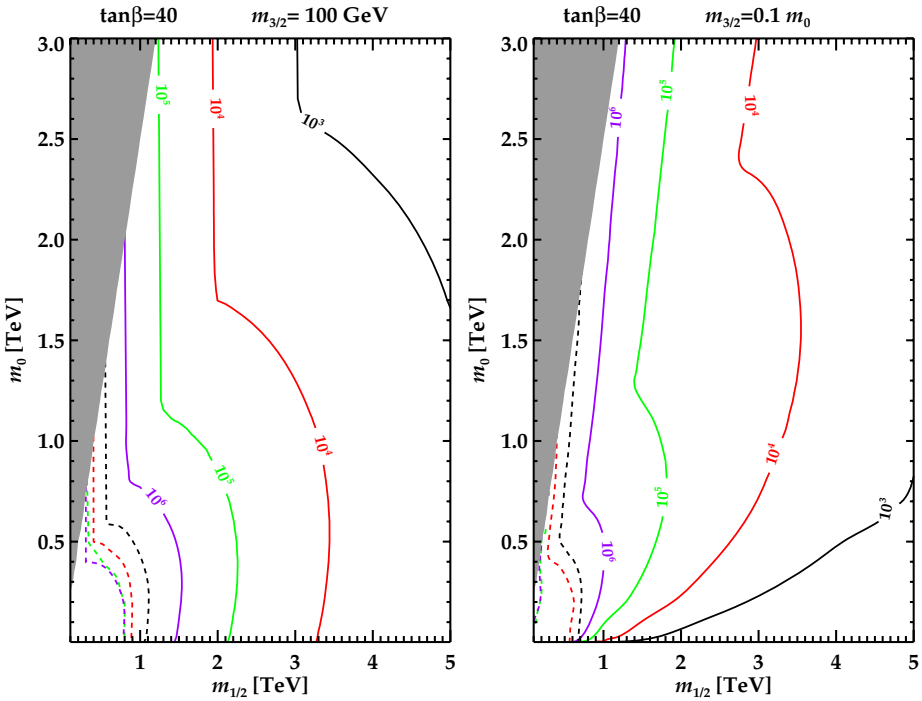

Figure 7. The NLSP lifetime in the $(m_{1/2}, m_0)$ plane for $A_0 = 2.5\,m_0$, $\tan\beta = 40$ and $m_{3/2} = 100\,\mathrm{GeV}$ (left) and $m_{3/2} = 0.1\,m_0$ (right).

abundance, the lower left panel the ^{6}Li/^{7}Li ratio, the lower middle panel the ^{7}Li/H ratio, and the lower right panel the ^{9}Be/H ratio. As a general rule, we consider the regions left unshaded to be compatible with observation, whereas the yellow regions are problematic, and the red and magenta regions are progressively more strongly excluded. Solid shadings are used for regions with excess abundances, and hashed shadings for regions with low abundances. The criteria adopted for the light-element abundances are similar to those used in our previous work, and are summarized in table 4.[3]

D/H. We assume the mean value given in [104]

$$\left(\frac{\mathrm{D}}{\mathrm{H}}\right)_p = (3.0 \pm 0.7) \times 10^{-5}\,, \tag{7.1}$$

corresponding to the deuterium abundance measured in 10 quasar absorption systems [105], and the quoted uncertainty is given by the sample variance in the data. This is considerably larger than the error in the mean, which is only 0.2. Therefore, we consider any value outside the range $(2.3-3.7)\times 10^{-5}$ as problematic, as indicated in table 4, which also includes ranges that we consider to be (strongly) excluded.

^{3}He/D. Whilst it is difficult to use ^{3}He to constrain BBN, it is possible to use the ratio ^{3}He/D [106]. Although ^{3}He may be created or destroyed in stars, D is always destroyed in the pre-main sequence of stellar evolution and, as a result, the ratio ^{3}He/D is a monotonically

[3]The values corresponding to 'strong exclusion' are somewhat arbitrary, but serve to indicate how rapidly the abundances are varying in relevant regions of parameter space.

JCAP12(2012)037

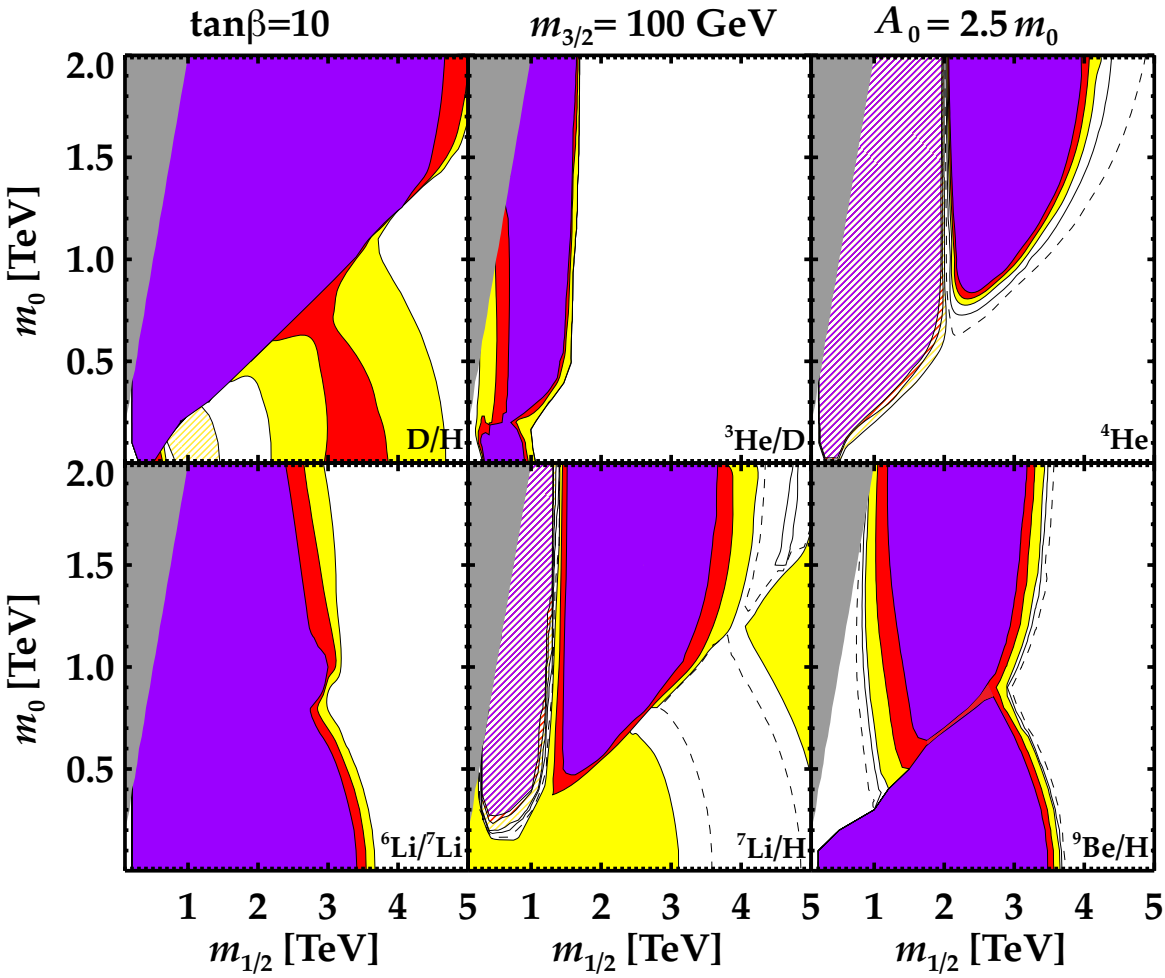

Figure 8. Light-element abundances in the $(m_{1/2}, m_0)$ plane for $A_0 = 2.5m_0$, $\tan\beta = 10$ and $m_{3/2} = 100\,\text{GeV}$.

Comparison with observation	D/H ($\times 10^{-5}$)	^{3}He/D	^{4}He	^{6}Li/^{7}Li	^{7}Li/H $\times 10^{-10}$	^{9}Be/H $\times 10^{-13}$
Strongly excluded	< 0.5	–	< 0.22	–	< 0.1	–
Excluded	< 1.0	–	< 0.23	–	< 0.2	–
Problematic	< 2.3	–	< 0.24	–	< 0.5	–
Acceptable	[2.3, 3.7]	[0.3, 1.0]	[0.24, 0.27]	< 0.05	[0.5, 2.75]	< 0.3
Problematic	> 3.7	> 1.0	> 0.27	> 0.05	> 2.75	> 0.3
Excluded	> 5.0	> 3.0	> 0.28	> 0.1	> 10	> 1.0
Strongly excluded	> 10	> 5.0	> 0.29	> 0.2	> 30	> 3.0

Table 4. The ranges of light-element abundances whose comparisons with observation we consider in this work to be acceptable, problematic and (strongly) excluded, as shown in the unshaded/yellow/red/magenta regions in the figures.

JCAP12(2012)037

increasing function of time. Thus one can use the solar ratio of about 1 [107] to constrain the BBN ratio. Because ^{3}He can be produced and/or D can be destroyed, we do not assume a lower bound to the ratio.

^{4}He. Although the determination of the ^{4}He abundance in extragalactic HII regions is dominated by systematic uncertainties [108], using the Markov Chain-Monte Carlo methods described in [109] and data compiled in [110], one finds [111]

$$Y_p = 0.2534 \pm 0.0083 \tag{7.2}$$

based on a regression of Y vs. O/H and

$$\langle Y \rangle = 0.2574 \pm 0.0036 \tag{7.3}$$

based on a weighted mean. As we will see, once the standard BBN value of Y_p is affected by NLSP decays, it varies very rapidly and it suffices to consider values outside the range [0.24, 0.27] to be problematic.

^{6}Li/^{7}Li. Some observations of Li absorption lines in halo dwarf stars have claimed evidence for a relatively large ratio of ^{6}Li/^{7}Li $\simeq 0.05$ [112] over a broad range of metallicities, though it remains possible that these observations are also dominated by systematic uncertainties [113]. There are a few reliable observations of stars with a similar ratio of ^{6}Li/^{7}Li in a very narrow range of metallicity [66] consistent with galactic cosmic-ray nucleosynthesis [114]. However, no observations indicate a ratio greater than 0.05 which we set as our lower boundary of the problematic range.

^{7}Li/H. The cosmological ^{7}Li problem [53] is now well established. There are many observations of ^{7}Li in halo dwarf stars [64, 65] that indicate a far lower ^{7}Li/H abundance than predicted in standard BBN. We adopt the range found in the plateau of Lithium versus metallicity [115], namely

$$\left(\frac{^7\mathrm{Li}}{\mathrm{H}}\right)_{\mathrm{halo}*} = (1.23^{+0.34}_{-0.16}) \times 10^{-10}, \tag{7.4}$$

although the lithium abundance observed in globular cluster stars may be a factor ~ 2 higher [116]. In addition, one should bear in mind that the thin plateau in ^{7}Li/H vs Fe/H seems to drop off and develop a large dispersion at [Fe/H] < -3 [65]. This seems to suggest some lithium destruction has taken place in these metal-poor stars; why the dispersion is not seen at higher metallicities remains unclear.

Although the preferred range in (7.4) is rather narrow, we deem that any reduction from the BBN value of[4] ^{7}Li/H $= (5.07^{+0.71}_{-0.62}) \times 10^{-10}$ [53] to $< 2.75 \times 10^{-10}$ represents a significant improvement in the ^{7}Li problem, and we take this to be the lower bound of our problematic region. NLSP decays can also destroy too much ^{7}Li and we will consider any value below 0.5×10^{-10} as similarly problematic.

[4]This corresponds to the BBN value at a baryon-to-photon ratio of $\eta = 6.16 \times 10^{-10}$ [51]. A similar value of $(5.24 \pm 0.5) \times 10^{-10}$ was found in another recent analysis [88].

JCAP12(2012)037

^{9}Be/H. Finally, ^{9}Be is also observed in halo dwarf stars, and is found to vary strongly with metallicity, as seen in a recent set of observations [117]. These observations extend down to [O/H] of about -2.5 with a ^{9}Be/H abundance of 3×10^{-14}. Though there is a single observation [118] of ^{9}Be with an abundance about 3 times lower, conservatively we will consider problematic any 'primordial' abundance in excess of the highest value seen at the lowest metallicity.

In the cases of ^{3}He/D, ^{6}Li/^{7}Li and ^{9}Be/H, there are no observational lower limits, so we do not quote ranges of abundances that we consider too low. Within the unshaded regions, we also display extra contours for the ^{4}He abundance = 0.25 and 0.26 (dashed and solid lines, respectively), for ^{7}Li/H $= 0.91, 1.91 \times 10^{-10}$ (dashed and solid) and ^{9}Be/H $= 1, 2 \times 10^{-14}$ (dashed and solid). In the case of ^{7}Li/H, as already discussed, it is well known that standard BBN gives a ratio significantly higher than that indicated by observations. Therefore, large parts of the regions coloured yellow in the ^{7}Li panels yield an abundance that is no worse than in standard cosmology, and may even be in somewhat better agreement with observation. Depending how seriously one takes the cosmological ^{7}Li problem, the favoured (unshaded) regions in subsequent plots could be expanded. In general, we see discontinuities in the colouring along a rising diagonal line: above it, the lightest neutralino is the NLSP, and below it the lighter stau is the NLSP, which is the case of main interest here.

We recall from previous analyses that hadronic processes are mostly relevant for lifetimes $\lesssim 10^4$ s, whereas electromagnetic processes are generally dominant for longer lifetimes, i.e., at smaller $m_{1/2}$ for any fixed value of m_0. We also note that, for any fixed $m_{1/2}$, the abundance of metastable relic particles (before decay) is generally largest at large m_0. We therefore expect hadronic processes to be most important when both $m_{1/2}$ and m_0 are large. Indeed, in the upper right parts of the ^{4}He panels in figure 8 and later figures we see triangular regions where the ^{4}He abundance is enhanced unacceptably by hadroproduction. This is generally accompanied by hadronic depletion of the ^{3}He/D ratio and enhancements in D/H, ^{6}Li/^{7}Li, ^{7}Li/H and ^{9}Be/H. On the other hand, staying at large m_0, the dominant electromagnetic processes at smaller $m_{1/2}$ include photodestruction of ^{4}He and ^{7}Li, accompanied by photoproduction of ^{3}He/D and D/H.

7.2 Application to the CMSSM with a metastable Stau NLSP

We see in the upper panels of figure 8 that for $A_0 = 2.5\, m_0$, $\tan\beta = 10$ and $m_{3/2} = 100\,$GeV the D/H ratio is acceptable in arcs with $m_{1/2} \sim 2\,$TeV and $> 4\,$TeV, whereas the ^{3}He/D ratio is generally acceptable for $m_{1/2} > 1.6\,$TeV and the ^{4}He abundance is acceptable throughout the stau NLSP wedge of the $(m_{1/2}, m_0)$ plane (This demarkation is displayed in the summary plot below). In the lower panels of figure 8 we see that the ^{6}Li/^{7}Li ratio is unacceptable for $m_{1/2} < 3\,$TeV, that the ^{7}Li/H ratio is acceptable in an arc with $m_{1/2} > 2.5\,$TeV, as well as in the neutralino NLSP region with $m_{1/2} > 4\,$TeV at large m_0. The ^{9}Be/H ratio favours either $m_{1/2} > 3\,$TeV or a triangular region with a neutralino NLSP with $m_{1/2} \lesssim 1\,$TeV. The overall conclusion is that all the light-element abundances are acceptable in a narrow arc starting on the stau/neutralino NLSP boundary where $(m_{1/2}, m_0) \sim (4.0, 1.1)\,$TeV and extending to larger $m_{1/2}$ at lower m_0.[5] Note that there is excessive photo-destruction of both ^{4}He and ^{7}Li in the low mass neutralino NLSP region. While there is a narrow strip along $m_{1/2} \approx 1.4\,$TeV

[5] We note in passing that there is no region of the neutralino NLSP wedge where all the light-element abundances are acceptable.

JCAP12(2012)037

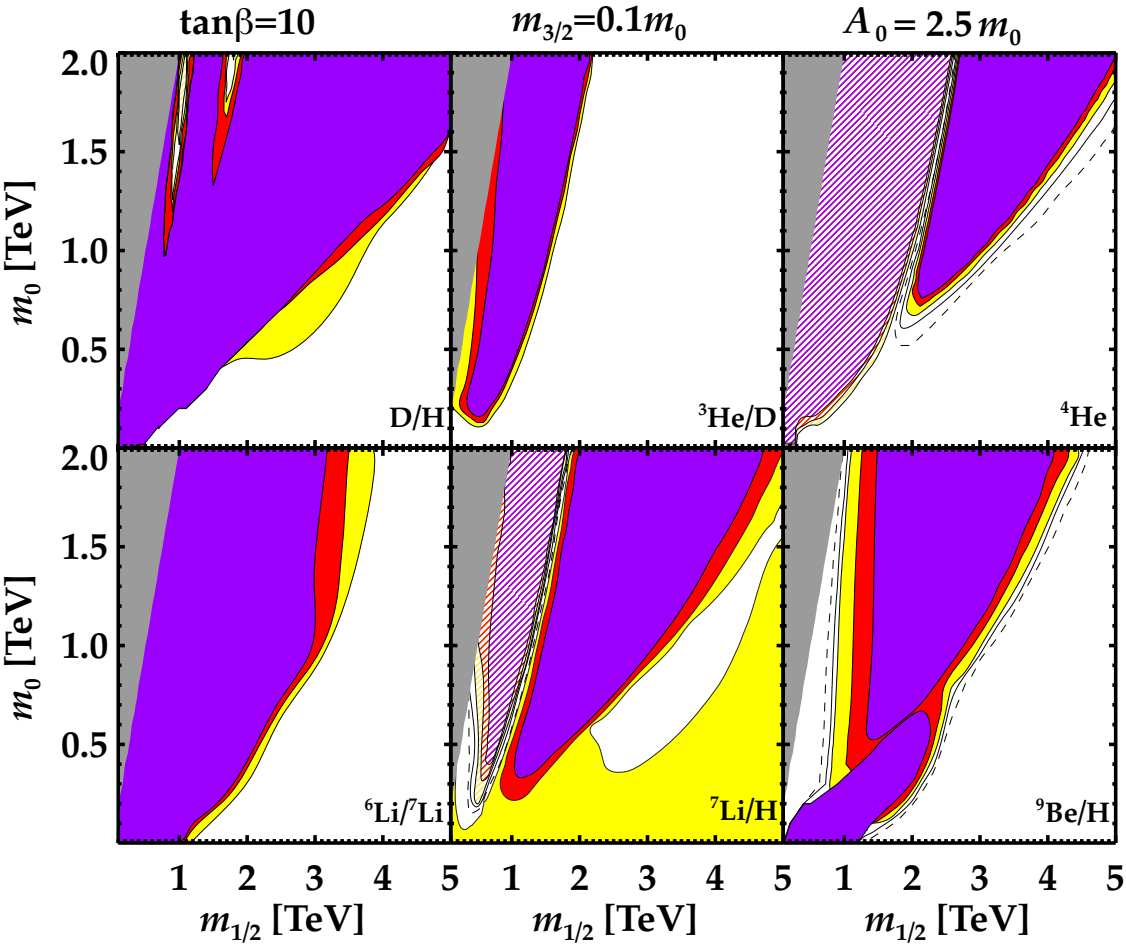

Figure 9. Light-element abundances in the $(m_{1/2}, m_0)$ plane for $A_0 = 2.5\,m_0$, $\tan\beta = 10$ and $m_{3/2} = 0.1\,m_0$.

where ^{7}Li is just right, this strip is excluded by many of the other light elements. This behaviour is also seen in the subsequent parameter choices.

Figure 9 displays a similar analysis for the same CMSSM parameters $A_0 = 2.5\,m_0$, $\tan\beta = 10$, but with $m_{3/2} = 0.1\,m_0$. In this case, we see that the light-element abundances are all acceptable in a narrow arc through the stau NLSP region between $(m_{1/2}, m_0) \sim (2.3, 0.4)$ TeV and $\sim (4.8, 1.5)$ TeV, that is defined essentially by the D/H and ^{7}Li/H constraints.[6]

Figure 10 summarizes our results for the CMSSM $(m_{1/2}, m_0)$ planes for $A_0 = 2.5m_0$, $\tan\beta = 10$, with $m_{3/2} = 100$ GeV (left) and $m_{3/2} = 0.1\,m_0$ (right). Here and in subsequent similar figures, the magenta regions are strongly excluded by one or more constraints, the red regions are excluded by one or more constraints, and the yellow regions are problematic for at least one constraint. We see explicitly the unshaded narrow arcs where all the constraints are satisfied. These are the regions where the cosmological ^{7}Li problem is solved in the presence of metastable stau NLSPs: they are all below the grey line that marks the boundary between the neutralino and stau NLSP wedges.

[6] Again, there is no acceptable region where the neutralino is the NLSP.

JCAP12(2012)037

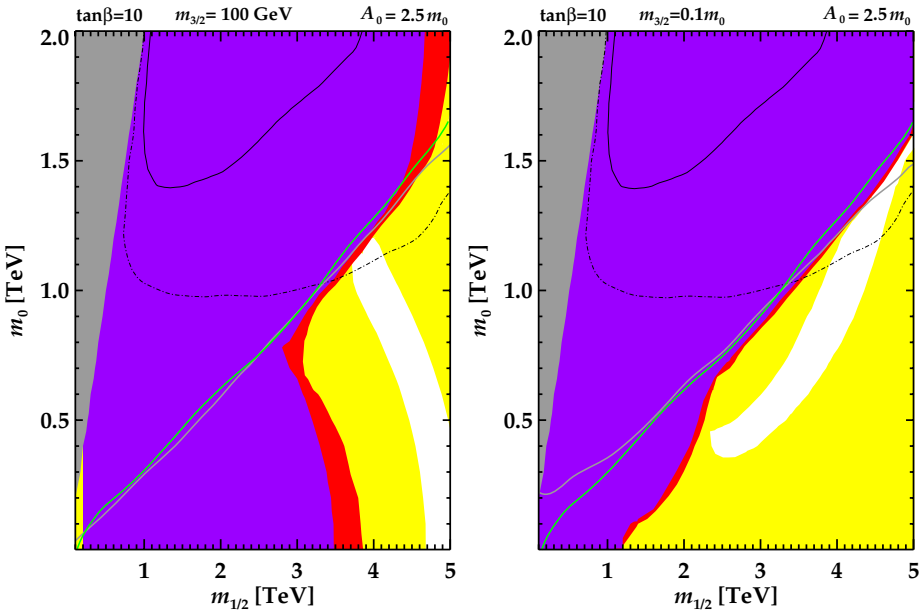

Figure 10. Summary of the light-element-abundance constraints in the $(m_{1/2}, m_0)$ plane for $A_0 = 2.5\,m_0$, $\tan\beta = 10$ and $m_{3/2} = 100\,\text{GeV}$ (left) and $m_{3/2} = 0.1\,m_0$ (right).

Also shown is a green line, above which the gravitinos arising from NLSP decays have a density greater than the range allowed by WMAP and other observations [51]. This line corresponds to the gravitino relic abundance determined from NLSP decays

$$\Omega_{3/2}h^2 = \Omega_{\text{NLSP}}h^2 \left(\frac{m_{3/2}}{m_{\text{NLSP}}}\right) , \tag{7.5}$$

where Ω_{NLSP} is the thermal relic density of NLSPs left over after annihilations. We note that there may be other sources of gravitinos such as reheating after inflation which would further strengthen this bound. This constraint excludes almost completely the neutralino NLSP regions in figure 10 and the subsequent analogous figures, but does not impact the white regions compatible with all the light-element constraints. Also shown in this and subsequent summary figures are some contours of calculated values of $M_h = 124\,\text{GeV}$ (dash-dotted), 125 GeV (solid), 126 GeV (dotted) and 127 GeV (dashed). The present experimental and theoretical uncertainties are such that no calculated value of $M_h \in [124, 127]\,\text{GeV}$ can currently be excluded, and an even larger range may be permitted at large $m_{1/2}$, where the `FeynHiggs` code [96] warns of theoretical uncertainties considerably exceeding 1.5 GeV.

Looking back at the contours of constant τ_{NLSP} in described arcs in figure 5, we see that in the stau NLSP segment of the $(m_{1/2}, m_0)$ plane they parallel the contours in the corresponding regions of the $(m_{1/2}, m_0)$ planes in figures 8 and 9 for the different light-element abundances. This confirms the important influence of τ_{NLSP}. Comparing with the summary of this case displayed in the left panel of figure 10, we see that in this case the optimal lifetime for solving the cosmological Lithium problem is $\tau_{\text{NLSP}} \sim \text{few} \times 10^2$ s. In the case when $m_{3/2} = 0.1\,m_0$ (right panel of figure 5), we see that in the stau NLSP segment the contours of constant τ_{NLSP} parallel those of constant $^6\text{Li}/^7\text{Li}$ and $^9\text{Be/H}$ ratios, though the shapes of the D/H and $^7\text{Li/H}$ contours are quite different. Looking at the right panel of

JCAP12(2012)037

figure 10, we see that in this case the optimal lifetime for solving the cosmological Lithium problem is $\tau_{\rm NLSP} \sim$ few $\times\, 10^3$ s.

Though we do not show the results here, we have studied other choices for the gravitino mass for the values of $\tan\beta = 10$ and $A_0 = 2.5\, m_0$. For example, for a larger fixed gravitino mass of 500 GeV, one must consider larger $m_{1/2} \gtrsim 1$ TeV to ensure a gravitino LSP. For a given gaugino mass, the NLSP lifetime is longer. As a result, the acceptable arc of D/H moves to larger $m_{1/2}$. More importantly, the ^{6}Li constraint would now exclude all values of $m_{1/2}$ between 1 and 5 TeV. The ^{9}Be constraint similarly would exclude the entire stau NLSP region displayed. Had we chosen instead $m_{3/2} = m_0$, a gravitino LSP would be present only in the lower right half of the plane. Once again lifetimes would typically be longer, affecting the light element abundances. In this case, only a small corner of the parameter space at very large $m_{1/2}$ and very small m_0 would survive all constraints.

We now describe an analogous analysis for the CMSSM $(m_{1/2}, m_0)$ planes for $A_0 = 2\, m_0$, $\tan\beta = 40$. Figure 11 displays our results for the option $m_{3/2} = 100$ GeV. In this case, the D/H constraint would allow most of the lower half of the parameter plane. This regions would be allowed by both the ^{3}He/D (except for a small area with low $m_{1/2}$ and m_0) and ^{4}He constraints, but much of it is excluded by the ^{6}Li/^{7}Li ratio, and more strongly excluded by the ^{9}Be/H ratio. Improvement in the ^{7}Li/H ratio only occurs around an arc starting at $(m_{1/2}, m_0) = (3.2, 2)$ TeV. This arc is for the most part allowed by the other constraints.

Figure 12 displays the results of a similar analysis for $m_{3/2} = 0.1\, m_0$, but with the same values of the CMSSM parameters. Once again, the neutralino NLSP region is excluded by the D/H ratio, which is also problematic for a large area with $m_0 > 1$ TeV. The ^{3}He/D and ^{4}He constraints are qualitatively similar to the previous case. However, the effect of the ^{6}Li/^{7}Li constraint is somewhat different: it excludes a bulbous region of the stau NLSP segment extending almost to $m_{1/2} \sim 5$ TeV as does the ^{9}Be constraint. In this case, the arc allowed by the ^{7}Li/H ratio is wider and has shifted to larger masses. As a result, the only region that has a chance of being compatible with all the light-element constraints has $m_{1/2} \sim 5$ TeV and $m_0 \sim 1$ TeV.

The results in the $(m_{1/2}, m_0)$ planes for $A_0 = 2\, m_0$ and $\tan\beta = 40$ are summarized in figure 13. In the case of $m_{3/2} = 100$ GeV (left panel) we see an allowed arc across the stau NLSP region extending from $(m_{1/2}, m_0) \sim (3.2, 2)$ TeV to $\sim (5, 1.5)$ TeV. In the case of $m_{3/2} = 0.1\, m_0$ (right panel), there is only a very small region of marginal consistency close to $(m_{1/2}, m_0) \sim (5, 1)$ TeV. In the stau NLSP region the contours of the light-element constraints displayed in figures 11 and 12 (except for the D/H ratio in the latter case) again parallel the contours of constant $\tau_{\rm NLSP}$ in figure 6, and we see in figure 13 that the preferred ranges of $\tau_{\rm NLSP}$ are somewhat below and above 10^3 s, respectively.

For the same choice of $\tan\beta = 40$ and $A_0 = 2.0 m_0$, had we taken $m_{3/2} = 500$ GeV we would have found that, due to the increased lifetimes, virtually the entire parameter plane with a gravitino LSP would be strongly excluded by the ^{6}Li/^{7}Li ratio. The ^{9}Be constraint also would strongly exclude the stau NLSP region shown. For $m_{3/2} = m_0$, we would once again be forced into a tiny area in the lower right corner of the $(m_{1/2}, m_0)$ plane.

Turning now to the case $A_0 = 2.5\, m_0$, $\tan\beta = 40$ and $m_{3/2} = 100$ GeV shown in figure 14, we note in particular that there is virtually no improvement over standard BBN in the ^{7}Li/H abundance throughout almost all the stau NLSP region. Only a small region close to the stau-neutralino NLSP boundary extending to higher masses from $m_{1/2} \sim 3$ TeV is consistent with this constraint. The ^{6}Li/^{7}Li and ^{9}Be constraints once again dominate in the stau NLSP region.

JCAP12(2012)037

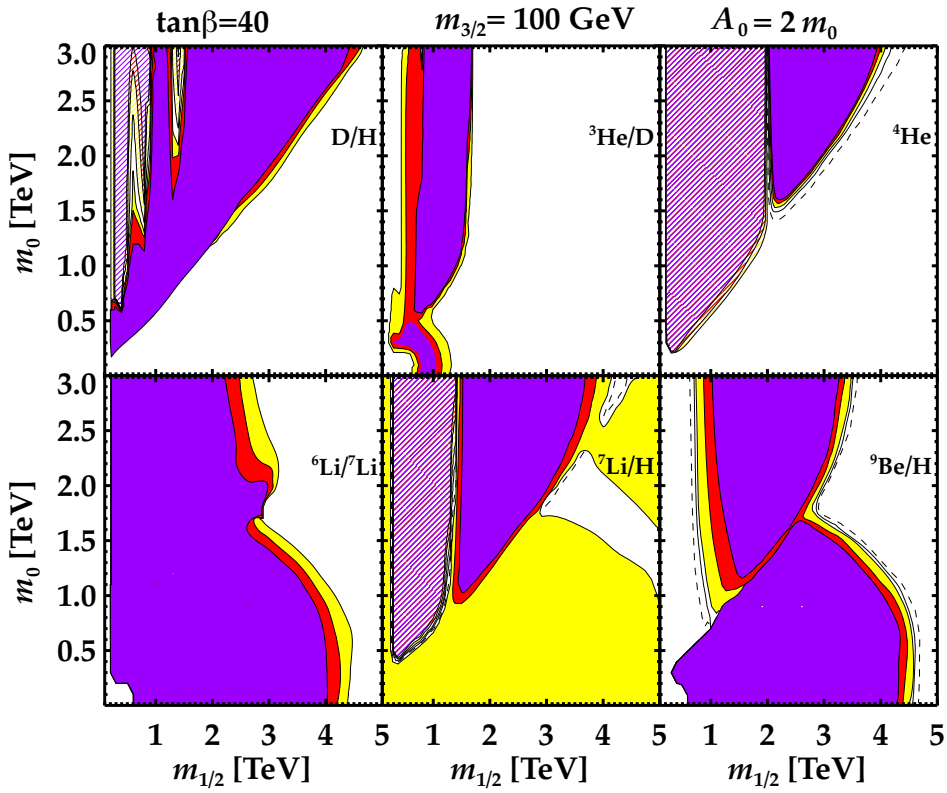

Figure 11. Light-element abundances in the $(m_{1/2}, m_0)$ plane for $A_0 = 2\,m_0$, $\tan\beta = 40$ and $m_{3/2} = 100\,\mathrm{GeV}$.

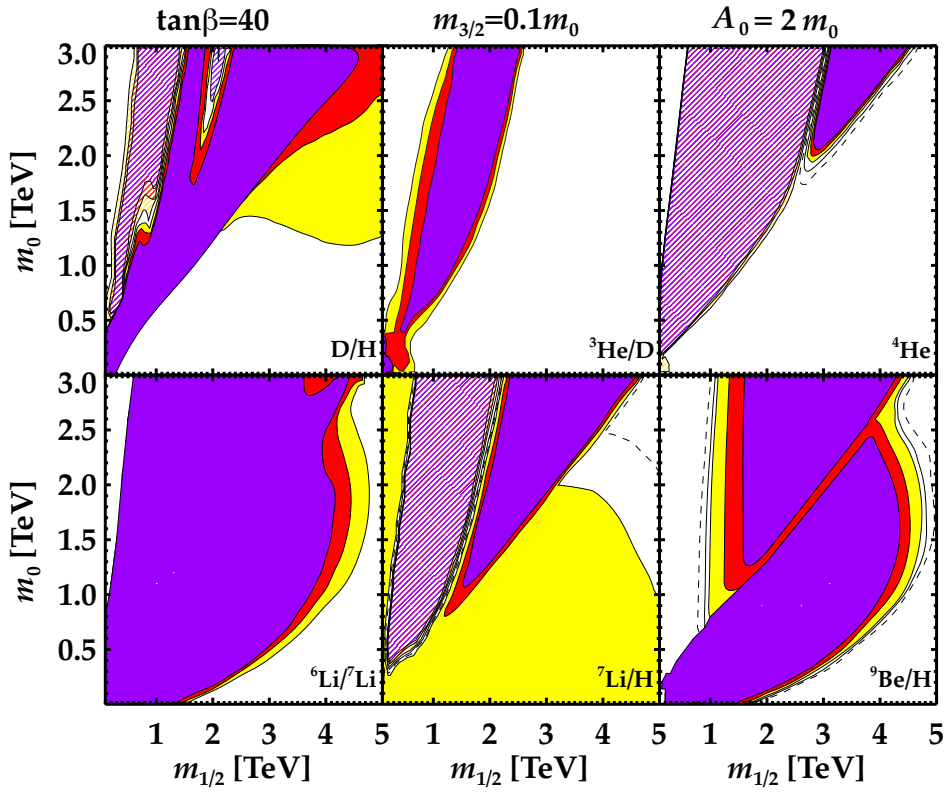

Figure 12. Light-element abundances in the $(m_{1/2}, m_0)$ plane for $A_0 = 2\,m_0$, $\tan\beta = 40$ and $m_{3/2} = 0.1\,m_0$.

JCAP12(2012)037

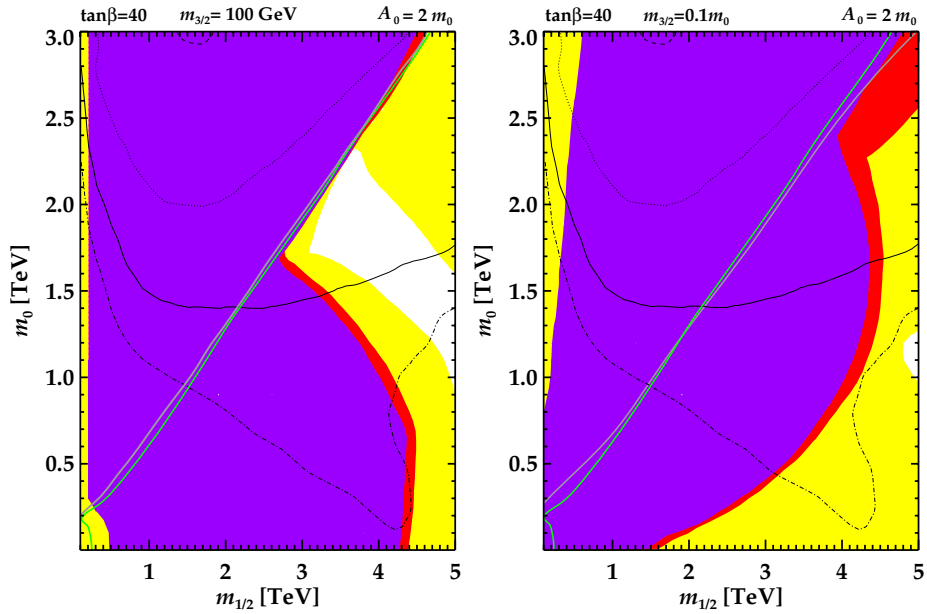

Figure 13. Summary of the light-element-abundance constraints in the $(m_{1/2}, m_0)$ plane for $A_0 = 2\,m_0$, $\tan\beta = 40$ and $m_{3/2} = 100\,\mathrm{GeV}$ (left) and $m_{3/2} = 0.1\,m_0$ (right).

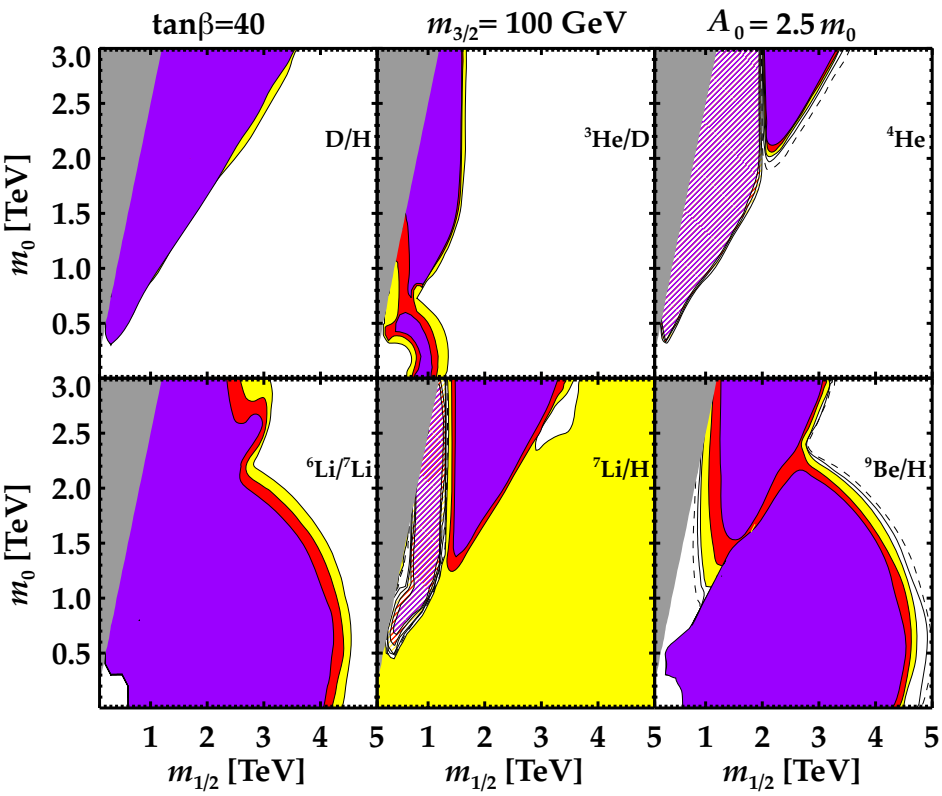

Figure 14. Light-element abundances in the $(m_{1/2}, m_0)$ plane for $A_0 = 2.5\,m_0$, $\tan\beta = 40$ and $m_{3/2} = 100\,\mathrm{GeV}$.

JCAP12(2012)037

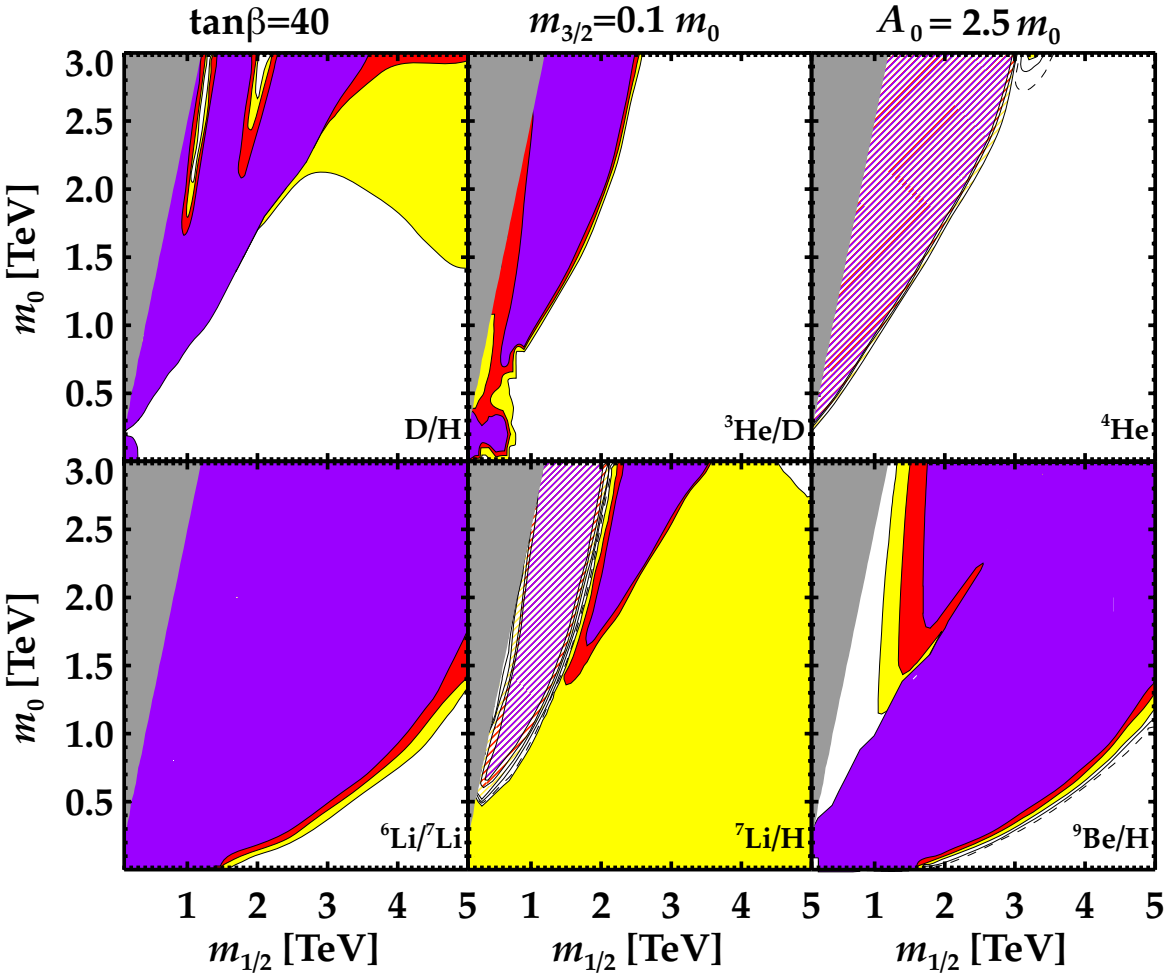

Figure 15. Light-element abundances in the $(m_{1/2}, m_0)$ plane for $A_0 = 2.5\,m_0$, $\tan\beta = 40$ and $m_{3/2} = 0.1\,m_0$.

Even this small region of consistency is eradicated in the case $A_0 = 2.5\,m_0$, $\tan\beta = 40$ and $m_{3/2} = 0.1\,m_0$ shown in figure 15. Now, the improvement in ^{7}Li/H is limited to a small region at very large masses $(m_{1/2}, m_0) \sim (5, 3)$ TeV, and this corner of parameter space is excluded by both the ^{6}Li/^{7}Li and ^{9}Be/H ratios.

These results are summarized in figure 16. We see in the left panel for $m_{3/2} = 100$ GeV that only a very small region with $(m_{1/2}, m_0) \sim (3.5, 2.8)$ TeV is compatible with all the constraints, whereas we see no allowed region in the right panel for $m_{3/2} = 0.1\,m_0$. Comparing the lifetime contours in figure 7 with figures 14, 15 and 16, we again see that the preferred ranges of $\tau_{\rm NLSP}$ are $\sim 10^3$ s. Choosing the gravitino masses $m_{3/2} = 500$ GeV or $= m_0$ would leave us with results very similar to those described for $A_0 = 2m_0$.

The results shown above have been for slices through the CMSSM parameter space corresponding to $(m_{1/2}, m_0)$ planes for fixed $\tan\beta$ and A_0. We have also explored how the results for $\tan\beta = 40$ vary as functions of A_0 for a couple of values of $m_0 = 1000, 3000$ GeV, with the results summarized in figure 17. The left panel is for $m_0 = 1000$ GeV, which is typical of the range of m_0 in the unshaded regions in the cases studied above. We see that

JCAP12(2012)037

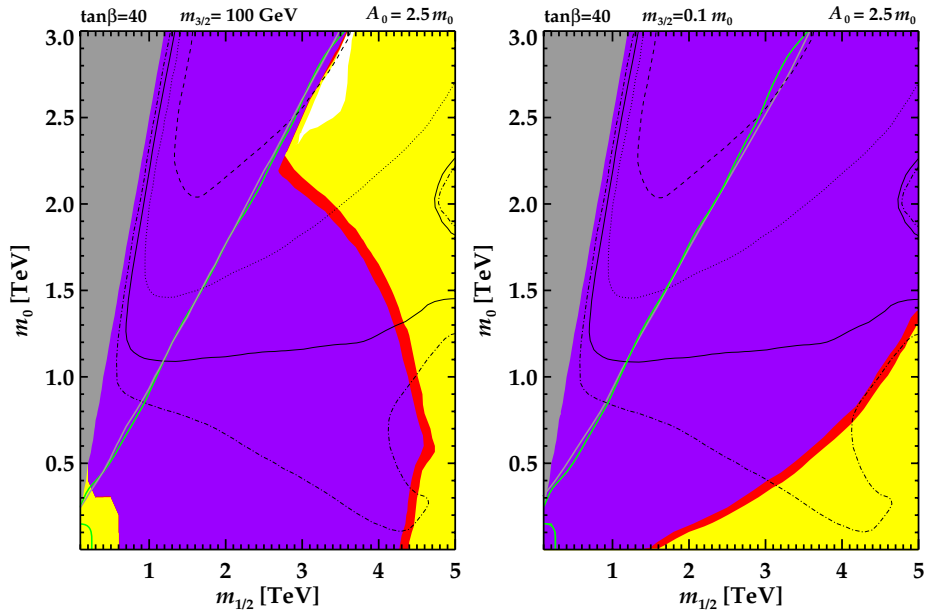

Figure 16. Summary of the light-element-abundance constraints in the $(m_{1/2}, m_0)$ plane for $A_0 = 2.5\,m_0$, $\tan\beta = 40$ and $m_{3/2} = 100\,\mathrm{GeV}$ (left) and $m_{3/2} = 0.1\,m_0$ (right).

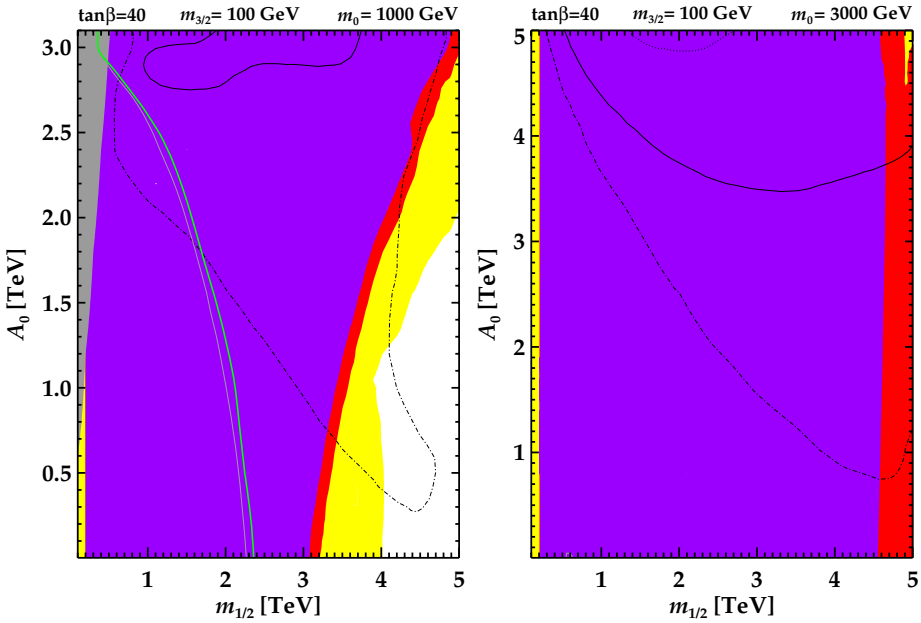

Figure 17. Summary of the light-element-abundance constraints in the $(m_{1/2}, A_0)$ plane for $\tan\beta = 40$ and $m_{3/2} = 100\,\mathrm{GeV}$ with $m_0 = 1000\,\mathrm{GeV}$ (left) and $m_0 = 3000\,\mathrm{GeV}$ (right).

a large region with $m_{1/2} > 4\,\mathrm{TeV}$ and $A_0 < 2\,\mathrm{TeV}$ is unshaded and hence ^{7}Li-compatible. On the other hand, we see no unshaded region in the right panel for $m_0 = 3000\,\mathrm{GeV}$, which is less typical of the values of m_0 found in the unshaded regions of previous summary plots. Therefore, we expect that the features found earlier are quite generic.

JCAP12(2012)037

Also shown in figures 10, 13, 16 and 17 are some representative contours of the lightest MSSM Higgs boson M_h, as calculated using the `FeynHiggs` code [96]. This code is generally thought to have an uncertainty $\sim 1.5\,\mathrm{GeV}$ for generic sets of CMSSM parameters, but warns of larger uncertainties at the large values of $m_{1/2}$ of interest here.[7] Accordingly, we consider calculated values of $M_h \in [124, 127]\,\mathrm{GeV}$ to be compatible with the observed range of 125 to 126 GeV [95], and an even larger range of calculated values of M_h may be acceptable at large $m_{1/2}$. In the cases displayed in figure 10, we see that the ends of the BBN-compatible arcs with higher m_0 have $M_h \sim 124\,\mathrm{GeV}$, i.e., within the acceptable range, and hence may be preferred. In figures 13 we see that the preferred arc for $m_{3/2} = 100\,\mathrm{GeV}$ corresponds to $M_h \sim 124$ to 126 GeV, all within the range suggested by the LHC, whereas in the case $m_{3/2} = 0.1\,m_0$ the BBN-compatible region has $M_h \sim 124\,\mathrm{GeV}$. In figure 16 we see that the small BBN-compatible region for $m_{3/2} = 100\,\mathrm{GeV}$ corresponds to a nominal value of $M_h \sim 127\,\mathrm{GeV}$, at the upper end of the LHC-compatible range. Finally, in figure 17 we see that the unshaded region in the left panel corresponds generally to $M_h \sim 124\,\mathrm{GeV}$, which is compatible within theoretical uncertainties with the LHC discovery.

7.3 Bound-state effects and uncertainties

We conclude this section with a brief discussion of the importance of bound-state effects and their uncertainties.

Figure 18 shows how our results in the $(m_{1/2}, m_0)$ plane for $A_0 = 2\,m_0$, $\tan\beta = 40$ and $m_{3/2} = 100\,\mathrm{GeV}$ would change if all bound-state effects were to be switched off, but with decay effects retained. Comparing with figure 11, we see that the D/H, ^{3}He/D and ^{7}Li/H ratios are unaffected, as is the ^{4}He abundance. However, there are major changes in the ^{6}Li/^{7}Li ratio and ^{9}Be abundance. In particular, arcs at small $m_{1/2}$ and m_0 that would have been permitted (modulo the lack of improvement in the ^{7}Li/H abundance) in the absence of bound-state effects are robustly excluded by both the ^{6}Li/^{7}Li and ^{9}Be/H ratios once bound-state effects are included. On the other hand, the allowed arc at larger $m_{1/2}$ and m_0 is quite unaffected by bound-state effects, as seen by comparing the left panel of figure 19 with the left panel of figure 13. Even more dramatically, we see that the stau NLSP region excluded by ^{9}Be was entirely due to bound state effects.

The constraints from the ^{6}Li/^{7}Li ratio rely on the observed ^{6}Li abundances. The difficulties in measuring ^{6}Li and inferring its abundance thus propagate into uncertainties in the ^{6}Li/^{7}Li constraints. As noted in § 7.1, isotopic lithium measurements in halo stars are very challenging, with only a few stars showing unambiguous detections. Moreover, if the stars have burned some lithium, then the observed isotopic ratio could be different from (lower than) the initial ratio in the star. But at least for the two best determinations, we are unaware of claims of ^{6}Li depletion. Furthermore, it is known that the measured ^{6}Li/H must also include a component produced by Galactic (and possibly pre-Galactic) cosmic rays [125]; our neglect of any such production strengthens our upper limit. In any case, the rapid rise of the ^{6}Li/^{7}Li contours indicates that our ^{6}Li constraint is insensitive to details of the adopted abundances. We find, for example, that when all the acceptable, problematic and (strongly) excluded ranges for ^{6}Li/^{7}Li are increased by a factor of 2 (as perhaps could occur in the case of stellar depletion) the ^{6}Li contours relax by about 200 GeV.

As discussed in section 2, bound-state ^{9}Be production hinges on two principal uncertainties in our bound-state analysis. One of these uncertainties is the (^{8}BeX) binding energy,

[7] This may be linked with the irregular behaviours of some calculated contours of M_h in figures 13, 16 and 17.

JCAP12(2012)037

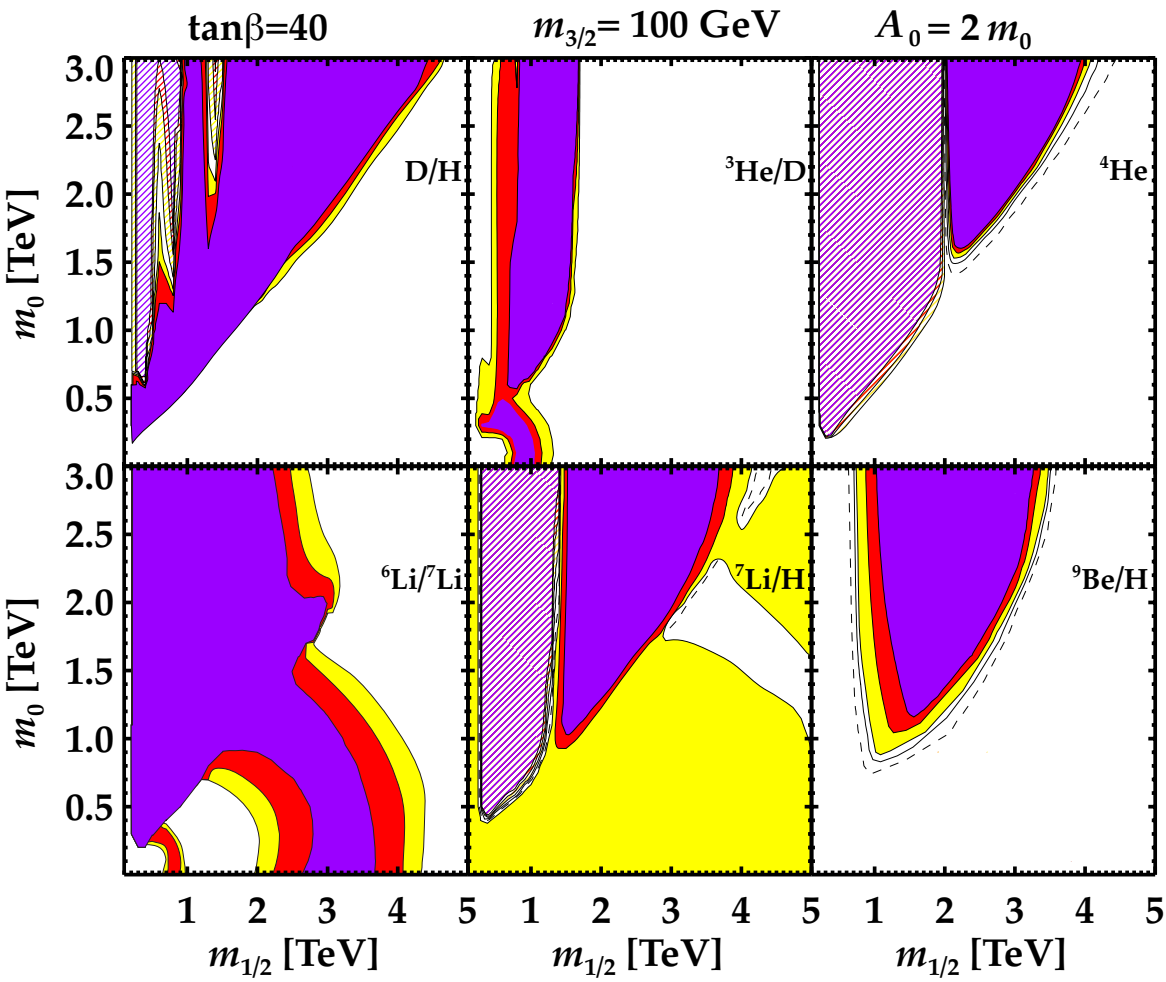

Figure 18. Light-element abundances in the $(m_{1/2}, m_0)$ plane for $A_0 = 2\,m_0$, $\tan\beta = 40$ and $m_{3/2} = 100\,\mathrm{GeV}$, with decay effects retained but all bound-state effects switched off.

must be high enough to allow for $(^4\mathrm{He}X^-) + {}^4\mathrm{He} \to (^8\mathrm{Be}X^-) + \gamma$ to be exothermic, i.e., $Q > 0$ (cf. eq. (2.1)). Our analysis has assumed as default the $B_8 = 1.1679\,\mathrm{MeV}$ value of ref. [77], which implies the formation reaction is strongly exothermic, and thus the reverse photodissociation of $(^8\mathrm{Be}X^-)$ is strongly suppressed. We have also considered both greater and smaller values of the binding energy. Using the larger value $B_8 = 1.408\,\mathrm{MeV}$ [78] makes the reaction even more exothermic; this gives results that are almost identical to our default analysis, since the bound-state formation rate remains very similar. The central panel of figure 19 summarizes the overall effect on the allowed region of $(m_{1/2}, m_0)$ plane for $A_0 = 2\,m_0$, $\tan\beta = 40$ and $m_{3/2} = 100\,\mathrm{GeV}$, which is almost indistinguishable from the default result shown in the left panel of figure 13.

Our own three-body estimate of the $(^8\mathrm{Be}X^-)$ binding energy in section 2 gives $B_8 = 492 \pm 50$ keV, a value that exceeds the effective 'no-go' limit in eq. (2.1) only by $Q = B_8 - B_8^{\mathrm{min}} = 53$ keV. In this situation, $(^8\mathrm{Be}X^-)$ production is weakly exothermic but remains highly vulnerable to photodissociation back to $(^4\mathrm{He}X^-) + {}^4\mathrm{He}$. This reverse reaction suppresses $(^8\mathrm{Be}X^-)$ formation until the temperature drops to $\sim Q/|\ln\eta| \sim 2$ keV. But at

JCAP12(2012)037

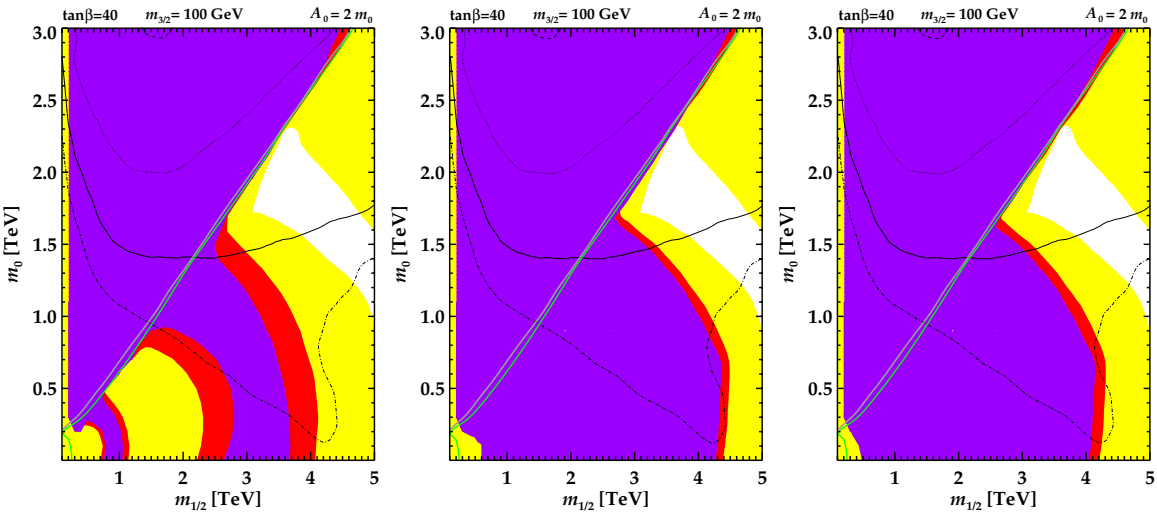

Figure 19. Summary of the light-element-abundance constraints in the $(m_{1/2}, m_0)$ plane for $A_0 = 2.5\,m_0$, $\tan\beta = 40$ and $m_{3/2} = 100\,\mathrm{GeV}$, if all bound-state effects were switched off (left), with greater ^{8}Be-X binding energy than our default choice (centre) and with ^{9}Be bound-state production suppressed (right).

this late time, no free neutrons are available, and the result is effectively that no bound-state ^{9}Be production occurs. Results for this case appear in figure 20. We see that in the lower-right region, where bound-state effects are important, the ^{9}Be production is now missing. Indeed, we have checked that the results are unchanged if bound-state ^{9}Be production is switched off entirely, as would be the case if the if $(^8\mathrm{Be}X)$ binding energy drops below the limit in eq. (2.1). Note also that even in the absence of bound-state production, ^{9}Be contours do remain in the upper-left region in figure 20. In this regine the thermalized ^{4}He fragments deuterium, tritium and ^{3}He are overproduced, and these can still make ^{9}Be via reactions with background ^{7}Be.

The right panel of figure 19 summarizes the overall effect of suppressed ^{9}Be bound-state production on the allowed region of the $(m_{1/2}, m_0)$ plane for $A_0 = 2\,m_0$, $\tan\beta = 40$ and $m_{3/2} = 100\,\mathrm{GeV}$. Perhaps surprisingly, there is little visible effect, and specifically none on the allowed unshaded arc at large $m_{1/2}$ and m_0. This is because the ^{9}Be and ^{6}Li/^{7}Li constraint contours very closely shadow each other in the lower part of the $(m_{1/2}, m_0)$ plane.

A second uncertainty in ^{9}Be production comes from the requirement that the $(^8\mathrm{Be}X^-) + n \to (^9\mathrm{Be}X^-) + \gamma$ reaction is on resonance with the first excited state of $(^9\mathrm{Be}^*X^-)$. As noted in section 2, this requires that the $(^8\mathrm{Be}X^-)$ and $(^9\mathrm{Be}^*X^-)$ bindings conspire in such a way that the entrance channel is on resonance, as would be the case for the larger binding energy $B_8 = 1.408\,\mathrm{MeV}$. Because the $(^9\mathrm{Be}^*X^-)$ binding is quite uncertain, this possibility remains viable. However, if the excited state level turns out to fall far ($\gtrsim$ 100 keV) from the $(^8\mathrm{Be}X^-) + n$ entrance, then the reaction will be non-resonant and suppressed. And here again, the bound-state ^{9}Be production would become unimportant, similar to the results in figure 20 and in the right panel of figure 19.

We conclude that, whereas the overall bound-state effects are very important, the principal uncertainties associated with the $(^8\mathrm{Be}X)$ binding energy have little effect on our final results. This comes about because the regions excluded by bound-state ^{9}Be production overlap almost completely with those also excluded by bound-state ^{6}Li production. In particular,

JCAP12(2012)037

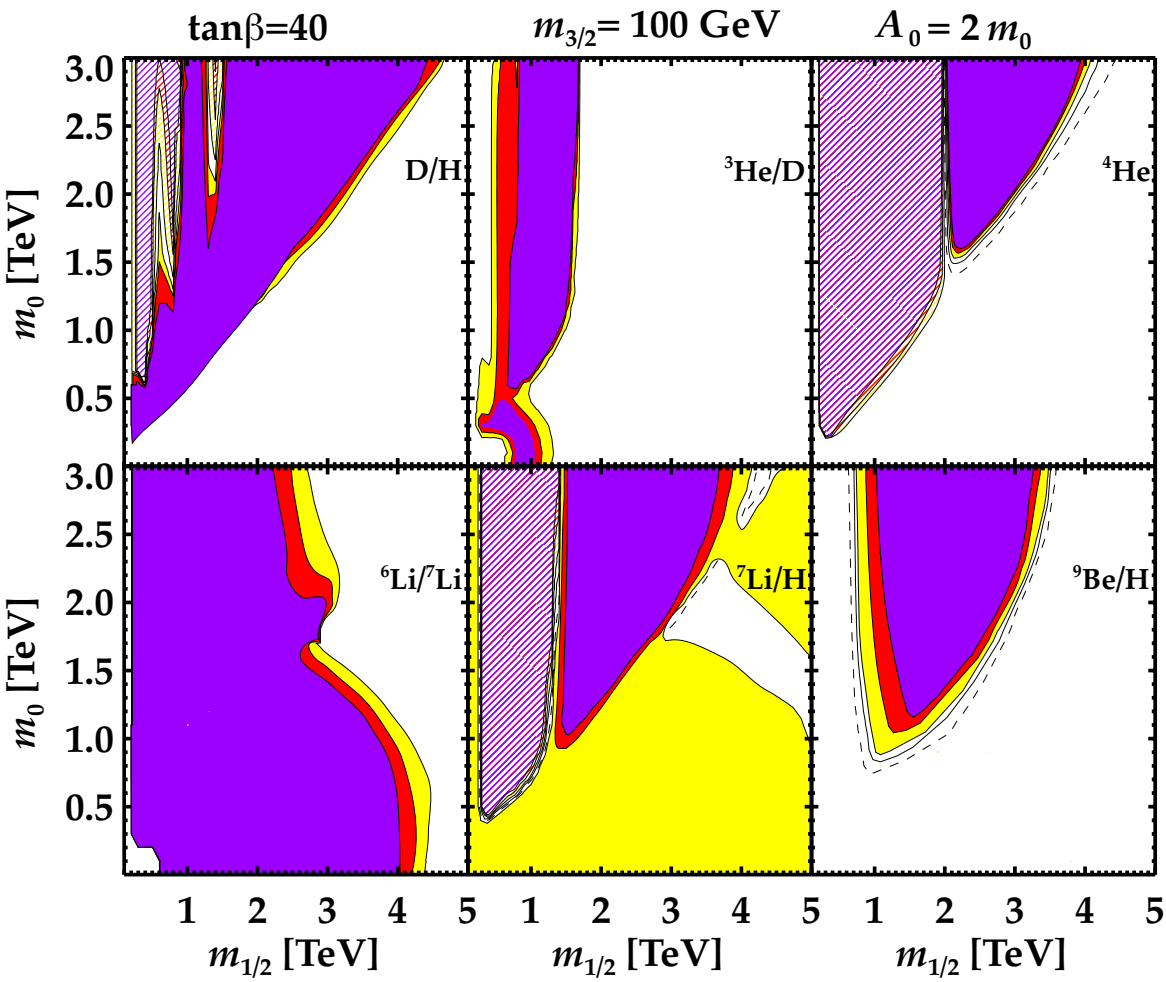

Figure 20. Light-element abundances in the $(m_{1/2}, m_0)$ plane for $A_0 = 2\,m_0$, $\tan\beta = 40$ and $m_{3/2} = 100\,\mathrm{GeV}$, with bound-state ^{9}Be production suppressed.

though our analysis incorporated the resonant $(^9\mathrm{Be}^* X^-)$ reaction rate postulated in [78], our final results are not very sensitive to this assumption.

8 Summary

We have presented in this paper a new treatment of the possible effects of bound states of metastable charged particles in the light-element abundances yielded by Big-Bang Nucleosynthesis (BBN), including in our analysis calculations of the abundances of D, ^{3}He, ^{4}He, ^{6}Li, ^{7}Li and ^{9}Be. We have applied our code to the case of metastable $\tilde{\tau}_1$ NLSPs in the framework of the CMSSM with a gravitino LSP. Motivated by the discovery of (apparently) a Higgs boson weighing ~ 125 to $126\,\mathrm{GeV}$, we have concentrated on regions of the CMSSM in which this may be interpreted as the lightest neutral Higgs boson, specifically $(m_{1/2}, m_0)$ planes with $A_0 \geq 2\,m_0$.

We find interesting examples in which the light-element abundances are as consistent with observations as are calculations of standard homogeneous BBN with no metastable relic particles. Indeed, we find generic strips of the CMSSM parameter space in which the

JCAP12(2012)037

cosmological ^{7}Li problem may be solved without altering unacceptably the abundances of the other light elements. Examples are given for $\tan\beta = 10$ and 40 with Higgs masses compatible with the LHC discovery.

Characteristics of these models include relatively large values of the soft supersymmetry-breaking parameters $m_{1/2}$ and m_0, with heavy supersymmetric particles that could not be detected directly at the LHC. Another characteristic of these models is that the $\tilde{\tau}_1$ lifetime is $\mathcal{O}(10^3)$ s. Avenues for future research include a more complete examination of the CMSSM parameter space, possible extensions to more general supersymmetric models, as well as to non-supersymmetric scenarios. In addition, we reiterate the need for careful study of the nuclear physics behind bound-state ^{8}Be and ^{9}Be production.

The observational situation with the ^{6}Li and ^{7}Li abundances is still evolving, and the fat lady has not yet sung the final aria in the cosmological lithium saga. It is perhaps still possible that the current discrepancy with standard homogeneous BBN will eventually dissipate. However, we have shown that, should it survive, it could have a plausible supersymmetric solution.

Acknowledgments

B.D.F. is pleased to acknowledge illuminating discussions with Chris Hirata regarding bound-state recombination, and we thank Sven Heinemeyer for discussions about `FeynHiggs` calculations. The work of R.H.C. was supported by the U.S. National Science Foundation Grants PHY-02-016783 and PHY-08-22648 (JINA). The work of J.E. and F.L. was supported in part by the London Centre for Terauniverse Studies (LCTS), using funding from the European Research Council via the Advanced Investigator Grant 267352: this also supported visits by K.A.O. and V.C.S. to the CERN TH Division, which they thank for its hospitality. The work of B.D.F. was partially supported by the U.S. National Science Foundation Grant PHY-1214082. The work of F.L. and K.A.O. was supported in part by DOE grant DE-FG02-94ER-40823 at the University of Minnesota, and the work of F.L. was also supported in part by the Doctoral Dissertation Fellowship at the University of Minnesota. The work of V.C.S. was supported by Marie Curie International Reintegration grant SUSYDM-PHEN, MIRG-CT-2007-203189.

A Recombination of X bound states

A comparison of (AX^-) recombination with that of ordinary hydrogen recombination reveals important similarities but also crucial differences. The recombination of ordinary cosmic hydrogen and helium does not proceed primarily through $pe \to (pe)_1$ transitions directly to the $n = 1$ ground state. This is because such recombinations emit Lyman limit photons with energy $E_\gamma = B_{(pe)} = 13.6\,\mathrm{eV}$, which have a large cross section. Thus, during the era of (ordinary) recombination, these photons have a short mean free path against absorption by neighboring ground-state hydrogen atoms. Thus, at this epoch the universe is optically thick to Lyman limit photons. Consequently, the overwhelming majority of recombinations to the ground state in one atom lead to a reionization of a neighboring atom, and there is no net change in the number of atoms.

Ordinary recombination therefore proceeds via transitions initially to excited states, particularly the $n = 2$ first excited state, and then to the ground state. However, the cosmic plasma is also optically thick to $2P \to 1S$ Lyman-α photons, and so the transition to the

JCAP12(2012)037

ground state is dominated by the much slower two-photon $2S \to 1S$ transition. Because of these effects, ordinary hydrogen recombination is not instantaneous, but delayed due to the 'bottleneck' of the large optical depth for Lyman series photons.

Our NLSP case of $pX^- \to (pX)$ and $^4\mathrm{He}X^- \to (^4\mathrm{He}X)$ recombination is controlled by the same underlying atomic physics, and under conditions of a similar matter-to-photon ratio. It thus is worthwhile to check whether we expect similar effects.

For the hydrogen and NLSP recombination, we are interested in the absorption of Lyα and 'XLyα' photons, respectively, by ground-state atoms:

$$\gamma_{1\to 2} + (\mathcal{A}p)_1 \to (\mathcal{A}p)_2 \ , \tag{A.1}$$

where the 'anion' $\mathcal{A} \in (e, X)$ corresponds to ordinary and NLSP recombination, respectively. Note, however, that in the NLSP case the proton, being lighter, plays the role of the electron in setting the relevant reduced mass μ, so $\mu = m_e$ for hydrogen and $\mu = m_p$ for NLSP. On the other hand, the atomic mass $m_p + m_{\mathcal{A}} - B_{\mathcal{A}}$ is well approximated by $m = m_p$ for hydrogen and $m = m_X$ for NLSP.

The XLyα photon optical depth against absorption by (pX) atoms is

$$\tau_\alpha(\mathcal{A}p) = \sigma_\alpha(\mathcal{A}p)\ n_{\mathcal{A}}\ d_{\rm hor} \approx \sigma_\alpha(\mathcal{A}p)\ n_{\mathcal{A}}\ t \ , \tag{A.2}$$

so the ratio of hydrogen and NLSP optical depths is

$$\frac{\tau_\alpha(Xp)}{\tau_\alpha(ep)} = \frac{\sigma_\alpha(Xp)}{\sigma_\alpha(ep)} \frac{n_X}{n_e} \frac{t_{\rm bbn}}{t_{\rm cmb}}. \tag{A.3}$$

The XLyα resonance cross section is, in the notation of ref. [126],

$$\sigma_\alpha = \frac{3}{8\pi}\lambda_\alpha^2 \frac{\Gamma_{2p\to 1s}^2}{(\omega-\omega_\alpha)^2 + \Gamma_{2p\to 1s}^2/4}\,, \tag{A.4}$$

where $\lambda_\alpha \propto 1/E_\alpha \sim (\alpha^2\mu)^{-1}$, and $\Gamma_{2p\to 1s} \propto \mu$ is the decay rate. Thermal broadening dominates over this width, with $\delta\omega/\omega \sim v_T/c \sim \sqrt{T/m}$ where m is the atomic mass. Thus we have an effective mean cross section

$$\bar{\sigma}_\alpha \sim \lambda_\alpha^2 \frac{\Gamma_{2p\to 1s}^2}{\delta\omega^2} \sim \lambda_\alpha^2 \frac{\Gamma_{2p\to 1s}^2}{\omega_\alpha^2}\frac{m}{T} \propto \mu^{-2}\frac{m}{T} \propto \mu^{-2}\frac{m}{T_0}(1+z)^{-1}. \tag{A.5}$$

where z is the redshift. The appropriate number densities are the physical, not comoving, values, and are set by $n_e \approx n_p$, and by $n_X = Y_X n_p$, with $n_p \sim n_{\rm B} \propto (1+z)^3$. Finally, in the ordinary recombination case we have $z_{\rm cmb} \sim 1000$ and $t_{\rm cmb} \sim 400,000$ yr $\sim 10^{13}$ sec, whereas in the NLSP case we have $z_{\rm bbn} \sim 4\times 10^8$ and $t_{\rm bbn} \sim 100$ sec.

Putting the above information together, we have

$$\frac{\tau_\alpha(Xp)}{\tau_\alpha(ep)} = \left(\frac{m_e}{m_p}\right)^2 \left(\frac{m_X}{m_p}\right)\ Y_X \left(\frac{1+z_{\rm bbn}}{1+z_{\rm cmb}}\right)^2 \frac{t_{\rm bbn}}{t_{\rm cmb}} \tag{A.6}$$

$$\approx 5\times 10^{-7} \left(\frac{Y_X}{0.01}\right) \left(\frac{m_X}{100\ \mathrm{GeV}}\right). \tag{A.7}$$

Thus we see that the XLyα optical depth at NLSP recombination is much smaller than that of ordinary recombination. However, the optical depth for ordinary recombination is enormous, $\tau(ep) \sim 10^9$, so

$$\tau_\alpha(Xp) \sim 500 \left(\frac{Y_X}{0.01}\right) \left(\frac{m_X}{100\ \mathrm{GeV}}\right) \ . \tag{A.8}$$

JCAP12(2012)037

We find an optical depth against (pX) absorption that is much larger than unity. Hence it would seem that this effect could also be important for the NLSP recombination case.

However, in the case of NLSP recombination there is an additional process to be considered that has no analogue in ordinary recombination, namely the Compton scattering of XLyα photons on free electrons and positrons. In ordinary recombination, electrons act as both the dominant photon scattering agent when they are unbound, and as the negatively-charged partners in the bound states. However, in our (AX^-) case, these roles are now separated to $e^\pm$ and X^- respectively. The optical depth against electron scattering can be estimated using the ordinary Thomson cross section $\sigma_{\rm T}$:

$$\tau_{e\gamma} = n_{e,\rm net}^{\rm bbn}\sigma_{\rm T} t_{\rm bbn} \geq n_{\rm B}^{\rm bbn}\sigma_{\rm T} t_{\rm bbn} \tag{A.9}$$

$$\sim 5\times 10^7 \left(\frac{T_{\rm bbn}}{100\ {\rm keV}}\right). \tag{A.10}$$

This is a lower bound, because we have used the *net* electron number $n_{e,\rm net} = n_{e^-} - n_{e^+} \simeq n_{\rm B}$, whereas pairs dominate the *total* $e^\pm$ budget:

$$\frac{n_{e^-}+n_{e^+}}{n_{\rm B}} \sim \eta^{-1}\left(\frac{m_e}{T}\right)^{3/2} e^{-m_e/T} \gg 1 \tag{A.11}$$

down to $T \sim m_e/\ln\eta^{-1} \simeq m_e/25 \sim 20$ keV. Note that during ordinary recombination, the optical depth against Thompson scattering drops below $\tau_{e\gamma} \sim 1$, and cannot compete successfully with resonant Lyα scattering.

We see that an XLyα photon will typically suffer at least $\sim \tau_{e\gamma}/\tau_\alpha(Xp) \sim 500$ Compton scatterings before encountering a bound state that it could reionize. Each of these scatterings degrades the photon energy, pulling it out of resonance. If the scattering were off a nonrelativistic electron, the photon would lose energy according to the Compton formula

$$E'_\gamma = \frac{E_\gamma}{1+\frac{E_\gamma}{m_e}(1-\cos\theta)}, \tag{A.12}$$

and we would expect an approximate mean energy loss per scattering of

$$\frac{\Delta E_\gamma}{E_\gamma} \sim \frac{E_\gamma}{m_e}. \tag{A.13}$$

The Lyman photons of interest have $E(X{\rm Ly}\alpha) = 3/4\ B(AX)$, and we have $B(^4{\rm He}X) = 348$ keV and $B(pX) = 25$ keV; each species recombines at roughly $T \sim B/\ln\eta^{-1} \sim B/25$.

Thus ^{4}He recombination occurs when pairs are abundant, whereas protons recombine when pairs have completely annihilated. In either case, the Compton opacity dominates the resonance opacity, so that Lyman photons scatter many times before encountering a bound state. Moreover, in the first scattering the Lyman photons suffer energy losses $\Delta E/E \sim \mathcal{O}(1)$ for $(^4{\rm He}X)$ and $\Delta E/E \sim \mathcal{O}(10^{-1})$ for (pX). The Lyman photons are thus thermalized rapidly, long before they interact with any ground state atoms. We conclude that NLSP recombination to the ground state can occur unimpeded, unlike the case of ordinary recombination.

B Specification of the supersymmetric model framework

In this paper we analyze the possible implications of bound states of massive metastable particles on Big-Bang Nucleosynthesis in the context of the minimal supersymmetric extension

JCAP12(2012)037

of the Standard Model (MSSM). In this model, there is a supersymmetric partner for each Standard Model particle, and there are two Higgs doublet supermultiplets linked via a mixing parameter μ. The interactions are restricted to the same gauge and Yukawa interactions as in the Standard Model, so the quantity $R = (-1)^{3B+L+2S}$ is conserved multiplicatively, where B and L are the baryon and lepton numbers, respectively, and S is the spin. As a consequence of R conservation, the lightest supersymmetric particle (LSP) is stable, and a candidate for cosmological dark matter.

We further assume the presence of soft supersymmetry-breaking fermion masses $m_{1/2}$, scalar masses m_0 and trilinear parameters A_0 which are each universal at the grand unification scale, a framework known as the constrained MSSM (CMSSM) [97, 119]. In addition to $m_{1/2}, m_0$ and A_0, we treat the ratio of Higgs vacuum expectation values, $\tan\beta$, as a free parameter. Motivated by the apparent discrepancy between the experimental measurement [120] of the anomalous magnetic moment of the muon, $g_\mu - 2$, and theoretical calculations within the Standard Model [121] we assume that the MSSM Higgs mixing parameter μ is positive. As specified, the CMSSM includes no prediction for the mass of the gravitino, $m_{3/2}$, which we treat as a free and independent parameter.

We consider here the case in which the gravitino is the LSP, and the next-to-lightest supersymmetric particle (NLSP) is the spartner of one of the Standard Model particles. Possible candidates include the lightest neutralino χ, the lighter stau slepton $\tilde{\tau}_1$, the spartner of the right-handed electron or muon, $\tilde{e}_R$ or $\tilde{\mu}_R$, or the lighter stop squark $\tilde{t}_1$. In the CMSSM as described above with a gravitino LSP, the most generic of these candidates for the NLSP are the lightest neutralino χ and the lighter stau slepton $\tilde{\tau}_1$, and the latter is the candidate we consider as an example of a charged metastable NLSP.

C Three-body Stau decays

We give here the matrix elements for $\tilde{\tau}^- \to \widetilde{G}\,\tau^- Z$ and $\tilde{\tau}^- \to \widetilde{G}\,\nu_\tau W^-$, which are the three-body stau decay processes that are most relevant for our study. In the Feynman diagrams for these two processes, the vertices involving the outgoing gravitino are given in appendix A of [122], and the vertices involving only the MSSM fields are given in [123] and [124]. In the context of the CMSSM, left-right mixing needs to be taken into account only for the third generation of sfermion fields. Neutrinos are treated the same way as in the Standard Model, i.e., as massless, purely left-handed neutrinos (and right-handed antineutrinos). Following appendix B of [41], we write the relation between the mass eigenstates, $\tilde{\tau}_{1,2}$, and the interaction eigenstates, $\tilde{\tau}_{L,R}$, as

$$\begin{pmatrix} \tilde{\tau}_L \\ \tilde{\tau}_R \end{pmatrix} = \begin{pmatrix} U_{\tilde{\tau}\,1L} & U_{\tilde{\tau}\,2L} \\ U_{\tilde{\tau}\,1R} & U_{\tilde{\tau}\,2R} \end{pmatrix} \begin{pmatrix} \tilde{\tau}_1 \\ \tilde{\tau}_2 \end{pmatrix}. \tag{C.1}$$

In order to be quite general, we give expressions for $\tilde{\tau}_j^-$ $(j = 1, 2)$, where the stau NLSP is the lighter of the two mass eigenstates.

At tree-level, the Feynman diagrams contributing to $\tilde{\tau}_j^-(p_1) \to \widetilde{G}(p_2)\,\tau^-(p_3)\,Z(p_4)$ are the contact diagram and the τ^-, $\tilde{\tau}_k^-$ $(k = 1, 2)$ and neutralino $\tilde{\chi}_k^0$ $(k = 1 - 4)$ exchange diagrams. The partial matrix elements for each of these diagrams (suppressing spin and

JCAP12(2012)037

polarization indices) are

$$i\mathcal{M}_{\text{contact}} = \bar{\psi}_\mu(p_2)\left(-\frac{i\sqrt{2}}{M_P}\frac{g}{\cos\theta_W}\right)\left[\left(T_f^3 - Q_f\sin^2\theta_W\right)U_{\tilde{\tau}\,jL}P_R + Q_f\sin^2\theta_W U_{\tilde{\tau}\,jR}P_L\right]\eta^{\mu\nu} \cdot v(p_3)\,\epsilon_\nu^*(p_4), \tag{C.2}$$

$$i\mathcal{M}_{\tilde{\tau}_j^- \to \widetilde{G}\tau^{-*} \to \widetilde{G}Z\tau^-} = \bar{\psi}_\mu(p_2)\left(-\frac{i\sqrt{2}}{M_P}\right)\left(U_{\tilde{\tau}\,jR}P_L - U_{\tilde{\tau}\,jL}P_R\right)p_1^\mu\,\frac{i\left(-\not{p}_1 + \not{p}_2 + m_\tau\right)}{(p_1-p_2)^2 - m_\tau^2} \cdot\left(\frac{ig}{\cos\theta_W}\right)\gamma^\nu\left[\left(T_f^3 - Q_f\sin^2\theta_W\right)P_R - Q_f\sin^2\theta_W P_L\right]v(p_3)\,\epsilon_\nu^*(p_4), \tag{C.3}$$

$$i\mathcal{M}_{\tilde{\tau}_j^- \to Z\tilde{\tau}_k^{-*} \to Z\widetilde{G}\tau^-} = \bar{\psi}_\mu(p_2)\left(-\frac{i\sqrt{2}}{M_P}\right)\left(U_{\tilde{\tau}\,kR}P_L - U_{\tilde{\tau}\,kL}P_R\right)(p_1-p_4)^\mu\,\frac{i}{(p_1-p_4)^2 - m_{\tilde{\tau}_k}^2} \cdot\left(-\frac{ig}{\cos\theta_W}\right)\left[\left(T_f^3 - Q_f\sin^2\theta_W\right)U_{\tilde{\tau}\,jL}U_{\tilde{\tau}\,kL}^* - Q_f\sin^2\theta_W U_{\tilde{\tau}\,jR}U_{\tilde{\tau}\,kR}^*\right] \cdot(2p_1-p_4)^\nu\,v(p_3)\,\epsilon_\nu^*(p_4), \tag{C.4}$$

$$i\mathcal{M}_{\tilde{\tau}_j^- \to \tau^-\tilde{\chi}_k^{0*} \to \tau^-\widetilde{G}Z} = \bar{\psi}_\mu(p_2)\left(-\frac{i}{M_P}\right)\left[\left(H_L\,\eta^{\mu\nu} - \frac{1}{4}G_L\left[\not{p}_4, \gamma^\nu\right]\gamma^\mu\right)P_L + \left(H_R\,\eta^{\mu\nu} - \frac{1}{4}G_R\left[\not{p}_4, \gamma^\nu\right]\gamma^\mu\right)P_R\right]\frac{i\left(\not{p}_1 - \not{p}_3 + m_{\tilde{\chi}_k^0}\right)}{(p_1-p_3)^2 - m_{\tilde{\chi}_k^0}^2} \cdot i\left[\left(C_L U_{\tilde{\tau}\,jL} + D_L U_{\tilde{\tau}\,jR}\right)P_L + \left(C_R U_{\tilde{\tau}\,jR} + D_R U_{\tilde{\tau}\,jL}\right)P_R\right]v(p_3)\,\epsilon_\nu^*(p_4), \tag{C.5}$$

where $\bar{\psi}_\mu(p_2)$ represents the outgoing gravitino with momentum p_2, $v(p_3)$ represents the outgoing chiral fermion with momentum p_3, $\epsilon_\nu^*(p_4)$ is the polarization four-vector for the outgoing gauge boson with momentum p_4, $\eta^{\mu\nu}$ is the flat-space Lorentz metric tensor, $H_L = m_Z\left(\cos\beta N_{k3}^* - \sin\beta N_{k4}^*\right)$, $G_L = \cos\theta_W N_{k2}^* - \sin\theta_W N_{k1}^*$, $H_R = H_L^*$, $G_R = G_L^*$, $C_L = -(g m_\tau N_{k3}^*)/(\sqrt{2}m_W\cos\beta)$, $D_L = \sqrt{2}g N_{k1}^*\tan\theta_W Q_f$, $C_R = C_L^*$, $D_R = -\sqrt{2}g\left[N_{k2}T_f^3 + \tan\theta_W N_{k1}\left(Q_f - T_f^3\right)\right]$, $T_f^3 = -1/2$, $Q_f = -1$ and N is the unitary matrix used to diagonalize the neutralino mass matrix (details can be found in [124]).

For $\tilde{\tau}_j(p_1) \to \widetilde{G}(p_2)\,\nu_\tau(p_3)\,W^-(p_4)$, the Feynman diagrams contributing to this process, corresponding to eq. (C.2), (C.3), (C.4) and (C.5), are the contact diagram, and the τ^-, $\tilde{\nu}_\tau$ and chargino $\tilde{\chi}_k^-$ $(k = 1, 2)$ exchange diagrams, respectively. The partial matrix elements are obtained by making the substitutions $g \to g\sqrt{2}\cos\theta_W$, $T_f \to 1/2$ and $Q_f \to 0$ in eq. (C.2)–(C.4), $m_{\tilde{\tau}_k} \to m_{\tilde{\nu}_\tau}$, $U_{\tilde{\tau}\,kR} \to 0$, $U_{\tilde{\tau}\,kL} \to 1$, $U_{\tilde{\tau}\,kR}^* \to 0$ and $U_{\tilde{\tau}\,kL}^* \to 1$ in eq. (C.4) since there is no right-handed sneutrino in the MSSM. Also, in eq. (C.5) $m_{\tilde{\chi}_k^0} \to m_{\tilde{\chi}_k^\pm}$, and now the coefficients are $H_L = \sqrt{2}m_W\cos\beta U_{k2}^*$, $G_L = U_{k1}^*$, $H_R = \sqrt{2}m_W\sin\beta V_{k2}$, $G_R = V_{k1}$, $C_L = D_L = 0$, $C_R = (g m_\tau U_{k2})\,/\left(\sqrt{2}m_W\cos\beta\right)$ and $D_R = -g U_{k1}$, where U and V are the unitary matrices used to diagonalize the chargino mass matrix.

JCAP12(2012)037

References

[1] D. Lindley, *Cosmological Constraints on the Lifetime of Massive Particles*, *Astrophys. J.* **294** (1985) 1 [INSPIRE].

[2] J.R. Ellis, D.V. Nanopoulos and S. Sarkar, *The Cosmology of Decaying Gravitinos*, *Nucl. Phys.* **B 259** (1985) 175 [INSPIRE].

[3] D. Lindley, *Hadronic Decays of Cosmological Gravitinos*, *Phys. Lett.* **B 171** (1986) 235 [INSPIRE].

[4] R.J. Scherrer and M.S. Turner, *Primordial Nucleosynthesis with Decaying Particles. 1. Entropy Producing Decays. 2. Inert Decays*, *Astrophys. J.* **331** (1988) 19 [INSPIRE].

[5] M.H. Reno and D. Seckel, *Primordial Nucleosynthesis: The Effects of Injecting Hadrons*, *Phys. Rev.* **D 37** (1988) 3441 [INSPIRE].

[6] S. Dimopoulos, R. Esmailzadeh, L.J. Hall and G. Starkman, *Is the universe closed by baryons? Nucleosynthesis with a late decaying massive particle*, *Astrophys. J.* **330** (1988) 545 [INSPIRE]; *Limits on late decaying particles from nucleosynthesis*, *Nucl. Phys.* **B 311** (1989) 699 [INSPIRE].

[7] J.R. Ellis, G. Gelmini, J.L. Lopez, D.V. Nanopoulos and S. Sarkar, *Astrophysical constraints on massive unstable neutral relic particles*, *Nucl. Phys.* **B 373** (1992) 399 [INSPIRE].

[8] M. Kawasaki and T. Moroi, *Gravitino production in the inflationary universe and the effects on big bang nucleosynthesis*, *Prog. Theor. Phys.* **93** (1995) 879 [hep-ph/9403364] [INSPIRE].

[9] M. Kawasaki and T. Moroi, *Electromagnetic cascade in the early universe and its application to the big bang nucleosynthesis*, *Astrophys. J.* **452** (1995) 506 [astro-ph/9412055] [INSPIRE].

[10] M.Y. Khlopov, Y. Levitan, E. Sedelnikov and I. Sobol, *Nonequilibrium cosmological nucleosynthesis of light elements: Calculations by the Monte Carlo method*, *Phys. Atom. Nucl.* **57** (1994) 1393 [*Yad. Fiz.* **57** (1994) 1466] [INSPIRE]; E.V. Sedelnikov, S.S. Filippov and M.Y. Khlopov, *Kinetic theory of nonequilibrium cosmological nucleosynthesis*, *Phys. Atom. Nucl.* **58** (1995) 235 [*Yad. Fiz.* **58** (1995) 280] [INSPIRE].

[11] E. Holtmann, M. Kawasaki, K. Kohri and T. Moroi, *Radiative decay of a longlived particle and big bang nucleosynthesis*, *Phys. Rev.* **D 60** (1999) 023506 [hep-ph/9805405] [INSPIRE].

[12] K. Jedamzik, *Lithium 6: A Probe of the early universe*, *Phys. Rev. Lett.* **84** (2000) 3248 [astro-ph/9909445] [INSPIRE].

[13] M. Kawasaki, K. Kohri and T. Moroi, *Radiative decay of a massive particle and the nonthermal process in primordial nucleosynthesis*, *Phys. Rev.* **D 63** (2001) 103502 [hep-ph/0012279] [INSPIRE].

[14] K. Kohri, *Primordial nucleosynthesis and hadronic decay of a massive particle with a relatively short lifetime*, *Phys. Rev.* **D 64** (2001) 043515 [astro-ph/0103411] [INSPIRE].

[15] R.H. Cyburt, J.R. Ellis, B.D. Fields and K.A. Olive, *Updated nucleosynthesis constraints on unstable relic particles*, *Phys. Rev.* **D 67** (2003) 103521 [astro-ph/0211258] [INSPIRE].

[16] K. Jedamzik, *Did something decay, evaporate, or annihilate during Big Bang nucleosynthesis?*, *Phys. Rev.* **D 70** (2004) 063524 [astro-ph/0402344] [INSPIRE]; *Neutralinos and Big Bang nucleosynthesis*, *Phys. Rev.* **D 70** (2004) 083510 [astro-ph/0405583] [INSPIRE].

[17] M. Kawasaki, K. Kohri and T. Moroi, *Hadronic decay of late-decaying particles and Big-Bang Nucleosynthesis*, *Phys. Lett.* **B 625** (2005) 7 [astro-ph/0402490] [INSPIRE]; *Big-Bang nucleosynthesis and hadronic decay of long-lived massive particles*, *Phys. Rev.* **D 71** (2005) 083502 [astro-ph/0408426] [INSPIRE].

JCAP12(2012)037

[18] J.R. Ellis, K.A. Olive and E. Vangioni, *Effects of unstable particles on light-element abundances: Lithium versus deuterium and He-3*, Phys. Lett. **B 619** (2005) 30 [astro-ph/0503023] [INSPIRE].

[19] K. Kohri, T. Moroi and A. Yotsuyanagi, *Big-bang nucleosynthesis with unstable gravitino and upper bound on the reheating temperature*, Phys. Rev. **D 73** (2006) 123511 [hep-ph/0507245] [INSPIRE].

[20] D.G. Cerdeno, K.-Y. Choi, K. Jedamzik, L. Roszkowski and R. Ruiz de Austri, *Gravitino dark matter in the CMSSM with improved constraints from BBN*, JCAP **06** (2006) 005 [hep-ph/0509275] [INSPIRE].

[21] K. Jedamzik, K.-Y. Choi, L. Roszkowski and R. Ruiz de Austri, *Solving the cosmic lithium problems with gravitino dark matter in the CMSSM*, JCAP **07** (2006) 007 [hep-ph/0512044] [INSPIRE].

[22] K. Jedamzik, *Big bang nucleosynthesis constraints on hadronically and electromagnetically decaying relic neutral particles*, Phys. Rev. **D 74** (2006) 103509 [hep-ph/0604251] [INSPIRE].

[23] F.D. Steffen, *Gravitino dark matter and cosmological constraints*, JCAP **09** (2006) 001 [hep-ph/0605306] [INSPIRE].

[24] M. Pospelov, *Particle physics catalysis of thermal Big Bang Nucleosynthesis*, Phys. Rev. Lett. **98** (2007) 231301 [hep-ph/0605215] [INSPIRE].

[25] K. Kohri and F. Takayama, *Big bang nucleosynthesis with long lived charged massive particles*, Phys. Rev. **D 76** (2007) 063507 [hep-ph/0605243] [INSPIRE].

[26] M. Kusakabe, T. Kajino and G.J. Mathews, *Li-6 Production by the Radiative Decay of Long-Lived Particles*, Phys. Rev. **D 74** (2006) 023526 [astro-ph/0605255] [INSPIRE].

[27] R.H. Cyburt, J.R. Ellis, B.D. Fields, K.A. Olive and V.C. Spanos, *Bound-State Effects on Light-Element Abundances in Gravitino Dark Matter Scenarios*, JCAP **11** (2006) 014 [astro-ph/0608562] [INSPIRE].

[28] K. Hamaguchi, T. Hatsuda, M. Kamimura, Y. Kino and T. Yanagida, *Stau-catalyzed ^{6}Li Production in Big-Bang Nucleosynthesis*, Phys. Lett. **B 650** (2007) 268 [hep-ph/0702274] [INSPIRE].

[29] C. Bird, K. Koopmans and M. Pospelov, *Primordial Lithium Abundance in Catalyzed Big Bang Nucleosynthesis*, Phys. Rev. **D 78** (2008) 083010 [hep-ph/0703096] [INSPIRE].

[30] M. Kawasaki, K. Kohri and T. Moroi, *Big-Bang Nucleosynthesis with Long-Lived Charged Slepton*, Phys. Lett. **B 649** (2007) 436 [hep-ph/0703122] [INSPIRE].

[31] T. Jittoh, K. Kohri, M. Koike, J. Sato, T. Shimomura, et al., *Possible solution to the Li-7 problem by the long lived stau*, Phys. Rev. **D 76** (2007) 125023 [arXiv:0704.2914] [INSPIRE]; *Big-bang nucleosynthesis and the relic abundance of dark matter in a stau-neutralino coannihilation scenario*, Phys. Rev. **D 78** (2008) 055007 [arXiv:0805.3389] [INSPIRE]; T. Jittoh, K. Kohri, M. Koike, J. Sato, T. Shimomura and M. Yamanaka, *Stau relic density at the Big-Bang nucleosynthesis era consistent with the abundance of the light element nuclei in the coannihilation scenario*, Phys. Rev. **D 82** (2010) 115030 [arXiv:1001.1217] [INSPIRE]; T. Jittoh, K. Kohri, M. Koike, J. Sato, K. Sugai, et al., *Big-bang nucleosynthesis with a long-lived charged massive particle including ^{4}He spallation processes*, Phys. Rev. **D 84** (2011) 035008 [arXiv:1105.1431] [INSPIRE].

[32] K. Jedamzik, *The cosmic Li-6 and Li-7 problems and BBN with long-lived charged massive particles*, Phys. Rev. **D 77** (2008) 063524 [arXiv:0707.2070] [INSPIRE]; *Bounds on long-lived charged massive particles from Big Bang nucleosynthesis*, JCAP **03** (2008) 008 [arXiv:0710.5153] [INSPIRE].

JCAP12(2012)037

[33] D. Cumberbatch, K. Ichikawa, M. Kawasaki, K. Kohri, J. Silk, et al., *Solving the cosmic lithium problems with primordial late-decaying particles*, *Phys. Rev.* **D 76** (2007) 123005 [arXiv:0708.0095] [INSPIRE].

[34] J. Pradler and F.D. Steffen, *Implications of Catalyzed BBN in the CMSSM with Gravitino Dark Matter*, *Phys. Lett.* **B 666** (2008) 181 [arXiv:0710.2213] [INSPIRE].

[35] M. Kusakabe, T. Kajino, R.N. Boyd, T. Yoshida and G.J. Mathews, *A Simultaneous Solution to the ^{6}Li and ^{7}Li Big Bang Nucleosynthesis Problems from a Long-Lived Negatively-Charged Leptonic Particle*, *Phys. Rev.* **D 76** (2007) 121302 [arXiv:0711.3854] [INSPIRE]; *The X^- Solution to the ^{6}Li and ^{7}Li Big Bang Nucleosynthesis Problems*, arXiv:0711.3858 [INSPIRE].

[36] M. Kawasaki, K. Kohri, T. Moroi and A. Yotsuyanagi, *Big-Bang Nucleosynthesis and Gravitino*, *Phys. Rev.* **D 78** (2008) 065011 [arXiv:0804.3745] [INSPIRE].

[37] M. Pospelov, J. Pradler and F.D. Steffen, *Constraints on Supersymmetric Models from Catalytic Primordial Nucleosynthesis of Beryllium*, *JCAP* **11** (2008) 020 [arXiv:0807.4287] [INSPIRE].

[38] S. Bailly, K. Jedamzik and G. Moultaka, *Gravitino Dark Matter and the Cosmic Lithium Abundances*, *Phys. Rev.* **D 80** (2009) 063509 [arXiv:0812.0788] [INSPIRE].

[39] M. Kusakabe, T. Kajino, T. Yoshida and G.J. Mathews, *Effect of Long-lived Strongly Interacting Relic Particles on Big Bang Nucleosynthesis*, *Phys. Rev.* **D 80** (2009) 103501 [arXiv:0906.3516] [INSPIRE].

[40] K. Jedamzik and M. Pospelov, *Big Bang Nucleosynthesis and Particle Dark Matter*, *New J. Phys.* **11** (2009) 105028 [arXiv:0906.2087] [INSPIRE].

[41] R.H. Cyburt, J. Ellis, B.D. Fields, F. Luo, K.A. Olive, et al., *Nucleosynthesis Constraints on a Massive Gravitino in Neutralino Dark Matter Scenarios*, *JCAP* **10** (2009) 021 [arXiv:0907.5003] [INSPIRE].

[42] M. Kusakabe, T. Kajino, T. Yoshida and G.J. Mathews, *New results on catalyzed BBN with a long-lived negatively-charged massive particle*, *Phys. Rev.* **D 81** (2010) 083521 [arXiv:1001.1410] [INSPIRE].

[43] M. Pospelov and J. Pradler, *Metastable GeV-scale particles as a solution to the cosmological lithium problem*, *Phys. Rev.* **D 82** (2010) 103514 [arXiv:1006.4172] [INSPIRE].

[44] R.H. Cyburt, J. Ellis, B.D. Fields, F. Luo, K.A. Olive, et al., *Nuclear Reaction Uncertainties, Massive Gravitino Decays and the Cosmological Lithium Problem*, *JCAP* **10** (2010) 032 [arXiv:1007.4173] [INSPIRE].

[45] M. Pospelov and J. Pradler, *Primordial beryllium as a big bang calorimeter*, *Phys. Rev. Lett.* **106** (2011) 121305 [arXiv:1010.4079] [INSPIRE].

[46] M. Pospelov and J. Pradler, *Big Bang Nucleosynthesis as a Probe of New Physics*, *Ann. Rev. Nucl. Part. Sci.* **60** (2010) 539 [arXiv:1011.1054] [INSPIRE].

[47] M. Kawasaki and M. Kusakabe, *Destruction of ^{7}Be in big bang nucleosynthesis via long-lived sub-strongly interacting massive particles as a solution to the Li problem*, *Phys. Rev.* **D 83** (2011) 055011 [arXiv:1012.0435] [INSPIRE].

[48] D. Albornoz Vasquez, A. Belikov, A. Coc, J. Silk and E. Vangioni, *Neutron injection during primordial nucleosynthesis alleviates the primordial 7Li problem*, *Phys. Rev.* **D 86** (2012) 063501 [arXiv:1208.0443] [INSPIRE].

[49] B.D. Fields, *The primordial lithium problem*, *Ann. Rev. Nucl. Part. Sci.* **61** (2011) 47 [arXiv:1203.3551] [INSPIRE].

JCAP12(2012)037

[50] G. Steigman, *Primordial Nucleosynthesis in the Precision Cosmology Era*, *Ann. Rev. Nucl. Part. Sci.* **57** (2007) 463 [arXiv:0712.1100] [INSPIRE].

[51] WMAP collaboration, E. Komatsu et al., *Seven-Year Wilkinson Microwave Anisotropy Probe (WMAP) Observations: Cosmological Interpretation*, *Astrophys. J. Suppl.* **192** (2011) 18 [arXiv:1001.4538] [INSPIRE].

[52] R.H. Cyburt, B.D. Fields and K.A. Olive, *Primordial nucleosynthesis with CMB inputs: Probing the early universe and light element astrophysics*, *Astropart. Phys.* **17** (2002) 87 [astro-ph/0105397] [INSPIRE].

[53] R.H. Cyburt, B.D. Fields and K.A. Olive, *Primordial nucleosynthesis in light of WMAP*, *Phys. Lett.* **B 567** (2003) 227 [astro-ph/0302431] [INSPIRE]; *An Update on the big bang nucleosynthesis prediction for Li-7: The problem worsens*, *JCAP* **11** (2008) 012 [arXiv:0808.2818] [INSPIRE].

[54] A. Coc, E. Vangioni-Flam, P. Descouvemont, A. Adahchour and C. Angulo, *Updated Big Bang nucleosynthesis confronted to WMAP observations and to the abundance of light elements*, *Astrophys. J.* **600** (2004) 544 [astro-ph/0309480] [INSPIRE].

[55] R.H. Cyburt, B.D. Fields and K.A. Olive, *Solar neutrino constraints on the BBN production of Li*, *Phys. Rev.* **D 69** (2004) 123519 [astro-ph/0312629] [INSPIRE].

[56] C. Angulo, E. Casarejos, M. Couder, P. Demaret, P. Leleux, et al., *The Be-7(d,p)2-alpha cross section at big bang energies and the primordial Li-7 abundances*, *Astrophys. J.* **630** (2005) L105 [astro-ph/0508454] [INSPIRE].

[57] R.N. Boyd, C.R. Brune, G.M. Fuller and C.J. Smith, *New Nuclear Physics for Big Bang Nucleosynthesis*, *Phys. Rev.* **D 82** (2010) 105005 [arXiv:1008.0848] [INSPIRE].

[58] R.H. Cyburt and M. Pospelov, *Resonant enhancement of nuclear reactions as a possible solution to the cosmological lithium problem*, *Int. J. Mod. Phys.* **E 21** (2012) 1250004 [arXiv:0906.4373] [INSPIRE].

[59] N. Chakraborty, B.D. Fields and K.A. Olive, *Resonant Destruction as a Possible Solution to the Cosmological Lithium Problem*, *Phys. Rev.* **D 83** (2011) 063006 [arXiv:1011.0722] [INSPIRE].

[60] C. Broggini, L. Canton, G. Fiorentini and F. Villante, *The cosmological 7Li problem from a nuclear physics perspective*, *JCAP* **06** (2012) 030 [arXiv:1202.5232] [INSPIRE].

[61] P.D. O'Malley, D.W. Bardayan, A.S. Adekola, S. Ahn, K.Y. Chae, et al., *Search for a resonant enhancement of the Be-7 + d reaction and primordial Li-7 abundances*, *Phys. Rev.* **C 84** (2011) 042801 [INSPIRE].

[62] O.S. Kirsebom and B. Davids, *One fewer solution to the cosmological lithium problem*, *Phys. Rev.* **C 84** (2011) 058801 [arXiv:1109.4690] [INSPIRE].

[63] S. Vauclair and C. Charbonnel, *Element segregation in low metallicity stars and the primordial lithium abundance*, astro-ph/9802315 [INSPIRE];
M. Pinsonneault, T. Walker, G. Steigman and V. Narayanan, *Halo star lithium depletion*, *Astrophys. J.* **527** (2002) 180 [astro-ph/9803073] [INSPIRE];
M. Pinsonneault, G. Steigman, T. Walker and V. Narayanans, *Stellar mixing and the primordial lithium abundance*, *Astrophys. J.* **574** (2002) 398 [astro-ph/0105439] [INSPIRE];
O. Richard, G. Michaud and J. Richer, *Implications of WMAP observations on Li abundance and stellar evolution models*, *Astrophys. J.* **619** (2005) 538 [astro-ph/0409672] [INSPIRE];
A.J. Korn, F. Grundahl, O. Richard, P. Barklem, L. Mashonkina, et al., *A probable stellar solution to the cosmological lithium discrepancy*, *Nature* **442** (2006) 657 [astro-ph/0608201] [INSPIRE];
A.E. García Peréz, S. Inoue, W. Aoki, and S.G. Ryan, in *Precision Spectroscopy in Astrophysics*, proceedings of the ESO/Lisbon/Aveiro Conference, 9 (2008).

JCAP12(2012)037

[64] F. Spite and M. Spite, *Abundance of lithium in unevolved halo stars and old disk stars: Interpretation and consequences*, *Astron. Astrophys.* **115** (1982) 357 [INSPIRE];
S.G. Ryan, J.E. Norris and T.C. Beers, *The spite lithium plateau: ultrathin but post primordial*, *Astrophys. J.* **523** (1999) 654 [astro-ph/9903059] [INSPIRE];
W. Aoki et al., *Lithium Abundances of Extremely Metal-Poor Turn-off Stars*, *Astrophys. J.* **698** (2009) 1803 [arXiv:0904.1448] [INSPIRE].

[65] L. Sbordone et al., *The metal-poor end of the Spite plateau. 1: Stellar parameters, metallicities and lithium abundances*, *Astron. Astrophys.* **522** (2010) A26 [arXiv:1003.4510] [INSPIRE].

[66] V.V. Smith, D.L. Lambert and P.E. Nissen, *The 6Li/7Li ratio in the metal-poor halo dwarfs HD 19445 and HD 84937*, *Astrophys. J.* **408** (1993) 262 [INSPIRE]; *Isotopic Lithium Abundances in Nine Halo Stars*, *Astrophys. J.* **506** (1998) 405;
L.M. Hobbs and J.A. Thorburn, *Lithium isotope ratios in six halo stars*, *Astrophys. J. Lett.* **428** (1994) L25; *Lithium isotope ratios in halo stars. II.*, *Astrophys. J.* **491** (1997) 772;
R. Cayrel, M. Spite, F. Spite, E. Vangioni-Flam, M. Cassé and J. Audouze, *New high S/N observations of li6/li7 blend in HD 84937 and two other metal-poor stars*, *Astron. Astrophys.* **343** (1999) 923;
P.E. Nissen, M. Asplund, V. Hill and S. D'Odorico, *The lithium isotope ratio in the metal-poor halo star G271-162 from VLT/UVES observations*, *Astron. Astrophys.* **357** (2000) L49.

[67] J. Melendez and I. Ramirez, *Reappraising the Spite lithium plateau: Extremely thin and marginally consistent with WMAP*, *Astrophys. J.* **615** (2004) L33 [astro-ph/0409383] [INSPIRE].

[68] A. Hosford, A.G. Perez, R. Collet, S. Ryan, J. Norris, et al., *Lithium abundances of halo dwarfs based on excitation temperatures. II. NLTE*, arXiv:1004.0863 [INSPIRE];
A. Hosford, S.G. Ryan, A.E. García Pérez, J.E. Norris and K.A. Olive, *Lithium abundances of halo dwarfs based on excitation temperature. I. Local thermodynamic equilibrium*, *Astron. Astrophys.* **493** (2009) 601 [arXiv:0811.2506].

[69] J.C. Howk, N. Lehner, B.D. Fields and G.J. Mathews, *The detection of interstellar lithium in a low-metallicity galaxy*, *Nature* **489** (2012) 121 [arXiv:1207.3081] [INSPIRE].

[70] Particle Data Group collaboration, C. Amsler et al., *Review of Particle Physics*, *Phys. Lett.* **B 667** (2008) 1 [INSPIRE].

[71] I. Sick and D. Trautmann, *On the rms radius of the deuteron*, *Nucl. Phys.* **A 637** (1998) 559.

[72] D. Beck, S. Kowalski, M. Schulze, W. Turchinetz, J. Lightbody, et al., *Tritium form-factors at low q*, *Phys. Rev.* **C 30** (1984) 1403 [INSPIRE];
TUNL Nuclear Data Evaluation http://www.tunl.duke.edu/nucldata/.

[73] P. Mueller, I. Sulai, A. Villari, J. Alcantara-Núñez, R. Alves-Conde, et al., *Nuclear charge radius of He-5*, *Phys. Rev. Lett.* **99** (2007) 252501 [arXiv:0801.0601] [INSPIRE].

[74] I. Sick, *Precise root-mean-square radius of He-4*, *Phys. Rev.* **C 77** (2008) 041302 [INSPIRE].

[75] R. Sanchez, W. Nortershauser, G. Ewald, D. Albers, J. Behr, et al., *Nuclear Charge Radii of* ^{9}*Li,* ^{11}*Li: The Influence of Halo Neutrons*, *Phys. Rev. Lett.* **96** (2006) 033002 [INSPIRE].

[76] W. Nortershauser, D. Tiedemann, M. Zakova, Z. Andjelkovic, K. Blaum, et al., *Nuclear Charge Radii of* ^{7}*Be,* ^{9}*Be,* ^{10}*Be and the one-neutron halo nucleus* ^{11}*Be*, *Phys. Rev. Lett.* **102** (2009) 062503 [arXiv:0809.2607] [INSPIRE].

[77] M. Kamimura, Y. Kino and E. Hiyama, *Stau-catalyzed big-bang nucleosynthesis and nuclear cluster model*, *Int. J. Mod. Phys.* **A 24** (2009) 2076 [INSPIRE].

[78] M. Pospelov, *Bridging the primordial A=8 divide with catalyzed big bang nucleosynthesis*, arXiv:0712.0647 [INSPIRE].

JCAP12(2012)037

[79] K. Arai, P. Descouvemont, D. Baye and W. Catford, *Resonance structure of Be-9 and B-9 in a microscopic cluster model*, *Phys. Rev.* **C 68** (2003) 014310 [INSPIRE];
K. Arai, *Structure of the excited states of Be-10 in a microscopic cluster model*, *Phys. Rev.* **C 69** (2004) 014309 [INSPIRE].

[80] K. Varga and Y. Suzuki, *Solution of few body problems with the stochastic variational method: 1. Central forces*, *Comput. Phys. Commun.* **106** (1997) 157 [nucl-th/9702034] [INSPIRE].

[81] S. Ali, and A.R. Bodmer, *Phenomenological α-α potentials*, *Nucl. Phys.* **80** (1966) 99.

[82] S. Ali, and A. Afzal, *Phenomenological α-α potential and the ground state of ^{8}Be*, *Nuovo Cim.* **50** (1967) 355.

[83] D.R. Tilley, et al., *Energy Levels of Light Nuclei A = 20*, *Nucl. Phys.* **A 636** (1998) 247.

[84] G.R. Caughlan and W. A. Fowler, *Thermonuclear reaction rates. 5.*, *Atom. Data Nucl. Data Tabl.* **40** (1988) 283.

[85] C. Angulo, M. Arnould, M. Rayet, P. Descouvemont, D. Baye, et al., *A compilation of charged-particle induced thermonuclear reaction rates*, *Nucl. Phys.* **A 656** (1999) 3 [INSPIRE].

[86] R. Malaney and W. Fowler, *Late time neutron diffusion and nucleosynthesis in a post Qcd inhomogeneous Omega (B) = 1 Universe*, *Astrophys. J.* **333** (1988) 14 [*Annals Phys.* **192** (1989) 45] [INSPIRE].

[87] R.H. Cyburt, *Primordial nucleosynthesis for the new cosmology: Determining uncertainties and examining concordance*, *Phys. Rev.* **D 70** (2004) 023505 [astro-ph/0401091] [INSPIRE].

[88] A. Coc, S. Goriely, Y. Xu, M. Saimpert and E. Vangioni, *Standard Big-Bang Nucleosynthesis up to CNO with an improved extended nuclear network*, *Astrophys. J.* **744** (2012) 158 [arXiv:1107.1117] [INSPIRE].

[89] E. Matt, H. Pfander, H. Rieseberg and V. Soergel, *Beta decay from ^{8}B to the 16.67 MeV level in ^{8}Be*, *Phys. Lett.* **9** (1964) 174.

[90] J.L. Feng, A. Rajaraman and F. Takayama, *SuperWIMP dark matter signals from the early universe*, *Phys. Rev.* **D 68** (2003) 063504 [hep-ph/0306024] [INSPIRE];
J.L. Feng, S.-f. Su and F. Takayama, *SuperWIMP gravitino dark matter from slepton and sneutrino decays*, *Phys. Rev.* **D 70** (2004) 063514 [hep-ph/0404198] [INSPIRE].

[91] J.L. Feng, S. Su and F. Takayama, *Supergravity with a gravitino LSP*, *Phys. Rev.* **D 70** (2004) 075019 [hep-ph/0404231] [INSPIRE].

[92] J.R. Ellis, K.A. Olive, Y. Santoso and V.C. Spanos, *Gravitino dark matter in the CMSSM*, *Phys. Lett.* **B 588** (2004) 7 [hep-ph/0312262] [INSPIRE].

[93] J.R. Ellis, K.A. Olive, Y. Santoso and V.C. Spanos, *Very constrained minimal supersymmetric standard models*, *Phys. Rev.* **D 70** (2004) 055005 [hep-ph/0405110] [INSPIRE].

[94] T. Sjöstrand, P. Eden, C. Friberg, L. Lönnblad, G. Miu, et al., *High-energy physics event generation with PYTHIA 6.1*, *Comput. Phys. Commun.* **135** (2001) 238 [hep-ph/0010017] [INSPIRE].

[95] ATLAS collaboration, *Observation of a new particle in the search for the Standard Model Higgs boson with the ATLAS detector at the LHC*, *Phys. Lett.* **B 716** (2012) 1 [arXiv:1207.7214] [INSPIRE];
CMS collaboration, *Observation of a new boson at a mass of 125 GeV with the CMS experiment at the LHC*, *Phys. Lett.* **B 716** (2012) 30 [arXiv:1207.7235] [INSPIRE].

[96] G. Degrassi, S. Heinemeyer, W. Hollik, P. Slavich and G. Weiglein, *Towards high precision predictions for the MSSM Higgs sector*, *Eur. Phys. J.* **C 28** (2003) 133 [hep-ph/0212020] [INSPIRE];

JCAP12(2012)037

S. Heinemeyer, W. Hollik and G. Weiglein, *The Masses of the neutral CP-even Higgs bosons in the MSSM: Accurate analysis at the two loop level*, *Eur. Phys. J.* **C 9** (1999) 343 [hep-ph/9812472] [INSPIRE]; *FeynHiggs: A Program for the calculation of the masses of the neutral CP even Higgs bosons in the MSSM*, *Comput. Phys. Commun.* **124** (2000) 76 [hep-ph/9812320] [INSPIRE];
M. Frank, T. Hahn, S. Heinemeyer, W. Hollik, H. Rzehak, et al., *The Higgs Boson Masses and Mixings of the Complex MSSM in the Feynman-Diagrammatic Approach*, *JHEP* **02** (2007) 047 [hep-ph/0611326] [INSPIRE];
see http://www.feynhiggs.de/.

[97] J. Ellis and K.A. Olive, *Revisiting the Higgs Mass and Dark Matter in the CMSSM*, *Eur. Phys. J.* **C 72** (2012) 2005 [arXiv:1202.3262] [INSPIRE].

[98] O. Buchmueller, R. Cavanaugh, A. De Roeck, M. Dolan, J. Ellis, et al., *Higgs and Supersymmetry*, *Eur. Phys. J.* **C 72** (2012) 2020 [arXiv:1112.3564] [INSPIRE];
O. Buchmueller, R. Cavanaugh, M. Citron, A. De Roeck, M. Dolan, et al., *The CMSSM and NUHM1 in Light of 7 TeV LHC, $B_s \to \mu^+\mu^-$ and XENON100 Data*, *Eur. Phys. J.* **C 72** (2012) 2243 [arXiv:1207.7315] [INSPIRE].

[99] H. Baer, V. Barger and A. Mustafayev, *Implications of a 125 GeV Higgs scalar for LHC SUSY and neutralino dark matter searches*, *Phys. Rev.* **D 85** (2012) 075010 [arXiv:1112.3017] [INSPIRE];
A. Arbey, M. Battaglia, A. Djouadi, F. Mahmoudi and J. Quevillon, *Implications of a 125 GeV Higgs for supersymmetric models*, *Phys. Lett.* **B 708** (2012) 162 [arXiv:1112.3028] [INSPIRE];
L. Aparicio, D. Cerdeno and L. Ibáñez, *A 119-125 GeV Higgs from a string derived slice of the CMSSM*, *JHEP* **04** (2012) 126 [arXiv:1202.0822] [INSPIRE].

[100] ATLAS collaboration, *Search for the decay $B_s^0 \to \mu^+\mu^-$ with the ATLAS detector*, *Phys. Lett.* **B 713** (2012) 387 [arXiv:1204.0735] [INSPIRE];
CDF collaboration, T. Aaltonen et al., *Search for $B_s \to \mu^+\mu^-$ and $B_d \to \mu^+\mu^-$ Decays with CDF II*, *Phys. Rev. Lett.* **107** (2011) 239903 [arXiv:1107.2304] [INSPIRE];
CDF collaboration, T. Aaltonen et al., *Search for $B_s \to \mu^+\mu^-$ and $B_d \to \mu^+\mu^-$ Decays with CDF II*, *Phys. Rev. Lett.* **107** (2011) 239903 [arXiv:1107.2304] [INSPIRE];
CMS collaboration, *Search for B_s and B to dimuon decays in pp collisions at 7 TeV*, *Phys. Rev. Lett.* **107** (2011) 191802 [arXiv:1107.5834] [INSPIRE];
LHCb collaboration, *Search for the rare decays $B_s^0 \to \mu^+\mu^-$ and $B^0 \to \mu^+\mu^-$*, *Phys. Lett.* **B 699** (2011) 330 [arXiv:1103.2465] [INSPIRE];
LHCb collaboration, *Strong constraints on the rare decays $B_s \to \mu^+\mu^-$ and $B^0 \to \mu^+\mu^-$*, *Phys. Rev. Lett.* **108** (2012) 231801 [arXiv:1203.4493] [INSPIRE];
For an official combination of the ATLAS, CMS and LHCb results, see: ATLAS, CMS, and LHCb Collaborations, *Search for the rare decays $B_s^0 \to \mu^+\mu^-$ at the LHC with the ATLAS, CMS and LHCb experiments*, LHCb-CONF-2012-017.

[101] C. Bobeth, T. Ewerth, F. Krüger and J. Urban, *Analysis of neutral Higgs boson contributions to the decays $\bar{B}_s \to \ell^+\ell^-$ and $\bar{B} \to K\ell^+\ell^-$*, *Phys. Rev.* **D 64** (2001) 074014 [hep-ph/0104284] [INSPIRE];
A. Dedes, H.K. Dreiner and U. Nierste, *Correlation of $B_s \to \mu^+\mu^-$ and (g-2) (μ) in minimal supergravity*, *Phys. Rev. Lett.* **87** (2001) 251804 [hep-ph/0108037] [INSPIRE];
C. Bobeth, A.J. Buras, F. Krüger and J. Urban, *QCD corrections to $\bar{B} \to X_{d,s}\nu\bar{\nu}$, $\bar{B}_{d,s} \to \ell^+\ell^-$, $K \to \pi\nu\bar{\nu}$ and $K_L \to \mu^+\mu^-$ in the MSSM*, *Nucl. Phys.* **B 630** (2002) 87 [hep-ph/0112305] [INSPIRE];
J. Mizukoshi, X. Tata and Y. Wang, *Higgs mediated leptonic decays of B_s and B_d mesons as probes of supersymmetry*, *Phys. Rev.* **D 66** (2002) 115003 [hep-ph/0208078] [INSPIRE];
FIXME C. Bobeth, T. Ewerth, F. Krüger and J. Urban, *Enhancement of $B(\bar{B}_d \to \mu^+\mu^-)/B(\bar{B}_s \to \mu^+\mu^-$ in the MSSM with minimal flavor violation and large tan*

JCAP12(2012)037

beta, *Phys. Rev.* **D 66** (2002) 074021 [hep-ph/0204225] [INSPIRE];
A.J. Buras, P.H. Chankowski, J. Rosiek and L. Slawianowska, $\Delta M_{d,s}, B^0_{d,s} \to \mu^+\mu^-$ *and* $B \to X_s\gamma$ *in supersymmetry at large* $\tan\beta$, *Nucl. Phys.* **B 659** (2003) 3 [hep-ph/0210145] [INSPIRE];
A.J. Buras, M.V. Carlucci, S. Gori and G. Isidori, *Higgs-mediated FCNCs: Natural Flavour Conservation vs. Minimal Flavour Violation*, *JHEP* **10** (2010) 009 [arXiv:1005.5310] [INSPIRE].

[102] R.L. Arnowitt, B. Dutta, T. Kamon and M. Tanaka, *Detection of* $B_s \to \mu^+\mu^-$ *at the Tevatron run II and constraints on the SUSY parameter space*, *Phys. Lett.* **B 538** (2002) 121 [hep-ph/0203069] [INSPIRE];
S. Baek, P. Ko and W.Y. Song, *Implications on SUSY breaking mediation mechanisms from observing B(s) —¿* $\mu^+\mu^-$ *and the muon (g-2)*, *Phys. Rev. Lett.* **89** (2002) 271801 [hep-ph/0205259] [INSPIRE];
C.-S. Huang and X.-H. Wu, *B(s) —¿* $\mu^+\mu^-$ *and* $B \to X_s\mu^+\mu^-$ *in MSSM*, *Nucl. Phys.* **B 657** (2003) 304 [hep-ph/0212220] [INSPIRE];
S. Baek, Y.G. Kim and P. Ko, *Neutralino dark matter scattering and* $B_s \to \mu^+\mu^-$ *in SUSY models*, *JHEP* **02** (2005) 067 [hep-ph/0406033] [INSPIRE];
J.R. Ellis, K.A. Olive and V.C. Spanos, *On the interpretation of* $B_s \to \mu^+\mu^-$ *in the CMSSM*, *Phys. Lett.* **B 624** (2005) 47 [hep-ph/0504196] [INSPIRE];
J.R. Ellis, K.A. Olive, Y. Santoso and V.C. Spanos, *On* $B_s \to \mu^+\mu^-$ *and cold dark matter scattering in the MSSM with non-universal Higgs masses*, *JHEP* **05** (2006) 063 [hep-ph/0603136] [INSPIRE];
S. Heinemeyer, X. Miao, S. Su and G. Weiglein, B^- *Physics Observables and Electroweak Precision Data in the CMSSM, mGMSB and mAMSB*, *JHEP* **08** (2008) 087 [arXiv:0805.2359] [INSPIRE];
B. Dutta, Y. Mimura and Y. Santoso, $B_s \to \mu^+\mu^-$ *in Supersymmetric Grand Unified Theories*, *Phys. Lett.* **B 706** (2011) 188 [arXiv:1107.3020] [INSPIRE];
A. Akeroyd, F. Mahmoudi and D.M. Santos, *The decay* $B_s \to \mu^+\mu^-$*: updated SUSY constraints and prospects*, *JHEP* **12** (2011) 088 [arXiv:1108.3018] [INSPIRE];
F. Mahmoudi, S. Neshatpour and J. Orloff, *Supersymmetric constraints from* $B_s \to \mu^+\mu^-$ *and* $B \to K * \mu^+\mu^-$ *observables*, *JHEP* **08** (2012) 092 [arXiv:1205.1845] [INSPIRE].

[103] K. Kohri and Y. Santoso, *Cosmological scenario of stop NLSP with gravitino LSP and the cosmic lithium problem*, *Phys. Rev.* **D 79** (2009) 043514 [arXiv:0811.1119] [INSPIRE].

[104] K.A. Olive, P. Petitjean, E. Vangioni and J. Silk, *Higher D or Li: Probes of Physics beyond the Standard Model*, arXiv:1203.5701 [INSPIRE].

[105] S. Burles and D. Tytler, *The Deuterium abundance towards Q1937-1009*, *Astrophys. J.* **499** (1998) 699 [astro-ph/9712108] [INSPIRE]; *The Deuterium abundance toward QSO 1009+2956*, *Astrophys. J.* **507** (1998) 732 [astro-ph/9712109] [INSPIRE];
J.M. O'Meara, D. Tytler, D. Kirkman, N. Suzuki, J.X. Prochaska, et al., *The Deuterium to hydrogen abundance ratio towards a fourth QSO: HS 0105 + 1619*, *Astrophys. J.* **552** (2001) 718 [astro-ph/0011179] [INSPIRE];
M. Pettini and D.V. Bowen, *A new measurement of the primordial abundance of deuterium: toward convergence with the baryon density from the cmb?*, *Astrophys. J.* **560** (2001) 41 [astro-ph/0104474] [INSPIRE];
S. Levshakov, M. Dessauges-Zavadsky, S. D'Odorico and P. Molaro, *Molecular hydrogen, deuterium and metal abundances in the damped ly-alpha system at Z = 3.025 toward qso 0347-3819*, astro-ph/0105529 [INSPIRE];
D. Kirkman, D. Tytler, N. Suzuki, J.M. O'Meara and D. Lubin, *The Cosmological baryon density from the deuterium to hydrogen ratio towards QSO absorption systems: D/H towards Q1243+3047*, *Astrophys. J. Suppl.* **149** (2003) 1 [astro-ph/0302006] [INSPIRE];
J.M. O'Meara, S. Burles, J.X. Prochaska, G.E. Prochter, R.A. Bernstein, et al., *The*

JCAP12(2012)037

Deuterium to Hydrogen Abundance Ratio Towards the QSO SDSS1558-0031, *Astrophys. J.* **649** (2006) L61 [astro-ph/0608302] [INSPIRE];
M. Pettini, B.J. Zych, M.T. Murphy, A. Lewis and C.C. Steidel, *Deuterium Abundance in the Most Metal-Poor Damped Lyman alpha System: Converging on Omega_baryons*, arXiv:0805.0594 [INSPIRE];
R. Srianand, N. Gupta, P. Petitjean, P. Noterdaeme and C. Ledoux, *Detection of 21-cm, H2 and Deuterium absorption at z¿3 along the line-of-sight to J1337+3152*, arXiv:1002.4620 [INSPIRE];
M. Fumagalli, J.M. O'Meara and J.X. Prochaska, *Detection of Pristine Gas Two Billion Years after the Big Bang*, arXiv:1111.2334 [INSPIRE].

[106] G. Sigl, K. Jedamzik, D.N. Schramm and V.S. Berezinsky, *Helium photodisintegration and nucleosynthesis: Implications for topological defects, high-energy cosmic rays and massive black holes*, *Phys. Rev.* **D 52** (1995) 6682 [astro-ph/9503094] [INSPIRE].

[107] J. Geiss, *Primordial abundances of hydrogen and helium isotopes*, in *Origin and Evolution of the Elements*, N. Prantzos, E. Vangioni-Flam and M. Casse eds., Cambridge University Press, Cambridge, 89 (1993).

[108] K.A. Olive, and E.D. Skillman, *Uncertainties in ^{4}He abundance determinations in extragalactic H II regions* New Astron. **6** (2001) 119; *A Realistic determination of the error on the primordial helium abundance: Steps toward non-parametric nebular helium abundances*, *Astrophys. J.* **617** (2004) 29 [astro-ph/0405588] [INSPIRE].

[109] E. Aver, K.A. Olive and E.D. Skillman, *Mapping systematic errors in helium abundance determinations using Markov Chain Monte Carlo*, *JCAP* **03** (2011) 043 [arXiv:1012.2385] [INSPIRE].

[110] Y.I. Izotov, T. Thuan and G. Stasinska, *The primordial abundance of He-4: A self-consistent empirical analysis of systematic effects in a large sample of low-metallicity HII regions*, *Astrophys. J.* **662** (2007) 15 [astro-ph/0702072] [INSPIRE].

[111] E. Aver, K.A. Olive and E.D. Skillman, *An MCMC determination of the primordial helium abundance*, *JCAP* **04** (2012) 004 [arXiv:1112.3713] [INSPIRE].

[112] M. Asplund, D.L. Lambert, P.E. Nissen, F. Primas and V.V. Smith, *Lithium isotopic abundances in metal-poor halo stars*, *Astrophys. J.* **644** (2006) 229 [astro-ph/0510636] [INSPIRE].

[113] R. Cayrel et al., *Line shift, line asymmetry and the 6Li/7Li isotopic ratio determination*, arXiv:0708.3819 [INSPIRE];
M. Steffen, R. Cayrel, P. Bonifacio, H.-G. Ludwig and E. Caffau, *6Li in metal-poor halo stars: real or spurious?*, arXiv:0910.5917 [INSPIRE].

[114] G. Steigman, B.D. Fields, K.A. Olive, D.N. Schramm and T.P. Walker, *POP-II Li-6 as a probe of nucleosynthesis and stellar structure and evolution*, *Astrophys. J.* **415** (1993) L35 [INSPIRE];
B.D. Fields and K.A. Olive, *The Evolution of 6-Li in standard cosmic-ray nucleosynthesis*, astro-ph/9811183 [INSPIRE];
E. Vangioni-Flam, M. Casse, R. Cayrel, J. Audouze, M. Spite and F. Spite, *Lithium-6 : evolution from big bang to present*, *New Astron.* **4** (1999) 245 [astro-ph/9811327] [INSPIRE].

[115] S. Ryan, T. Beers, K.A. Olive, B. Fields and J. Norris, *Primordial lithium and big bang nucleosynthesis*, *Astrophys. J. Lett.* **530** (2000) L57 [astro-ph/9905211] [INSPIRE].

[116] J.I.G. Hernandez, P. Bonifacio, E. Caffau, M. Steffen, H.-G. Ludwig, et al., *Lithium in the Globular Cluster NGC 6397: Evidence for dependence on evolutionary status*, *Astron. Astrophys.* **505** (2009) L13 [arXiv:0909.0983] [INSPIRE];
L. Pasquini and P. Molaro, *Lithium abundance in the globular cluster NGC 6397*, *Astron. Astrophys.* **307** (1996) 761;
F. Thevenin et al., *Vlt observations of turnoff stars in the globular cluster ngc 6397*, *Astron. Astrophys.* **373** (2001) 905 [astro-ph/0105166] [INSPIRE];

JCAP12(2012)037

P. Bonifacio et al., *The lithium content of the globular cluster ngc 6397*, *Astron. Astrophys.* **390** (2002) 91 [astro-ph/0204332] [INSPIRE];
P. Bonifacio, *On the lithium content of the globular cluster M92*, *Astron. Astrophys.* **395** (2002) 515 [astro-ph/0209434] [INSPIRE];
K. Lind, F. Primas, C. Charbonnel, F. Grundahl and M. Asplund, *Signatures of intrinsic Li depletion and Li-Na anti-correlation in the metal-poor globular cluster NGC6397*, *Astron. Astrophys.* **503** (2009) 545 [arXiv:0906.2876] [INSPIRE].

[117] A.M. Boesgaard, J.A. Rich, E.M. Levesque and B.P. Bowler, *Beryllium and Alpha-Element Abundances in a Large Sample of Metal-Poor Stars*, *Astrophys. J.* **743** (2011) 140 [arXiv:1110.2823] [INSPIRE].

[118] H. Ito, W. Aoki, S. Honda and T.C. Beers, *BD +44 493: A Ninth Magnitude Messenger from the Early Universe: Carbon Enhanced and Beryllium Poor*, *Astrophys. J.* **698** (2009) L37 [arXiv:0905.0950] [INSPIRE].

[119] M. Drees and M.M. Nojiri, *The Neutralino relic density in minimal $N = 1$ supergravity*, *Phys. Rev.* **D 47** (1993) 376 [hep-ph/9207234] [INSPIRE];
G.L. Kane, C.F. Kolda, L. Roszkowski and J.D. Wells, *Study of constrained minimal supersymmetry*, *Phys. Rev.* **D 49** (1994) 6173 [hep-ph/9312272] [INSPIRE];
H. Baer and M. Brhlik, *Cosmological relic density from minimal supergravity with implications for collider physics*, *Phys. Rev.* **D 53** (1996) 597 [hep-ph/9508321] [INSPIRE]; *Neutralino dark matter in minimal supergravity: Direct detection versus collider searches*, *Phys. Rev.* **D 57** (1998) 567 [hep-ph/9706509] [INSPIRE];
J.R. Ellis, T. Falk, K.A. Olive and M. Schmitt, *Supersymmetric dark matter in the light of LEP-1.5*, *Phys. Lett.* **B 388** (1996) 97 [hep-ph/9607292] [INSPIRE]; *Constraints on neutralino dark matter from LEP-2 and cosmology*, *Phys. Lett.* **B 413** (1997) 355 [hep-ph/9705444] [INSPIRE];
J.R. Ellis, T. Falk, G. Ganis, K.A. Olive and M. Schmitt, *Charginos and neutralinos in the light of radiative corrections: Sealing the fate of Higgsino dark matter*, *Phys. Rev.* **D 58** (1998) 095002 [hep-ph/9801445] [INSPIRE];
V.D. Barger and C. Kao, *Relic density of neutralino dark matter in supergravity models*, *Phys. Rev.* **D 57** (1998) 3131 [hep-ph/9704403] [INSPIRE];
J.R. Ellis, T. Falk, G. Ganis and K.A. Olive, *Supersymmetric dark matter in the light of LEP and the Tevatron collider*, *Phys. Rev.* **D 62** (2000) 075010 [hep-ph/0004169] [INSPIRE];
H. Baer, M. Brhlik, M.A. Diaz, J. Ferrandis, P. Mercadante, et al., *Yukawa unified supersymmetric* SO(10) *model: Cosmology, rare decays and collider searches*, *Phys. Rev.* **D 63** (2000) 015007 [hep-ph/0005027] [INSPIRE];
J.R. Ellis, T. Falk, G. Ganis, K.A. Olive and M. Srednicki, *The CMSSM parameter space at large tan beta*, *Phys. Lett.* **B 510** (2001) 236 [hep-ph/0102098] [INSPIRE];
V.D. Barger and C. Kao, *Implications of new CMB data for neutralino dark matter*, *Phys. Lett.* **B 518** (2001) 117 [hep-ph/0106189] [INSPIRE];
L. Roszkowski, R. Ruiz de Austri and T. Nihei, *New cosmological and experimental constraints on the CMSSM*, *JHEP* **08** (2001) 024 [hep-ph/0106334] [INSPIRE];
A. Djouadi, M. Drees and J. Kneur, *Constraints on the minimal supergravity model and prospects for SUSY particle production at future linear e^+e^- colliders*, *JHEP* **08** (2001) 055 [hep-ph/0107316] [INSPIRE];
U. Chattopadhyay, A. Corsetti and P. Nath, *Supersymmetric dark matter and Yukawa unification*, *Phys. Rev.* **D 66** (2002) 035003 [hep-ph/0201001] [INSPIRE];
J.R. Ellis, K.A. Olive and Y. Santoso, *Constraining supersymmetry*, *New J. Phys.* **4** (2002) 32 [hep-ph/0202110] [INSPIRE];
H. Baer, C. Balázs, A. Belyaev, J.K. Mizukoshi, X. Tata, et al., *Updated constraints on the minimal supergravity model*, *JHEP* **07** (2002) 050 [hep-ph/0205325] [INSPIRE];
R.L. Arnowitt and B. Dutta, *Dark matter, muon g-2 and other accelerator constraints*, hep-ph/0211417 [INSPIRE];

JCAP12(2012)037

J.R. Ellis, K.A. Olive, Y. Santoso and V.C. Spanos, *Supersymmetric dark matter in light of WMAP*, *Phys. Lett.* **B 565** (2003) 176 [hep-ph/0303043] [INSPIRE];
H. Baer and C. Balázs, *Chi**2 analysis of the minimal supergravity model including WMAP, g(mu)-2 and b —¿ s gamma constraints*, *JCAP* **05** (2003) 006 [hep-ph/0303114] [INSPIRE];
A.B. Lahanas and D.V. Nanopoulos, *WMAPing out supersymmetric dark matter and phenomenology*, *Phys. Lett.* **B 568** (2003) 55 [hep-ph/0303130] [INSPIRE];
U. Chattopadhyay, A. Corsetti and P. Nath, *WMAP constraints, SUSY dark matter and implications for the direct detection of SUSY*, *Phys. Rev.* **D 68** (2003) 035005 [hep-ph/0303201] [INSPIRE];
C. Muñoz, *Dark matter detection in the light of recent experimental results*, *Int. J. Mod. Phys.* **A 19** (2004) 3093 [hep-ph/0309346] [INSPIRE];
R.L. Arnowitt, B. Dutta and B. Hu, *Dark matter, muon g-2 and other SUSY constraints*, hep-ph/0310103 [INSPIRE];
J. Ellis and K.A. Olive, *Supersymmetric Dark Matter Candidates*, arXiv:1001.3651 [INSPIRE].

[120] MUON G-2 collaboration, G. Bennett et al., *Measurement of the negative muon anomalous magnetic moment to 0.7 ppm*, *Phys. Rev. Lett.* **92** (2004) 161802 [hep-ex/0401008] [INSPIRE]; *Final Report of the Muon E821 Anomalous Magnetic Moment Measurement at BNL*, *Phys. Rev.* **D 73** (2006) 072003 [hep-ex/0602035] [INSPIRE].

[121] D. Stöckinger, *The Muon Magnetic Moment and Supersymmetry*, *J. Phys.* **G 34** (2007) R45 [hep-ph/0609168] [INSPIRE];
J.P. Miller, E. de Rafael and B.L. Roberts, *Muon (g-2): Experiment and theory*, *Rept. Prog. Phys.* **70** (2007) 795 [hep-ph/0703049] [INSPIRE];
J. Prades, E. de Rafael and A. Vainshtein, *Hadronic Light-by-Light Scattering Contribution to the Muon Anomalous Magnetic Moment*, arXiv:0901.0306 [INSPIRE];
F. Jegerlehner and A. Nyffeler, *The Muon g-2*, *Phys. Rept.* **477** (2009) 1 [arXiv:0902.3360] [INSPIRE];
M. Davier, A. Hoecker, B. Malaescu, C. Yuan and Z. Zhang, *Reevaluation of the hadronic contribution to the muon magnetic anomaly using new $e^+e^- \to \pi^+\pi^-$ cross section data from BABAR*, *Eur. Phys. J.* **C 66** (2010) 1 [arXiv:0908.4300] [INSPIRE];
J. Prades, *Standard Model Prediction of the Muon Anomalous Magnetic Moment*, *Acta Phys. Polon. Supp.* **3** (2010) 75 [arXiv:0909.2546] [INSPIRE];
T. Teubner, K. Hagiwara, R. Liao, A. Martin and D. Nomura, *Update of g-2 of the Muon and Delta Alpha*, *Chin. Phys.* **C 34** (2010) 728 [arXiv:1001.5401] [INSPIRE];
M. Davier, A. Hoecker, B. Malaescu and Z. Zhang, *Reevaluation of the Hadronic Contributions to the Muon g-2 and to alpha(MZ)*, *Eur. Phys. J.* **C 71** (2011) 1515 [*Erratum ibid.* **C 72** (2012) 1874] [arXiv:1010.4180] [INSPIRE].

[122] F. Luo, K.A. Olive and M. Peloso, *The Gravitino coupling to broken gauge theories applied to the MSSM*, *JHEP* **10** (2010) 024 [arXiv:1006.5570] [INSPIRE].

[123] H.E. Haber and G.L. Kane, *The Search for Supersymmetry: Probing Physics Beyond the Standard Model*, *Phys. Rept.* **117** (1985) 75 [INSPIRE].

[124] J. Gunion and H.E. Haber, *Higgs Bosons in Supersymmetric Models. 1.*, *Nucl. Phys.* **B 272** (1986) 1 [*Erratum ibid.* **B 402** (1993) 567-569] [INSPIRE].

[125] E. Vangioni-Flam, M. Casse, R. Cayrel, J. Audouze, M. Spite and F. Spite, *Lithium-6: evolution from big bang to present*, *New Astron.* **4** (1999) 245;
B. D. Fields and K. A. Olive, *The evolution of 6Li in standard cosmic-ray nucleosynthesis*, *New Astron.* **4** (1999) 255;
B.D. Fields and T. Prodanovic, *Lithium-6 and gamma rays: Complementary constraints on cosmic-ray history*, *Astrophys. J.* **623** (2005) 877 [astro-ph/0407314] [INSPIRE];
E. Rollinde, E. Vangioni and K.A. Olive, *Population III Generated Cosmic Rays and the Production of Li6*, *Astrophys. J.* **651** (2006) 658 [astro-ph/0605633] [INSPIRE].

[126] P.J.E. Peebles, *Principles of Physical Cosmology* (1993), see equations (6.100)–(6.104) and the surrounding discussion.

JCAP12(2012)037